40th Annual Condensed Matter and Materials Meeting

Wagga 2016

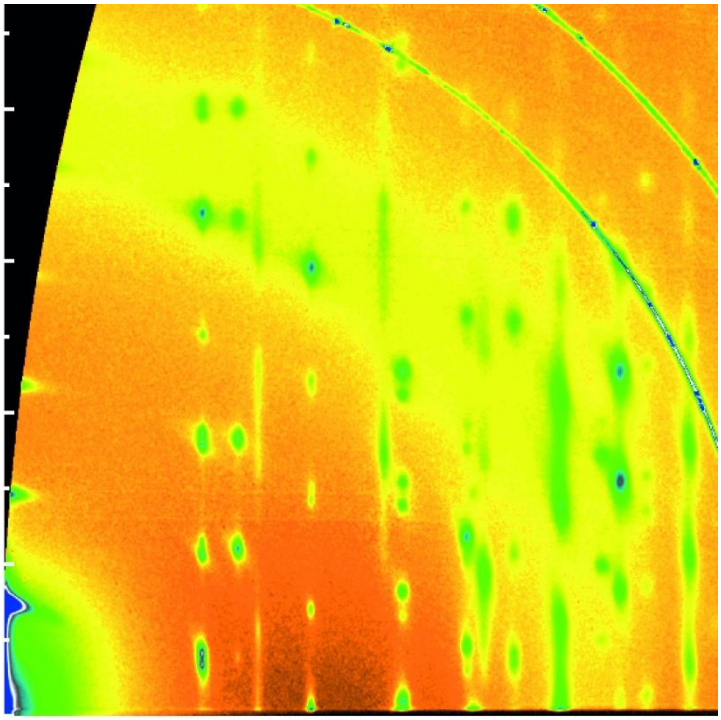

Charles Sturt University, Wagga Wagga, NSW
2nd February – 5th February, 2016

ISBN : 978-0-646-96433-1

Australian and New Zealand Institutes of Physics

40th Annual Condensed Matter and Materials Meeting

Charles Sturt University, Wagga Wagga, NSW
2nd February – 5th February, 2016

CONFERENCE HANDBOOK

ISBN : 978-0-646-96433-1

WW2016 Organising Committee

Anton Tadich
Helen Brand
Dominique Appadoo
Trevor Finlayson
Michael James

Australian Synchrotron
Clayton, VIC 3168, Australia

2016 : SPONSORS

scitek
total vacuum solutions

KPTechnology

ezzi vision
Vacuum & Thin Film Technology
www.ezzivision.com.au

AXAA
Australian X-ray Analytical Association

CRYSTRAN
UV · VISIBLE · IR SPECIALIST OPTICS

BOC
A Member of The Linde Group

Monash Centre for Atomically Thin Materials
INNOVATIVE MATERIALS | TRANSFORMATIVE TECHNOLOGY

BRUKER

scientaomicron

WW 2016 : CONTENTS

Front Cover Image:

This image is an example of a two dimensional Grazing-incidence Wide Angle X-ray Scattering (GIWAXS) pattern, collected in one second from a heated spin-coated thin organic film in-situ at SAXS/WAXS beamline at the Australian Synchrotron. Analysis of the peak locations and intensities reveals a unique crystalline structure, not seen at room temperature. Further analysis of how patterns such as these change at different temperatures reveals crystalline phase transitions and the thermal expansion of crystallites in these phases. Interestingly they also expose unexpected behaviours such as highly negative, and in other very similar molecules, highly positive linear thermal expansion coefficients. These different thermal expansion coefficients end up correlating very well with the varying performance of thin film transistors made of these materials annealed and quenched at different temperatures.

Courtesy: Dr Eliot Gann (Monash University / Australian Synchrotron)

WW2016 : MAPS

Wagga Wagga and the location of the Charles Sturt University campus

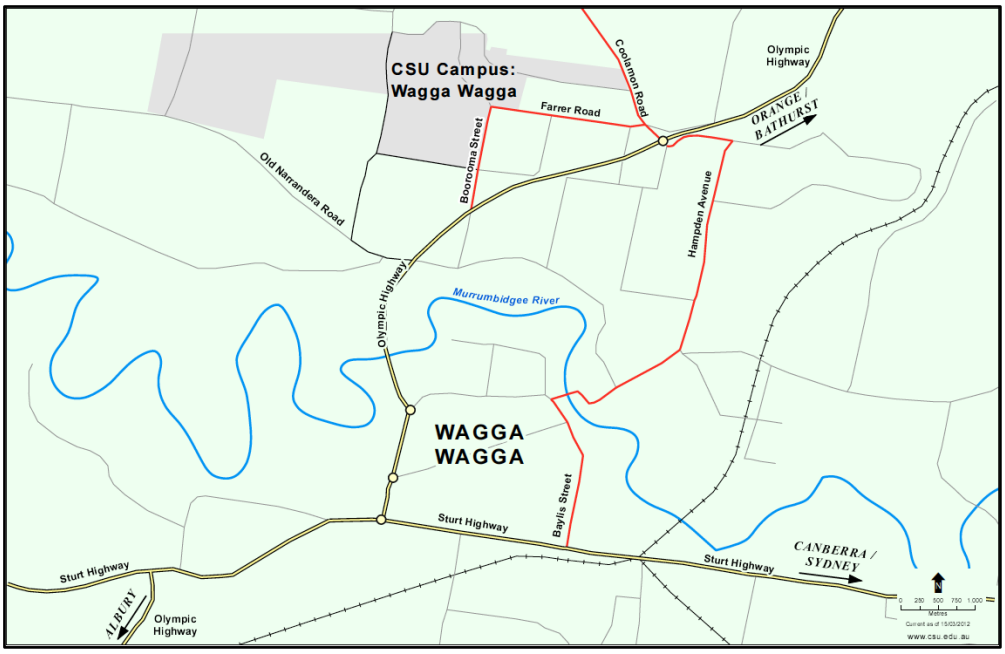

Location of Convention Centre and accommodation

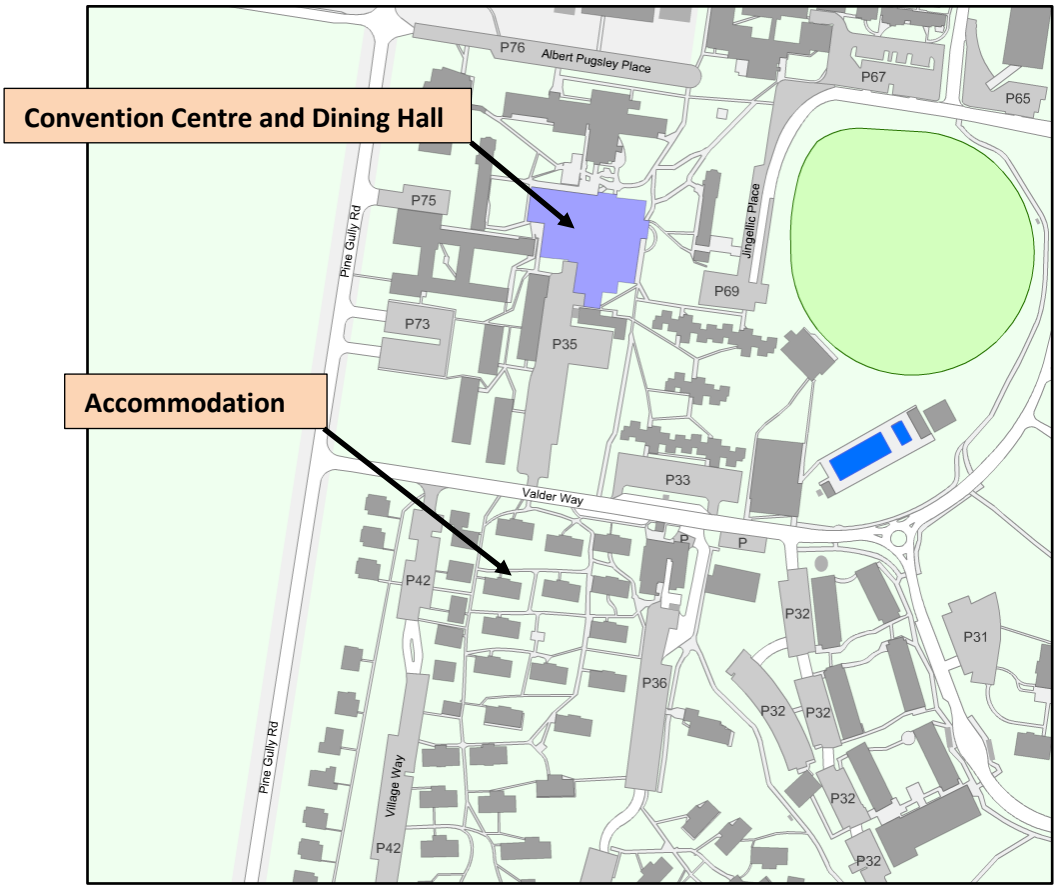

WW 2016 : CMM GROUP

Welcome to the "Wagga" community:

Just by attending the annual Condensed Matter and Materials (CMM) Meeting you are a member of the CMM topical group of the Australian Institute of Physics (AIP). There are no forms or membership fees involved.

Take a look at the CMM Group web site:

It can be accessed from the AIP national web site (**www.aip.org.au**) by clicking on **AIP Groups** listed under "Related Groups" in the column at the left of the home page and then selecting **Condensed Matter and Materials Group (CMM)**. Alternatively, you can go directly to **http://cmm-group.com.au/**

Please share your favourite "Wagga" experiences:

If you have some special group images of you and colleagues, interesting events and stories from previous "Waggas", please share them with us by passing them on to Glen Stewart (**g.stewart@adfa.edu.au**) who will have them incorporated into the history section of the CMM Group web site. Please include in your e-mail the year of the meeting and the names of those "Waggarites" you are able to identify in the images.

1978

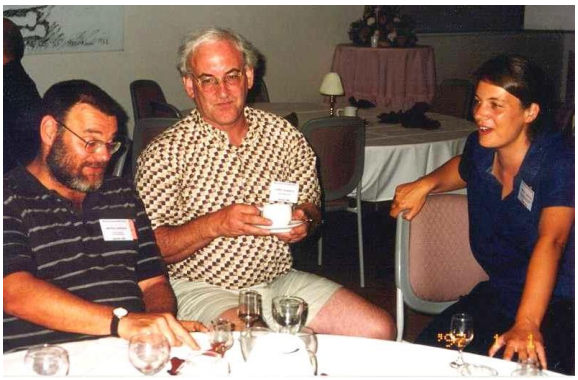

2002

WW 2016 : ATTENDEE INFORMATION

Scientific Program:

All poster sessions and lectures will be held at the Convention Centre. Chairpersons and speakers are asked to adhere closely to the schedule for the oral program. A PC laptop computer and data projector, overhead projector, pointer and microphone will be available. Please check that your presentation is compatible with the facilities provided as early as possible. Posters should be mounted as early as possible. Please remove your Wednesday session posters by early Thursday morning and your Thursday session posters by the close of the program on Friday.

Logistics:

Please wear your name tag at all times. Registration and all other administrative matters should be addressed to the registration desk or a committee member. For lost keys or if locked out of your room from 0900 to 1700, contact the Events Office for assistance 6933 4974; after hours, contact the Accommodation and Security Office near the corner of Valder Way and Park Way or phone them at 6933 2288. **Delegates must check out of their rooms on Friday morning, before 10:00am.**

Meals, Refreshments and Recreational Facilities:

All meals will be served in the "Food Bowl" dining room at Atkins Hall, except the Conference Dinner on Wednesday 3 February, which will be held in the Convention Centre. You will receive a dining room pass on registration and a ticket to the Conference Dinner. The dining room pass must be produced at every meal. It may also be required as identification for use of all other campus facilities, which are at your disposal.

Morning and afternoon tea will be served each day, as indicated in the timetable. Coffee and tea-making facilities are also available in the Common Room of each residence. In addition, on arrival on Tuesday afternoon and for the poster sessions, drinks will be available from the Conference Bar.

The swimming pool is open on weekdays from 06:00 until 21:00, as are the adjacent gymnasium and squash courts. A wide range of facilities such as exercise bikes, table tennis and basketball are available in the gymnasium. Access to these facilities is covered by your registration fee.

Organising Committee Contact Numbers:

Anton Tadich	Chair	0411747351
Helen Brand	Treasurer	0430679007
Dominique Appadoo	Secretary	0488346319

Convention Centre Contact Numbers:

Events Office Phone	(02) 6933 4974
After-hours Emergencies, Accommodation and Security Office	(02) 6933 2288

Wireless Internet:

Is available on site. Login details will be provided upon registration.

WW 2016 : EXHIBITORS

scitek
total vacuum solutions

www.scitek.com.au
Address: 4/12 Chaplin Dr, Lane Cove NSW 2066
Phone:(02) 9420 0477
Contact: Tobias Schappeler
Email: tobias@scitek.com.au

www.ezzivacuum.com.au
Address: 1 Dalmore Dr, Scoresby VIC 3179
Phone: 1800 463 994
Contact: Dr Adil Adamjee
Email: adil@ezzivacuum.com.au

ezzi vision
Vacuum & Thin Film Technology
www.ezzivision.com.au

www.crystan.co.uk
Address: Crystran Ltd1 Broom Road Business Park, Poole, Dorset
Phone: +44 (0) 1202 307650
Contact: Alaina Wright
Email: sales@crystran.co.uk

CRYSTRAN
UV · VISIBLE · IR SPECIALIST OPTICS

WW 2016 : PARTICIPANTS

	Participant		Affiliation	Email
1	ALBOHANI	Shaymaa	Murdoch University	dwlaird@iinet.net.au
2	ALKHALDI	Huda	Australian National University	huda.alkhaldi@anu.edu.au
3	ALSUBAIE	Abdullah	UNSW	a.alsubaie@student.unsw.edu.au
4	AMIN	Mohamad	RMIT University	mohamadhassan.amin@rmit.edu.au
5	APPADOO	Dominique	Australian Synchrotron	dominique.appadoo@synchrotron.org.au
6	AUCKETT	Josie	ANSTO	josie.auckett@sydney.edu.au
7	AVARO	Jonathan	Southern Cross University	jonathan.avaro@gmail.com
8	BARMI	Maryam	Murdoch University	m.barmi@murdoch.edu.au
9	BARRIE	Nicola	CSIRO North Ryde	nicola.gbarrie@gmail.com
10	BISWAL	Avijit	Murdoch University	avijitimmt@gmail.com
11	BLADWELL	Samuel	UNSW	leumas.llewdalb@gmail.com
12	BLEASDALE	Colin	University of Wollongong	colinbleasdale@gmail.com
13	BOOTH	Norman	ANSTO	normanb@ansto.gov.au
14	BRAND	Helen	Australian Synchrotron	helen.brand@synchrotron.org.au
15	BULANADI	Jerikho	CSIRO North Ryde	jerikho.bulanadi@csiro.au
16	CADOGAN	Sean	UNSW Canberra	s.cadogan@adfa.edu.au
17	CAMPBELL	Stewart	UNSW Canberra	stewart.campbell@adfa.edu.au
18	CASHION	John	Monash University	john.cashion@monash.edu
19	CAZORLA	Claudio	UNSW	c.cazorla@unsw.edu.au
20	CHANG	Fenfen	UNSW	fenfen.chang@unsw.edu.au
21	CHEN	Jingyu	Deakin University	jingyuc@deakin.edu.au
22	CHEN	Zhigang	University of Queensland	z.chen1@uq.edu.au
23	CHENG	Xiquan	SKLUWRE	chengxiquan@126.com
24	COLLA	Jarrod	University of Wollongong	jac050@uowmail.edu.au
25	COLLOCOTT	Stephen	CSIRO Lindfield	stephen.collocott@gmail.com
26	CORTIE	Michael	University of Technology Sydney	michael.cortie@uts.edu.au
27	DANIELS	John	UNSW	j.daniels@unsw.edu.au
28	DENG	Guochu	ANSTO	guochu.deng@ansto.gov.au
29	ELEWA	Nancy	UNSW Canberra	nancy.elewa@student.adfa.edu.au
30	EVANS	Jacob	Macquarie University	jacob.evans@students.mq.edu.au
31	FARAJI HESAR	Nastaran	UNSW	nastaran.faraji@student.unsw.edu.au
32	FINLAYSON	Trevor	University of Melbourne	trevorf@unimelb.edu.au
33	FLETCHER	Glen	University of Technology Sydney	glenflet@gmail.com
34	GANN	Eliot	Australian Synchrotron / Monash Uni	eliot.gann@synchrotron.org.au
35	GLEASON	Scott	UNSW	s.gleason@student.unsw.edu.au
36	GRAHAM	Paul	UNSW	p.j.graham@unsw.edu.au
37	GUANGQING	Liu	UNSW	z3426175@student.unsw.edu.au
38	HINTERSTEIN	Manuel	UNSW	m.hinterstein@unsw.edu.au
39	HIRAI	Tadahiko	CSIRO Clayton	tadahiko.hirai@csiro.au
40	HOSSAIN	Mohammad	UNSW	hossainjahangir1988@gmail.com
41	HOXLEY	David	La Trobe University	d.hoxley@latrobe.edu.au
42	HU	Songbai	UNSW	z3409292@student.unsw.edu.au
43	HUTCHISON	Wayne	UNSW Canberra	w.hutchison@adfa.edu.au
44	IACOPI	Francesca	Griffith University	f.iacopi@griffith.edu.au
45	ILES	Gail	ANSTO	gail.iles@ansto.gov.au
46	JAHANGIR	Solmaz	UNSW	s.jahangir@unsw.edu.au
47	JAMES	Michael	Australian Synchrotron	michael.james@synchrotron.org.au
48	KANEKO	Taka	Ezzi Vision	taka@ezzivacuum.com.au
49	KANG	Hyung-Been	University of Auckland	hkan026@aucklanduni.ac.nz
50	KASHI	Sima	RMIT University	s3406251@student.rmit.edu.au
51	KHANSUR	Neamul	UNSW	n.khansur@unsw.edu.au
52	KHARKOV	Yaroslav	UNSW	Y.Kharkov@gmail.com
53	KONDYURINA	Irina	University of Sydney	i.kondyurina@gmail.com
54	KONG	Scarlet	UNSW	scarlet.kong@gmail.com
55	LAIRD	Damian	Murdoch University	d.laird@murdoch.edu.au
56	LI	Jingliang	Deakin University	jli@deakin.edu.au

57	LI	Junda	University of Adelaide	junda.li@adelaide.edu.au
58	LISS	Klaus-Dieter	ANSTO	kdl@ansto.gov.au
59	LIU	Xinzhi	China Institute of Atomic Energies	liuxinzhi1984.cn@163.com
60	MABON	John	University of Wollongong	jm965@uowmail.edu.au
61	MACLEOD	Jennifer	Queensland University of Technology	jennifer.macleod@qut.edu.au
62	MANTRI	Sukriti	UNSW	s.mantri@student.unsw.edu.au
63	MAQBOOL	Muhammad	La Trobe University	s.maqbool@latrobe.edu.au
64	MARLTON	Frederick	UNSW	f.marlton@unsw.edu.au
65	MARSHALL	Craig	Venid Vacuum	craig@venidvacuum.com
66	MAYNARD-CASELY	Helen	ANSTO	helenmc@ansto.gov.au
67	MCINTYRE	Garry	ANSTO	garry.mcintyre@ansto.gov.au
68	MINAKSHI	Manickam	Murdoch University	minakshi@murdoch.edu.au
69	MISEREV	Dmitry	UNSW	erazorheader@gmail.com
70	MOTTA	Nunzio	Queensland University of Technology	n.motta@qut.edu.au
71	MYERS	Damian	University of Melbourne	damianem@unimelb.edu.au
72	NAHID	Masrur	Monash University	masrur.morshed.nahid@monash.edu
73	NESA	Faizun	ANSTO	faizunn@ansto.gov.au
74	OBBARD	Edward	UNSW	e.obbard@unsw.edu.au
75	OITMAA	Jaan	UNSW	j.oitmaa@unsw.edu.au
76	POSAR	Jessue	University of Wollongong	jap972@uowmail.edu.au
77	QI	Dongchen	La Trobe University	d.qi@latrobe.edu.au
78	REN	Qingyong	UNSW Canberra	qingyong.ren@student.adfa.edu.au
79	RIDLEY	Chris	University of Edinburgh	c.ridley@ed.ac.uk
80	RULE	Kirrily	ANSTO	kirrily.rule@ansto.gov.au
81	SANDERSON	Matthew	University of Wollongong	monkey_man_192@yahoo.com.au
82	SANDO	Daniel	UNSW	daniel.sando@unsw.edu.au
83	SANTOS	Rafael	University of Wollongong	jrls996@uowmail.edu.au
84	SCAMMELL	Harley	UNSW	h.scammell@unsw.edu.au
85	SELLAR	Jeffrey	Monash University	jeff.sellar@monash.edu
86	SIMULA	Tapio	Monash University	tapio.simula@monash.edu
87	SONG	Kay	Australian National University	u5783927@anu.edu.au
88	SQUIRES	Andrew	University of Wollongong	ads786@uowmail.edu.au
89	STACEY	Alastair	University of Melbourne	astacey@unimelb.edu.au
90	STAMPFL	Anton	ANSTO	aps@ansto.gov.au
91	STEWART	Glen	UNSW Canberra	g.stewart@adfa.edu.au
92	SUI	Zhan	Shanghai Institute of Laser Plasma	zhansui_caep@163.com
93	SUSHKOV	Oleg	UNSW	sushkov@phys.unsw.edu.au
94	SUSILO	Resta	UNSW Canberra	resta.susilo@student.adfa.edu.au
95	TADICH	Anton	Australian Synchrotron	anton.tadich@synchrotron.org.au
96	TATE	Matthew	ANSTO	matthew.tate@durham.ac.uk
97	THORNTON	John	DST Group	john.thornton@dsto.defence.gov.au
98	TIMMERS	Heiko	UNSW Canberra	h.timmers@adfa.edu.au
99	TUNG	Patrick	UNSW	tungpatrick@gmail.com
100	ULRICH	Clemens	UNSW	c.ulrich@unsw.edu.au
101	VALANOOR	Nagarajan	UNSW	nagarajan@unsw.edu.au
102	VAN'T SCHIP	Ken	Scitek	ken@scitek.com.au
103	WAHAB	Hud	UNSW Canberra	hud.abdulwahab@student.adfa.edu.au
104	WANG	Chin-Wei	NSRRC	wang.chin.wei.gm@gmail.com
105	WANG	Lijun	UNSW	z3409899@student.unsw.edu.au
106	WHITE	Reyner	UNSW Canberra	reyner.white@student.adfa.edu.au
107	WILLIAMS	Jim	University of Western Australia	jim.williams@uwa.edu.au
108	WILSON	Daniel	University of Auckland	daniel.j.wilson@auckland.ac.nz
109	WOODALL	Chris	University of Edinburgh	C.Woodall@ed.ac.uk
110	WOOLLEY	Matt	UNSW Canberra	m.woolley@adfa.edu.au
111	WU	Chun-Ming	NSRRC	muconic@hotmail.com
112	YAP	Emily	UNSW	emily.yap@student.unsw.edu.au
113	YUAN	Xiaodong	China Academy of Engineering Physics	xdyuan@caep.cn
114	ZHANG	Hao	University of Wollongong	hz968@uowmail.edu.au
115	ZHOU	Dongyi	UNSW	z_denny@hotmail.com
116	ZONNEVELDT	Matthew	DST Group	matthew.zonneveldt@dsto.defence.gov.au

WW 2016 : OVERALL TIMETABLE

Tuesday 2nd February

16:00 – 18:00	Registration desk open
	Conference bar open
18:00 – 19:30	*Dinner*
19:00 -	Posters WP1- WP33 to be mounted
19:30 – 21:00	*Wine Tasting*

Wednesday 3rd February

07:30 – 08:45	*Breakfast*
08:45 – 09:00	Conference opening
09:00 – 10:30	Oral Session: WM1 – WM4
10:30 – 11:00	*Morning tea*
11:00 – 12:30	Oral Session: WN1 – WN5
12:30 – 14:00	*Lunch*
14:00 – 15:30	Oral Session: WA1 – WA4
15:30 – 16:00	Poster Slam
16:00 – 18:00	Poster Session: WP1 – WP33
	Afternoon Tea
	Conference bar open
18:00 -	Posters**:** TP1 – TP37 to be mounted
18:30 – 22:00	*Wagga 2016 Conference Dinner*

Thursday 4th February

07:30 – 08:45	*Breakfast*
08:45 – 10:30	Oral Session: TM1 – TM6
10:30 – 11:00	*Morning tea*
11:00 – 12:30	Oral Session: TN1 – TN5
12:30 – 14:00	*Lunch*
14:00 – 15:30	Oral Session: TA1 – TA5
15:30 – 16:00	Poster Slam
16:00 – 18:00	Poster Session: TP1 – TP37
	Afternoon Tea
	Conference bar open
18:00 – 19:30	*Dinner*
19:30 – 22:00	Trivia Quiz (Lindsay Davis Cup)

Friday 5th February

07:30 – 08:45	*Breakfast*
08:45 – 10:30	Oral Session: FM1 – FM6
10:30 – 11:00	*Morning tea*
11:00 – 12:15	Oral Session: FN1 – FN4
12:15 – 12:30	Awards and Closing
12:30 –	*Lunch*

WW 2016 : PROGRAM DETAILS

Tuesday 2nd February

16:00 –	Registration desk open
16:00 – 18:00	Welcome reception
18:00 – 19:30	Dinner
19:30 – 21:00	Wine Tasting

Wednesday 3rd February

08:45 – 09:00		**Opening :** ***Anton Tadich, Australian Synchrotron***
09:00 – 10:30	**WM**	**Chairperson :** ***Garry McIntyre, ANSTO***
09:00 – 09:30	WM1	The Australian Synchrotron in 2015 – Turning Bright Ideas into Brilliant Outcomes *Michael James, Australian Synchrotron* *INVITED*
09:30 – 09:45	WM2	Reactions of dihalogenated 3,4-ethylenedioxythiophenes on metal surfaces *Jennifer Macleod, Queensland University of Technology*
09:45 – 10:00	WM3	Developing cryogenic high-pressure techniques on the WISH neutron diffractometer. *Chris Ridley, University of Edinburgh*
10:00 – 10:30	WM4	Crystalline self-stratification in polymer thin films *Eliot Gann, Australian Synchrotron* *INVITED*
10:30 – 11:00		**Morning tea**
11:00 – 12:30	**WN**	**Chairperson :** ***Patrick Tung, UNSW***
11:00 – 11:30	WN1	Quantitative Femtosecond Charge Transfer Dynamics at Organic/Electrode Interfaces Studied by Core-Hole Clock Spectroscopy *Dongchen Qi, La Trobe University* *INVITED*
11:30 - 11:45	WN2	Unconventional Molecular Weight Dependence of Charge Transport in a High Mobility *n*-type Semiconducting Polymer *Masrur Nahid, Monash University*
11:45 - 12:00	WN3	An Approach to Degradation Mechanisms using Numerical Model Fitting in Thermally Activated Delayed Fluorescence (TADF) Organic Light Emitting Diodes (OLEDs) *Tadahiko Hirai, CSIRO*
12:00 – 12:15	WN4	In situ characterisation of calcium carbonate prenucleation clusters around the solubility limit using Small Angle X-ray Scattering. *Jonathan Avaro, Southern Cross University*

12:15 – 12:30	WN5	Supramolecular assembly of small molecular gelators mediated by additives *Jingliang Li, Deakin University*
12:30 – 14:00		**Lunch**
14:00 – 15:30	**WA**	**Chairperson : *Francesca Iacopi, Griffith University***
14:00 – 14:30	WA1	Engineering the Diamond Surface for Quantum Technologies *Alastair Stacey, University of Melbourne* *INVITED*
14:30 – 14:45	WA2	Vacancy-mediated electrical conductivity in lithium fluoride upon moderate heating *David Hoxley, La Trobe University*
14:45 – 15:00	WA3	One-step synthesis of n-type Mg_2Ge *Rafael Santos, University of Wollongong*
15:00 – 15:30	WA4	Towards Realisation of High-Performance Thermoelectrics for Energy Conversion *Zhigang Chen, University of Queensland* *INVITED*
15:30 – 16:00		**Poster Slam**
16:00 – 18:00		**Poster Session WP1 – WP33**
18:30 – 22:00		**Conference dinner** After Dinner Talk "Pluto: The Next Frontier for Condensed Matter " *Helen Brand, Australian Synchrotron*

Thursday 4th February

08:45 – 10:30	**TM**	**Chairperson : *Dongchen Qi, La Trobe University***
08:45 – 09:15	TM1	The endless possibilities of graphene on heteroepitaxial silicon carbide *Francesca Iacopi, Griffith University* *INVITED*
09:15 – 09:30	TM2	Capturing the transition from 3C SiC(111) to graphene by XPS and STM in Ultra High Vacuum *Nunzio Motta, Queensland University of Technology*
09:30 – 09:45	TM3	NEXAFS Anisotropy of Molecular Excitations Preceding the Carbon Continuum Edge in CVD Graphene on Copper *Hud Wahab, University of New South Wales, Canberra*
09:45 – 10:00	TM4	Quest for Zero Loss: The Materials selection problem in plasmonics *Michael Cortie, University of Technology Sydney*
10:00 – 10:15	TM5	Preparation and Characterization of Poly Lactide and Poly (Butylene Adipate-co-Terephthalate) Nanocomposites Reinforced with Graphene Nanoplatelet *Sima Kashi, Royal Melbourne Institute of Technology*

10:15 – 10:30	TM6	Development of Hydrophilic Materials for Nanofiltration Membrane Achieving Dual Resistance to Fouling and Chlorine *Xi Quan Chen, Harbin Institute of Technology, China*
10:30 – 11:00		**Morning tea**
11:00 – 12:30	**TN**	**Chairperson : *Gail Iles, ANSTO***
11:00 – 11:30	TN1	Atomic-scale understanding of CO_2 adsorption processes in metal-organic framework (MOF) materials using neutron scattering and ab initio calculations *Josie Auckett, ANSTO* *INVITED*
11:30 - 11:45	TN2	Crystallographic and magnetic structure study in $SrCoO_{3-x}$ by high resolution X-ray and neutron powder diffraction *Fenfen Chang, University of New South Wales, Kensington*
11:45 - 12:00	TN3	Hydrates under pressure – new insights from sulfuric acid hydrates *Helen Maynard - Casely, ANSTO*
12:00 – 12:15	TN4	Inelastic neutron scattering as a means for determining the magnetic exchange interactions in the frustrated quantum spin chain, Linarite. *Kirrily Rule, ANSTO*
12:15 – 12:30	TN5	An investigation of magnetic structure and spin reorientation in Cr and Mn doped rare earth ferrites using neutron powder diffraction *Xinzhi Liu, ANSTO*
12:30 – 14:00		**Lunch**
14:00 – 15:30	**TA**	**Chairperson : *Helen Maynard-Casely, ANSTO***
14:00 – 14:30	TA1	X-radiation in health and disease: Novel approaches to the study of disease processes and therapy *Damian Myers, University of Melbourne* *INVITED*
14:30 – 14:45	TA2	Investigation of Targeting Capabilities of Peptide-conjugated Endocannabinoid-based lipid Nanoassemblies in the Treatment of Arthritis *Nicola Barrie, CSIRO*
14:45 – 15:00	TA3	Sodium for securing future renewable energy supply *Manickam Minakshi, Murdoch University*
15:00 – 15:15	TA4	Bi(III)-containing lanthanum germanium apatite-type oxide ion conductors and their structure-property relationships *Matthew Tate, ANSTO*
15:15 – 15:30	TA5	Low temperature effect of lithium diffusion in 18650-type MNC battery *Chun-ming Wu, National Synchrotron Radiation Research Centre, Taiwan*
15:30 – 16:00		**Poster Slam**
16:00 – 18:00		**Poster Session TP1 – TP37**

18:00 – 19:30		**Dinner**
19:30 – 22:00		**Trivia Night**

Friday 5th February

08:45 – 10:30	**FM**	**Chairperson : *Glen Stewart, UNSW Canberra***
08:45 – 09:15	FM1	A Morphotropic Phase Boundary in Samarium-modified Bismuth Ferrite Thin Films *Nagarajan Valanoor, University of New South Wales* *INVITED*
09:15 – 09:30	FM2	Reversible electrochromism, elasto-optic and thermo-optic effects in $BiFeO_3$ films *Daniel Sando, University of New South Wales, Kensington*
09:30 – 09:45	FM3	Effects of ^{18}O isotope substitution in multiferroic $RMnO_3$ (R=Tb, Dy) *Paul Graham, University of New South Wales, Kensington*
09:45 – 10:00	FM4	Growth and Properties of Strain-tuned $SrCoO_x$ ($2.5 \leq x < 3$) Thin Films *Hu Songbai, University of New South Wales, Kensington*
10:00 – 10:15	FM5	Experimental observations of grain-scale property coupling in electroceramics *John Daniels, University of New South Wales, Kensington*
10:15 – 10:30	FM6	Gamma irradiation effect on optical and laser damage performance of KDP crystals *Xiaodong Yuan, China Academy of Engineering Physics, China*
10:30 – 11:00		**Morning tea**
11:00 – 12:30	**FN**	**Chairperson : *Claudio Cazorla, UNSW***
11:00 – 11:30	FN1	Two-dimensional Coulomb gas at negative temperature *Tapio Simula, Monash University* *INVITED*
11:30 - 11:45	FN2	Multimode photon-assisted tunnelling in superconducting quantum circuits *Matthew Woolley, University of New South Wales, Canberra*
11:45 - 12:00	FN3	Focusing of electrons and holes in semiconductors: from semi-classical dynamics to spintronics *Samuel Bladwell, University of New South Wales, Kensington*
12:00 – 12:15	FN4	Amplitude of charge density wave in cuprates *Yaroslav Kharkov, University of New South Wales, Kensington*
12:15 – 12:30		**Awards and closing : *Anton Tadich, Australian Synchrotron***
12:30 – 14:00		**Lunch**

WW2016 : POSTER SESSIONS

Wednesday 3rd February : WP1 - WP34

WP1 Porosity in Ge and $Si_{1-x}Ge_x$ Alloys Induced by Ion Implantation
H. Alkhaldi, F. Kremer, T. Bierschenk, J.L. Hansen, A. Nylandsted-Larsen, J.S. Williams and M.C. Ridgway

WP2 Synthesis and characterisation of $CoMoO_4$ nanospheres with improved supercapacitive performance
M. Barmi and M. Minakshi

WP3 Electrolytic manganese dioxide from secondary sources for energy storage
A. Biswal, M. Minakshi and B. Tripathy

WP4 Do porosity templates improve the performance of supercapacitor electrode materials?
S. Albohani, D. Laird and M. Minakshi

WP5 Multigelator organogels-mixture of gelators assembled by different driving forces
J. Chen and J. Li

WP6 In situ characterisation of calcium carbonate prenucleation clusters around the solubility limit using Small Angle X-ray Scattering technique.
J. Avaro and A. Rose

WP7 Terahertz Characterisation of 3D Printed Plastics
J. Colla, A. Squires and R. Lewis

WP8 THz Spectroscopy of Artists' Pigments, Binders and Canvas
A. Squires, M. Kelly and R. Lewis

WP9 Steels and intermetallics under extreme conditions
K-D. Liss, A. Shiro, R. Dippenaar, K. Akita, K. Funakoshi, M. Reid, H. Suzuki, T. Shobu, Y. Higo, H. Saitoh, S. Zhang and Y. Tomota

WP10 Improved Micro-CT of SiC/SiC Ceramic Matrix Composites
J. Thornton, M. Zonneveldt, B. Arhatari, J. A. Kimpton, M. Sesso, S. Y. Kim and C. Hall

WP11 Mechanical meta-materials: beyond conventional property
L. Wang and J. Daniels

WP12 Curing of large size construction for space exploitation
A. Kondyurin

WP13 Polyurethane medical implants improved by plasma immersion ion implantation
I. Kondyurina, B. Bao, A. Kondyurin and M. Bilek

WP14 In-situ diffuse scattering experiment on stress-induced ferroelastic transformation in Ti-15Nb-2.5Zr-4Sn
E. Obbard, R. Burkovsky, H. Wang and Y. Hao

WP15 Prodrug Amphiphile Nanoparticles of Gemcitabine and 5- Fluorouracil
J. Bulanadi, M. Moghaddam, A. Xue, S. Julovi, S. Bal, X. Gong and R. Smith

WP16 Spin-polarized single and double electron spectroscopies
J. Williams and S. Samarin

WP17 Structures of Silane SAMs on Oxide Surfaces
A. Magerl, H-G. Steinruck, M. Deutsch and B. Ocko

WP18 Biocompatible magnesium based ultrastable metallic glass (SMG) thin films
S. Gleason, K. Laws, J. Jiang and M. Ferry

WP19 Epitaxial Growth of Spinel Iron Vanadate Thin Films on Perovskite Substrate
D. Zhou, Y. Zhou, N. Valanoor, Q. He and Y-H. Chu

WP20 Fingering instability in solid state dewetting of single crystal Ni films
S. Jahangir, N. Valanoor, C. Thompson, G.H Kim

WP21 Modelling TiO_2 supported Au cluster photocatalyst using DFT and SCC-DFTB approaches
J. Li, G. Metha and S. Irle

WP22 Photoconductivity of nanoscale grain boundaries in two dimensional ZnO platelets
N. Faraji Ouch Hesar

WP23 A Novel method for the preparation of a monolithic alumina catalyst support
M. H. Amin, S. Bhargava, J. Patel and M. Mazur

WP24 Refractive index of graphite and graphene at wavelengths spanning the carbon K edge
H. Wahab, C. Jansing, H. C. Mertins, S-H Choi and H. Timmers

WP25 Terahertz Spectroscopic Characterizations for Graphite Nanofibers and Graphite
H. Zhang, J. Horvat and R. Lewis

WP26 Optical bistability due to nonlinear surface plasmon polaritons in graphene
M. Sanderson, Y. Sin Ang and C. Zhang

WP27 Quantitative 3D Strain Mapping in Nanodiamonds using Bragg Coherent Diffractive Imaging (BCDI)
M. S. Maqbool, D. Hoxley, N. Phillips, A. Stacey, J. Clark, B. Chen, D. Langley, R. Harder, E. Balaur and B. Abbey

WP28 The role of dielectric function for the control of coupled dipole resonances in dimers of dissimilar metallic nanorods
G. Fletcher, M. Cortie and M. Arnold

WP29 Helium ion implantation dose dependent microstructure and laser damage of sapphire
Z. Sui

WP30 Theory of controlling avalanche process of carrier in short pulse laser irradiated dielectrics
X. Yuan, H. Deng and X. Xu

WP31 Cooperative Behaviour of Physical Systems
T. Finlayson and J. Lashley

WP32 EPR Study of a 'Capsule' Brewed Coffee and its Decaffeinated Version
G. Troup and S. Drew

WP33 An EPR Study of Tawny Ports, and Coffee Favoured Liqueurs
G. Troup and S. Drew

Thursday 4th February : TP1 – TP37

TP1 First spectrum measured on EMU, the cold-neutron backscattering spectrometer at the Bragg Institute, ANSTO
N. De Souza, A. Klapproth, G. Iles

TP2 Development of high-pressure single-crystal neutron diffraction on the Laue diffractometer, KOALA, at OPAL
J. Binns, G. McIntrye, K. Kamenev, S. Moggach and S. Parsons

TP3 Advanced Sample Environment Support for Neutron Instruments at the Bragg Institute, ANSTO
P. Imperia, N. Booth, G. Davidson, S. Lee, T. D'Adam and A. Manning

TP4 Vibrational studies using neutrons
A. Stampfl

TP5 Development of a compact X-ray source
E.W.J. Yap, R. Preston, J. Tickner and J. Daniels

TP6 Investigations of the Structural and Magnetic Phase Behaviour of $MnSb_{2-x}Ta_xO_6$ Solid Solutions
H-B. Kang, F. Suzuki and T. Soehnel and

TP7 Low Pressure Synchrotron X-ray Powder Diffraction of $Cu_{5-x}M_xSbO_6$ (M = Cr, Mn, W)
D. J. Wilson, T. Soehnel, K. Smith, H. E. A. Brand, C. Ulrich, P. Graham, F. Chang, M. Allison and N. H. Vyborna

TP8 Neutron diffraction study of double tungstates $Li_2M^{II}(WO_4)_2$ (M=Co and Ni)
C-W. Wang, S. Karna, F. C. Chou and R. Sankar

TP9 Low-energy crystal-field excitations observed using inelastic Neutron Scattering
G. Iles, G. Stewart, R. Mole, W. Hutchison and S. Cadogan

TP10 Dynamical Mechanism of Phase Transitions in A-site Ferroelectric Relaxor $(Na_{0.5}Bi_{0.5})TiO_3$
G. Deng, S. Danilkin, H. Zhang, P. Imperia, X. Li, X. Zhao and H. Luo

TP11 Kaolinite and halloysite – does octahedral Fe^{2+} introduce the extra water into halloysite?
J. Cashion, W. Gates, J.M. Cadogan, J. Churchman and L. Aldridge

TP12 An ^{57}Fe Mössbauer Study of the Ordinary Chondrite meteorite Lynch-001
N. Elewa and S. Cadogan

TP13 Spin transitions in cementite
S. Clark

TP14 Non-equilibrium field theory and decay widths: a new golden rule
H. Scammell and O. Sushkov

TP15 Incommensurate magnetic order in $PrNiAl_4$
R. White, W. Hutchison, M. Avdeev and K. Nishimura

TP16 Skyrmions and Hopfions in frustrated ferromagnets
Y. Kharkov, M. Mostovoy and O. Sushkov

TP17 The magnetic properties and magnetocaloric effect in $(Mn_{1-x}Ni_x)CoGe$
Q. Ren, W. Hutchison, J. Wang, A. Studer and S. Campbell

TP18 Azimuthal dependence of planar orbits in the crossed fields diamagnetic Kepler problem in silicon
C. Bleasdale and R. Lewis

TP19 Temperature and magnetic field dependent magnetization of nanoparticulate $ZnFe_2O_4$ produced by mechanochemical synthesis
F. Nesa, X. Wang, J. Wang, S. Kennedy, S. Campbell and M. Hofmann

TP20 Pressure induced, reversible, fourfold enhancement of the magnetic ordering temperature in transition metal monomers
C. Woodall, J. Martinez Lillio, A. Prescimone, M. Misek, J. Cano, J. Faus, S. Parsons, K. Kamenev and E. Brechin

TP21 Physical, thermal and ^{57}Fe Mössbauer studies of $Y_2Fe_2Si_2C$
R. Susilo, S. Cadogan, C-H. Hsu, H. lin, W. Hutchison and S. Campbell

TP22 Mechanism of enhancement of the electron g-factor in quantum point contacts
G. Vionnet and O. Sushkov

TP23 Towards understanding the magnetic structure of DyN, a ferromagnetic semiconductor
J. Evans, G. Stewart, S. Cadogan, W. Hutchison, E. Mitchell and J. Downes

TP24 G-factors of hole bound states in spherically symmetric potentials in cubic semiconductors
D. Miserev and O. Sushkov

TP25 A ^{161}Dy-Mössbauer spectroscopy investigation of $DyCrO_4$
G. Stewart, S. Cadogan, W. Hutchison and D. Ryan

TP26 Spin drift in Rashba systems with tilted magnetic fields
S. Bladwell and O. Sushkov

TP27 Epitaxial (001) $BiFeO_3$ thin-films with excellent ferroelectric properties by chemical solution deposition-The role of gelation
Q. Zhang and N. Valanoor

TP28 Complex Magnetic Structure in strained nanoscale bismuth ferrite thin films
C. Ulrich, J. Bertinshaw, R. Maran, S. Callori, V. Ramesh, J. Cheung, S. Danilkin, S. Hu, J. Seidel and N. Valanoor

TP29 Nanoscale Ferroelectric domain structure of bismuth ferrite $BiFeO_3$ under different strains
A. Alsubaie, P. Sharma and J. Seidel

TP30 Generalised requirements for ferroelectric domain sharing over grain boundaries
S. Mantri and J. Daniels

TP31 Rational design of multiferroic superlattices
C. Cazorla

TP32 Positive effect of an internal depolarization field in ultrathin epitaxial ferroelectric films
G. Liu and N. Valanoor

TP33 Determining fundamental properties from diffraction: electric field induced strain and piezoelectric coefficient
M. Hinterstein, A. Studer and M. Hoffman

TP34 Diffuse X-ray Scattering: Probing the Nano-scale Disorder in the Lead-Free Piezoelectric $Na_{0.5}Bi_{0.5}TiO_3$
P. Tung, M. Major, J. Hudspeth and J. Daniels

TP35 Combinatorial synthesis of piezoelectric materials using an inkjet printer
F. Marlton, J. Daniels and O. Standard

TP36 Stress and electric-field dependence of the induced phase symmetry in BNT-xBT
M. J. Hossain, Z. Wang, N. Khansur, P. Tung and J. Daniels

TP37 Contrasting strain mechanisms in lead-free piezoelectric ceramics
N. H. Khansur and J. Daniels

2016

ABSTRACTS FOR ORAL SESSIONS

WM1

The Australian Synchrotron in 2015 – Turning Bright Ideas into Brilliant Outcomes

M. James

Australian Synchrotron, 800 Blackburn Rd, Clayton VIC 3168, Australia

When VIP visitors come to the Australian Synchrotron (Commonwealth Ministers & their minders, Directors of national and international laboratories & research institutes; VCs & DVCRs; my Mother-in-Law…) we like to play a little game to try and impress them and to demonstrate the impact of our efforts. It goes a little like this:

Mike: "*Pick a topic, any topic, and I will tell you how we make a difference to that, by research carried-out at the Australian Synchrotron*" (It helps a little if they have an interest in a specific disease or medical condition, but this is not essential).
VIP: "*Well…, How about…*"

And so on...

A strange way to try and achieve the much-needed financial security that our facility so needs I hear you say; and yes, when we face some of our more imaginative foes, the link to their topic can be more than a little tenuous. (Ok sometimes, we crash and burn). However, for the most part, with about 1000 experiments per year to choose from, we walk away with our heads held high. My talk will give a brief overview of the Australian Synchrotron, as well as its status and future as one of the most substantial pieces of research infrastructure in the country. I will present some recent research highlights, particularly pertaining to condensed matter research, and challenge you to challenge us to see how the Australian Synchrotron can make a difference to your research.

Pick a topic, any topic…

WM2

Reactions of dihalogenated 3,4-ethylenedioxythiophenes on metal surfaces

J. Macleod[1], I. Di Bernardo[2], M. Abyazisani[1], J. Lipton-Duffin[1], N. Motta[1] and P. Hines[1]

[1] Queensland University of Technology, Brisbane, Queensland 4000, Australia

[2] Sapienza University of Rome, Rome 00185, Italy

Conducting polymers are a key component of modern technologies: they are used in batteries and in displays, and they have a promising future in solar conversion and emerging technologies like flexible electronics. The polymer formed from 3,4-ethylenedioxythiophene, known as poly-3,4-ethylenedioxythiophene or PEDOT, is used in a variety of applications, primarily because of its low bandgap, transparency and stability. PEDOT is typically solution processed, and although this technique is simple, it offers limited control over the structure of the polymer. Surface-confined polymerization is emerging as an important technique for the structurally-controlled synthesis of materials like PEDOT [1,2]. In order to explore possibilities for the surface-confined synthesis of structurally well-defined PEDOT, we have studied the reactions of dibromoEDOT and dichloroEDOT on Cu(111), Ag(111) and Au(111). The function of these surfaces is twofold: they provide an ordered template for epitaxial growth, and they act as catalyst for the Ullmann dehalogenation of the precursor molecules. X-ray photoelectron spectroscopy (XPS) measurements were performed at the SXR beamline of the Australian Synchrotron to benchmark the reaction temperatures for the successive steps in the on-surface reaction for both molecules on all three surfaces. Angle-resolved near-edge x-ray absorption fine structure (NEXAFS) spectra complement the information provided by XPS, and provide insight into the molecular adsorption geometry throughout the reaction pathway. Together, these data elucidate the benefits and drawbacks of different metal surfaces and different halogens in the context of the surface-confined synthesis of ordered PEDOT.

[1] M. El Garah, J.M. MacLeod and F Rosei, *Surf. Sci*. **613**, 6-14 (2013)

[2] J.A. Lipton-Duffin et al., *Proc. Nat. Acad. Sci*. **107** (25), 11200-11204 (2010)

WM3

Developing cryogenic high-pressure techniques on the WISH neutron diffractometer.

C. J. Ridley [a,b*], O.I. Kirichek [b], P. Manuel [b], D. Khalyavin [b] and K. Kamenev [a]

[a]*Centre for Science at Extreme Conditions, The University of Edinburgh, Edinburgh, UK*
[b]*ISIS, STFC, Rutherford Appleton Laboratory, Chilton, Didcot, UK*

Neutron diffraction is a powerful tool for investigating a variety of material characteristics such as structural and magnetic phenomena. Controlling temperature, pressure, and applied magnetic field allows transitions between phases to be studied very precisely. Neutron facilities such as the ILL and ISIS have a broad range of cryogenic equipment capable of reaching ~mK temperatures and magnets capable of generating continuous fields up to 15 T. High pressure instrumentation for neutron diffraction is currently limited by the need for large sample volumes, requiring large devices such as Paris-Edinburgh cells (P ~15 GPa), [1] which are not optimised for use down to the lowest temperatures (<70 K), or for use with applied fields due to the dimensions of the cell.

A compact opposed gem anvil system has been developed for use on the WISH diffractometer at the ISIS neutron facility. The cell is suitable for use in 100 mm cryostats/CCRs, with the ability to control, and continuously monitor, the applied pressure at base operating temperatures using a helium driven actuator and an in-situ ruby spectrometer. [2] Opposed gem anvil systems offer unrivalled pressure range, but at the cost of reduced sample volume. To improve the signal-to-noise, a novel 3D laser sintered collimator has been constructed, allowing data from 1mm^3 of sample to be refined in 1hr data sets. The cell operates with diamond and sapphire anvils; data from each will be presented, alongside data characterising the behaviour of the cell at base temperatures.

[1] JM. Besson, G. Weill, G. Hamel, RJ. Nelmes, JS. Loveday, S. Hull. *Phys. Rev. B.* **45**, 2613 (1992)
[2] MK. Jacobsen, CJ. Ridley et al. *Rev. Sci. Instrum*. **85**, 043904 (2014)

*c.ridley@ed.ac.uk

WM4

Crystalline self-stratification in polymer thin films

E. Gann and C. McNeill

Department of Materials Science and Engineering, Monash University, Victoria 3800, Australia

The orientation of molecules within thin films is of critical importance to the emerging field of organic electronics. Particularly in the case of solution processable polymers and small molecules, where alkyl side chains, included for solubility, impede conduction along that molecular direction, understanding and controlling the molecular orientation both at surfaces and in the bulk of thin films is increasingly important to further increase electronic performance. Grazing Incidence Wide Angle X-ray Scattering has been widely used to look at the orientation of crystallites within films, but a capability which has not been widely used is its potential to characterize the depth within films at which different kinds of molecular stacking occur. Using very fine control over the angle of incidence of the X-ray beam, we observe a distinct segregation of edge-on crystallinity in a film of the polymer PNDI-SVS which otherwise stacks in a highly face-on orientation. Using simulations of the X-ray Electric Field Intensity within the film, the angular variation of scattering intensity can be matched, resulting in the conclusion that the surface region extends 9 nm into the 72 nm film.

During the spin-coating deposition process, a face-on orientation is initially observed, likely the result of preaggregation in solution in combination with a relatively fast-drying solvent. The stratified morphology is produced by annealing the film for a brief time, while upon further annealing, the bulk of the film eventually reorients to become edge-on, suggesting that the stratification is a non-equilibrium, kinetically-trapped state. With brief annealing, only the surface region of the film has time to reorient to the ultimately lower energy edge-on orientation. The time and temperature of this reorganization can reveal the difference in energetics at different depths within the film, illustrating how grazing incidence scattering can open up the possibility of examining thin films in novel and important ways.

WN1

Quantitative Femtosecond Charge Transfer Dynamics at Organic/Electrode Interfaces Studied by Core-Hole Clock Spectroscopy

D. Qi

Department of Chemistry and Physics, La Trobe University, Victoria 3086, Australia

Organic semiconductors have important applications in organic electronics and other novel hybrid devices. In these devices, the transport of charge carriers across the interfaces between organic molecules and electrodes plays an important role in determining the device performance. Charge transfer dynamics at these interfaces usually occurs at the several femtoseconds timescale which presents tremendous challenges to conventional pump-probe based time-resolved techniques. In this talk, I will introduce our recent work in the application of synchrotron-based core-hole clock (CHC) spectroscopy on the quantitative characterisation of charge transfer dynamics in several model organic/electrode systems. The CHC technique allows us to quantify the interfacial charge transfer times with element and site/orbital specificity. Combined with other soft x-ray spectroscopies, it enables us to identify a few critical factors affecting the charge transfer dynamics at organic/electrode interfaces.

Reference

L. Cao, X.-Y. Gao, A. T. S. Wee, and D.-C. Qi, *Adv. Mater.* **26**, 7880 (2014)

WN2

Unconventional Molecular Weight Dependence of Charge Transport in a High Mobility n-type Semiconducting Polymer

M. Nahid, E. Gann and C. McNeill

Department of Materials Science and Engineering, Monash University, Victoria 3800, Australia

Semiconducting polymers are of interest for a range of applications including organic light-emitting diodes (OLEDs), polymer solar cells and flexible electronics. When used as the active layer in solution-processed organic field-effect transistors (OFETs) one usually finds that charge carrier mobility increases with increasing molecular weight, due to the ability of longer chains to bridge regions of local order. Here an unconventional molecular weight dependence of charge transport is reported in n-channel OFETs based on the semiconducting polymer poly{[N , N 0 -bis(2-octyldodecyl)- naphthalene-1,4,5,8-bis(dicarboximide)-2,6-diyl]-alt-5,50 -(2,20 -bithiophene)}, P(NDI2OD-T2). Five different molecular weights have been studied (10 kDa, 17 kDa, 30 kDa, 35 kDa and 41 kDa) with the charge carrier mobility in top gate bottom contact (TGBC) OFETs found to systematically increase with decreasing molecular weight. To understand the origin of this effect, the aggregating behaviour of polymer chains in solution has been studied, as well as the thin-film microstructure. From optical absorption measurements, which are sensitive to the polymer chain conformation, it is found that low molecular weight chains have an open coil conformation while higher molecular weight chains adopt a collapsed, or aggregated conformation. Analysis of Atomic Force Microscopy (AFM) measurements suggest a higher degree of polymer chain alignment in low molecular weight samples. Near Edge X-Ray Absorption Fine Structure (NEXAFS) spectroscopy measurements have also been performed that show a similar molecular orientation (backbone tilt) at the surface for all the molecular weight samples. Taken together, these results indicate that upon solution processing, the lower molecular weight samples are able to form more chain-extended thin-film morphologies that promote charge transport than the higher molecular weight samples that self-aggregate in solution produces less favourable morphologies.

WN3

An Approach to Degradation Mechanisms using Numerical Model Fitting in Thermally Activated Delayed Fluorescence (TADF) Organic Light Emitting Diodes (OLEDs)

T. Hirai[1], T. Shibata[2], K. Ueno[1], M. Bown[1] and C. Adachi[3]

[1] *Manufacturing, CSIRO, Clayton, Victoria 3168, Australia*

[2] *Japan Display Inc, Minato, Tokyo, Japan*

[3] *Kyushu University, Fukuoka, Fukuoka Prefecture, Japan*

We approach degradation mechanisms in green thermally activated delayed fluorescence (TADF) organic light emitting diodes (OLEDs) by a numerical model fitting method included a Schottky numerical model to evaluate barrier height of carrier injection at interfaces. Using temperature dependent current-voltage (I-V) behaviour of hole only (HOD) device ; glass / ITO (100nm) / HAT-CN (10) / Tris-PCz (70nm) / Al (100nm) , electron only device (EOD) ; glass / ITO (100nm) / Bpy-TP2 (40nm) /LiF (0.8nm) / Al (100nm) and our model, we have obtained values for the Richardson factor, and the barrier height. From the temperature dependent I-V characteristics of the HOD and our model fitting, we have estimated barrier height $\phi_B(H)$ = 0.370eV, Richardson factor $\boldsymbol{A}^*(H)=1.0\times10^{-2}$ $A/cm^2/K^2$ and threshold voltage $V_{TH}(H)$ = 1.5V for the injection of hole carriers. Notably, the $\boldsymbol{A}^*$ value of the ITO/HAT-CN/Tris-PCz interface is much smaller than that of a metal/Si interface. This suggests that $\boldsymbol{A}^*$ is strongly dependent on the combination of materials and its interface condition.

Likewise, we also obtained the device parameters for the electron injection interface from the temperature dependent I-V characteristics of the EOD. From the measurement data and our model fitting, we have estimated $\phi_B(E)$ = 0.285 eV, $A(E) = 1.0\times10^{-3}$ $A/cm^2/K^2$ and $V_{TH}(E)$ = 2.2 V. Therefore, we tried stress tests using 1 hour 500mA/cm^2 current stress for HOD and EOD. The parameter determined for the HOD show no significant change. In contrast to this the EOD parameters show significant change after current stressing; $\phi_B(E)$ = 0.285 → 0.345 eV, $\boldsymbol{A}^*(E) = 1.0\times10^{-3}$ → 1.0×10^{-2} $A/cm^2/K^2$ and $V_{TH}(E)$ = 2.2 → 2.5 V. It is apparent that the interface of electron injection side has undergone significant degradation during the current stressing as revealed by the change in the device parameters.

Hence, we have obtained the delayed response of luminescence under pulsed operation of delta-doped green TADF OLEDs ; glass / ITO (100nm) / HAT-CN (10) / Tris-PCz (30nm) / mCP:4CZIPN (15%,30nm) / T2T (10nm) / Bpy-TP2 (40nm) / LiF (0.8nm) / Al (100nm) after current stress. In order

to approach degradation mechanisms, we fabricated a half doped structure in the emission layer. The results of pulsed operation indicate the quick response of luminescence has been generated in a very thin region contacted to the electron injection side in the emission layer. On the other hand, STEM cross sectional images of the TADF green OLEDs show a different contrast at interface region of Bpy-TP2 as electron injection layer between before and after the current stress. The results are consistent with changes of parameters in the EOD after current stress. From our experimental and model fitting results, we describe a degradation model dominated at electron injection interface in TADF green OLEDs.

WN4

In situ characterisation of calcium carbonate prenucleation clusters around the solubility limit using Small Angle X-ray Scattering technique

J. Avaro and A. Rose

Southern Cross University, East Lismore, NSW 2480 Australia

In the classical nucleation theory, a mineral will form in supersaturated solution by the random collision of dissolved ions to yield transient clusters through a dynamic and reversible process. Random addition of dissolved ions eventually causes a "critical cluster" size to be reached, at which point the process becomes essentially irreversible and the first mineral crystal is considered to have formed. Nevertheless, it has been proven that calcium carbonates don't follow this theory. Instead, its abiotic precipitation proceeds by a novel mechanism involving formation of nanoparticle, between 1 and 250 nm in size and thermodynamically stable in under and supersaturated solution ($\Omega < 1$ and $\Omega > 1$). However, in situ studies aiming to characterise these nanoparticles have always been undertaken in highly oversaturated and simplistic conditions. Moreover, the exact role as well as their physical and chemical characteristics remains poorly understood. Here we've combined SAXS technics with an ultra-fast mixing device in order to acquire high quality data at extremely short reaction times (estimated < 1ms) representing the very early stage of calcium carbonate nanoparticles formation. With these technics we've been able to characterise the size and shape of these nanoparticles around the solubility limit ($\Omega < 1$ and $\Omega > 1$), varying pH.

WN5

Supramolecular assembly of small molecular gelators mediated by additives

J. Li

Deakin University, Geelong, Victoria 3220, Australia

Small molecule gel (SMG) is a class of supramolecular material that is formed by low molecular weight gelators in solvents. SMGs have important application in many fields such as foods, cosmetics and pharmaceutics. The properties of these materials depend on their multi-level (hierarchical) structure and affect their applications. Significant efforts in the past years have been devoted to developing novel gelators in order to achieve gels with desirable structure and properties. However, the molecular assembly property of a gelator is heavily dependent on solvent properties. Therefore, molecular design is not an efficient approach. Recently, it has been proven that the structure formation in SMGs is a nucleation and growth process. On the basis of this mechanism, the hierarchical structure and hence the properties of the gels can be conveniently manipulated by controlling the thermodynamics and kinetics of nucleation. In this presentation, different approaches, in particular, molecular additive-assisted approach, that have developed to control the hierarchical structures of SMGs will be covered.

WA1

Engineering the Diamond Surface for Quantum Technologies

A. Stacey[1], L. Hollenberg[2], J.P Tetienne[1], L. Hall[3] and D. Simpson[3]

[1] *Centre of Excellence for Quantum Computation and Communication Technology, University of Melbourne, Victoria 3010, Australia*

[2] *Thomas Baker Chair, School of Physics, University of Melbourne, Victoria 3010, Australia*

[3] *School of Physics, University of Melbourne, Victoria 3010, Australia*

Quantum technologies promise exciting and transformative futures in many areas of human endeavour. An example is the field of bio-sensing, where quantum probes are already being used to answer fundamental questions about living cells. In these applications diamond often takes centre stage, as a material which simultaneously exhibits both bio-friendly and quantum-friendly properties. This presentation will review efforts to exploit diamond for quantum bio-sensing applications, encompassing practical cellular measurements to the development of fundamentally new sensing techniques. In particular, I will address the biggest materials challenge we currently face, which is the presence of uncontrolled defects at the solid state surface, and detail the use of surface science techniques, based at the Australian Synchrotron, to understand and re-engineer this important quantum/life interface.

WA2

Vacancy-mediated electrical conductivity in lithium fluoride upon moderate heating

D. Hoxley[1], G. Van Riessen[1], D. Owen[2], K. Legge[3] , and M. Maketha[3] and N. Tran[3]

[1] *La Trobe University, Victoria 3086, Australia*

[2] *Ampacet Australia Pty Ltd, Mitcham, Victoria 3132, Australia*

[3] *La Trobe Institute of Molecular Science, La Trobe University, Victoria 3086, Australia*

The challenge posed by charge accumulation at the interfaces of low dimensional electronic devices has resulted in a wide range of novel architectures as well as potential applications in organic electronics such as organic photovoltaics. These devices include, among others, organic light-emitting diodes and organic thin-film transistors. Within such devices, the use of fluoride (LiF) as an inter-facial layer reduces the potential barrier at the interface which facilitates the efficient collection of photo-generated charge with minimal energy [1]. This manifests itself in minimising the band bending at interfaces of such devices and is attributed to the low work function of LiF, which reduces the effective work function at the interface [2] and in turn leads to efficient charge extraction/injection in the organic layer [3]. Thus the electrical properties of LiF are a subject of interest. While most alkali halides have been extensively investigated, LiF is an exception which, to date, has not been given enough attention. We show that lithium fluoride conducts electricity on heating to temperatures well below its melting point. By examining the variation in conductivity with heating along (111) plane, we show that the conductivity is due to a mechanism of ion hopping and vacancy migration through the host lattice sites. By fitting the data into the Nernst-Einstein relation the two linear regions were obtained from which upon extrapolation the activation energies for ion hopping were found to be 0.67 eV and 0.35 eV for high-temperature (region I) and low-temperature (region II) regions respectively as shown in the figure below. Conductivity of LiF has implications for its use as an inter-facial layer in photovoltaic device design and potential use in bio-sensing devices due to its cell tissue effective mass equivalence.

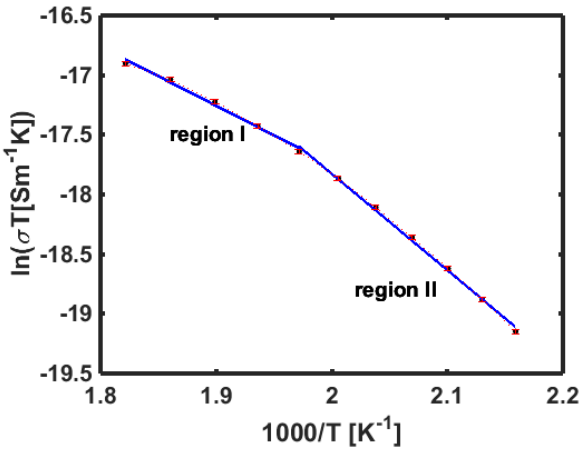

[1] F. Zhu, B. Low, K. Zhang, S. Chua, *Applied Physics Letters* **79**, 1205-1207 (2001)

[2] R. Schlaf, B. Parkinson, P. Lee, K. Nebesny, G. Jabbour, B. Kippelen, N. Peyghambarian, N. Armstrong, *Journal of Applied Physics* **84**, 6729-6736 (1998)

[3] K. G. Lim, M. R. Choi, J. H. Kim, D. H. Kim, G. H. Jung, Y. Park, J. L. Lee, T. W. Lee, *ChemSusChem* **7**, 1125-1132 (2014)

WA3

One-step synthesis of *n*-type Mg_2Ge

R. Santos and S. Aminorroaya-Yamini

Australian Institute of Innovative Materials (AIIM), University of Wollongong Wollongong, NSW 2522, Australia

Magnesium-based thermoelectric materials (Mg_2X, X = Si, Sn, Ge) have received considerable attention due to their availability, low toxicity and reasonably good thermoelectric performance. However, the synthesis of these materials with high purity is challenging due to the volatility and high vapor pressure of magnesium. In the current study, single phase *n*-type Mg_2Ge has been fabricated through the one-step reaction of elemental Ge and MgH_2 using spark plasma sintering (SPS). This technique was used previously on the synthesis of high purity nanocrystalline Mg_2Si as an alternative to melting procedures, believed to reduce the formation of oxides due to the liberation of hydrogen. X-ray diffraction (XRD) analysis of fabricated bulk samples shows single phase Mg_2Ge. Scanning electron microscopy (SEM) analysis equipped with energy-dispersive X-ray spectroscopy (EDS) indicates that the final composition has Mg deficiency, even when excess Mg of the stoichiometry is added to the starting materials. Previous reports highlighted the effect of non-stoichiometric amounts of Mg on the thermoelectric properties of Mg-based alloys, especially in *n*-type compounds where Mg vacancies act as electron acceptors and severely reduce the efficiency of dopants. Thermoelectric properties measurements show that intrinsic Mg_2Ge exhibits *n*-type behaviour. This work investigates the efficiency of Bi as dopant for one-step fabrication of *n*-type Mg_2Ge to improve its thermoelectric performance. Bismuth doping results in a significant reduction of electrical resistivity while the compound remains *n*-type, proving Bi as an electron donor in Mg_2Ge, as suggested by theoretical studies. However, the impact of Bi-doping on the thermoelectric properties of Mg_2Ge is much smaller than predicted values. Detailed microscopy analysis revealed the formation of Bi-rich precipitates at the grain boundaries of the Mg-deficient Mg_2Ge matrix, indicating very limited solubility of Bi in this compound. It suggests low efficiency of Bi as an *n*-type dopant for Mg_2Ge.

WA4

Towards Realisation of High-Performance Thermoelectrics for Energy Conversion

Z. Chen

School of Mechanical and Mining Engineering, University of Queensland, Brisbane 4072, Australia

Thermoelectric materials can directly harvest emission-free electricity from heat or achieve solid state cooling without any vibrational part [1][2] offering a promising solution for the energy shortage [3]. So far, extensive investigations have been made to improve the thermoelectric efficiency, which governed by the dimensionless figure-of-merit ZT ($ZT = S^2\sigma T / \kappa$), where σ is the electrical conductivity, S is the Seebeck coefficient, T is the absolute temperature, and k is the total thermal conductivity which is the sum of the contributions from its electron (k_e) and lattice (k_L) components [3][4]. For high thermoelectric performance, a high power factor ($S^2\sigma$) and a low κ are required. However, it is always a challenge to optimize the individual parameters of σ, S, and k for thermoelectric materials due to their interdependent and conflict[3]. Up to now, besides using band engineering through tuning band convergence [1] quantum confinement , and effective mass to maximizing $S^2\sigma$, most successful ZT enhancement has been achieved via structural and nanostructural engineering or hierarchical architecting to reduce κ.

Here, Dr Chen developed inexpensive, abundant, and low-toxic thermoelectrics for high-efficiency energy conversion using novel industry-level approach, coupled with nanostructure and band engineering strategies [3][5-8]. Through effective design of thermoelectric materials with engineered chemistry and unique structure, and advanced manufacturing, high-performance thermoelectrics has been realised in lab scale. Such innovative technology can be used for harvesting electricity from waste heat or body heat, which will pioneer the thermoelectric technology at the forefront of energy technologies and bring tremendous economic and environmental benefits to the community.

[1] Chen, Z. G.; Han, G.; Yang, L.; Cheng, L.; Zou, *J. Prog. Nat. Sci.* **22**(6), 535 (2012)

[2] Han, G.; Chen, Z.-G.; Drennan, J.; Zou, J. *Small* **10**(14), 2747 (2014)

[3] Yang, L.; Chen, Z.-G.; Han, G.; Hong, M.; Zou, Y.; Zou, J. *Nano Energy* **16,** 367 (2015)

[4] Hong, M.; Chen, Z.-G.; Yang, L.; Han, G.; Zou, J. *Advanced Electronic Materials* 1500025, 1-9 (2015)

[5] Han, G.; Chen, Z.-G.; Yang, L.; Hong, M.; Drennan, J.; Zou, J. *ACS Applied Materials & Interfaces* **7**(1), 989 (2015)

[6] Han, G.; Chen, Z.-G.; Sun, C.; Yang, L.; Cheng, L.; Li, Z.; Lu, W.; Gibbs, Z. M.; Snyder, G. J.; Jack, K.; Drennan, J.; Zou, *J. CrystEngComm* **16**(3), 393 (2014)

[7] Cheng, L.; Chen, Z.-G.; Yang, L.; Han, G.; Xu, H.-Y.; Snyder, G. J.; Lu, G.-Q.; Zou, *J. Journal of Physical Chemistry C* **117**(24), 12458 (2013)

[8] Cheng, L.; Chen, Z.-G.; Ma, S.; Zhang, Z.-d.; Wang, Y.; Xu, H.-Y.; Yang, L.; Han, G.; Jack, K.; Lu, G.; Zou, *J. Journal of the American Chemical Society* **134**(46), 18920 (2012)

TM1

The endless possibilities of graphene on heteroepitaxial silicon carbide

F. Iacopi

Queensland Micro and Nanotechnology Centre, Griffith University, Queensland 4111, Australia

Epitaxial graphene grown using solid source carbon from silicon carbide wafers has been for long time the only route to obtain high quality graphene directly grown at the wafer –level, which is crucial to realise the promise of graphene for nanodevices. Nonetheless, the capability of obtaining comparable quality of graphene on silicon as opposed to silicon carbide wafers, would open an immense opportunity for graphene in integrated circuits and micro-systems in general. While encouraging results have been obtained through thermal decomposition of heteroepitaxial SiC films on silicon wafers, this has usually been limited to small areas and to the use of Si (111) surfaces. Moreover, the obtained graphene quality tends to be strongly hampered by the upper limitation in synthesis temperature set by the melting temperature of silicon. We have recently demonstrated for the first time that most of those limitations can be overcome with the use of heteroepitaxial silicon carbide films in combination with a catalytic alloy of nickel and copper. With this approach we obtain 2 layers graphene on silicon carbide with uniform coverage over the silicon wafer and an average ID/IG ratio of about 0.2 +/- 0.05[1] indicating a substantial improvement as compared to a ratio of ˜1 and above of graphene through the more conventional thermal decomposition. This novel catalytic approach on silicon holds high promise for integrated applications also through the capability for straightforward graphene micropatterning through self-aligned synthesis on pre-structured silicon carbide on silicon [2]. Moreover, we have demonstrated the potential for this approach to fabricate high –performing electrodes for integrated supercapacitor structures [3].

[1] F.Iacopi, N.Mishra, B.V.Cunning, D.Goding, S.Dimitrijev, R.Brock, R.H.Dauskardt, B.Wood and J.J.Boeckl, "A catalytic alloy approach for highly uniform graphene on epitaxial SiC on silicon wafers", *J. Mater. Res* **30**(5), 609 (2015)

[2] B.V.Cunning, M.Ahmed, N.Mishra, A.R.Kermany, B.Wood, F.Iacopi, "Graphitized silicon carbide microbeams on silicon: wafer-level, self -aligned graphene on silicon wafers", *Nanotechnology* **25**, 325301 (2014)

[3] M.Ahmed, M.Khawaja, M.Notarianni, B.Wang, D.Goding, B.Gupta, J.J. Boeckl, A.Takshi, N.Motta, S.E.Saddow, F.Iacopi, "A thin film approach for SiC–derived graphene as an on-chip electrode for supercapacitors", *Nanotechnology* **26**, 434005 (2015)

TM2

Capturing the transition from 3C SiC(111) to graphene by XPS and STM in Ultra High Vacuum

N. Motta[1], B. Gupta[1], F. Zarotti[2], F. Iacopi[3], A. Sgarlata[2], M. Tomellini[2]
E. Placidi[2] and C. Hogan[2]
[1] *Queensland University of Technology, Brisbane, Queensland 4000, Australia*
[2] *University of Rome Tor Vergata, Rome 00173, Italy*
[3]*Queensland Micro and Nanotechnology Centre, Griffith University, Queensland 4111, Australia*

By using X-Ray Photoelectron Spectroscopy and Scanning Tunnelling Microscopy we have been able to follow the time evolution of graphene layers obtained by annealing 3C SiC(111)/Si(111) crystals at different temperatures. Analysis of the atomic resolution images and of the Carbon signal provides a clear picture of the graphene formation. We have been able to visualise by STM the first steps of graphene formation on the surface of SiC finding the sequence of reconstructions which lead from the SiC(111) surface to graphene, caused by the Si sublimation. We followed by XPS the evolution of the graphene thickness at different temperatures as a function of the annealing time, finding a power growth law with exponent 0.5. We show that a kinetic model, based on a bottom-up growth mechanism, provides a full explanation to the evolution of the graphene thickness as a function of time, allowing to calculate the effective activation energy of the process and the energy barriers, in excellent agreement with previous theoretical results. Our study provides a complete and exhaustive picture of the Si out-diffusion from SiC, establishing the conditions for a perfect control of the graphene growth by Si sublimation

[1] Gupta, B., M. Notarianni, N. Mishra, M. Shafiei, F. Iacopi, and N. Motta, "Evolution of epitaxial graphene layers on 3C SiC/Si (111) as a function of annealing temperature in UHV" *Carbon* **68**, 563-572 (2014)
[2] Gupta, B., E. Placidi, C. Hogan, N. Mishra, F. Iacopi, and N. Motta, The transition from 3C SiC(111) to graphene captured by Ultra High Vacuum Scanning Tunneling Microscopy. *Carbon* **91,** 378-385 (2015)

TM3

NEXAFS Anisotropy of Molecular Excitations Preceding the Carbon Continuum Edge in CVD Graphene on Copper

H. Wahab[a], R. Haverkamp[b], J. M. Cadogan[a], H.-C. Mertins[b], S.-H. Choi[c] and H. Timmers[a]

[a] *School of PEMS, University of New South Wales in Canberra, Canberra BC 2610, Australia.*

[b] *Department of Engineering Physics, Münster University of Applied Science, Germany.*

[c] *Kyung Hee University, Yongin 446-701, Korea.*

Technology development and device-design based upon graphene materials require reliable techniques for mass production that are time-robust and reproducible. CVD-synthesis is expected to be the prime candidate for such up-scaling. Copper is a preferred substrate for CVD. Details of the graphene-copper substrate interactions in regard to mechanical stability and electronic band structure are therefore crucial input for future device engineering. Such application will require that the electronic band-structure of different graphene materials is measured in detail and that graphene-substrate interactions are well understood. Both, the degree of sp^2-hybridisation and the electronic band-structure can be directly probed with NEXAFS. The spectroscopy technique enables detailed studies of structural changes at the graphene surface and at its substrate interface. Our NEXAFS studies at the Australian Synchrotron have produced new evidence for a contentious state in graphene near 288 eV. This resonance has been intermittently observed before by others and it is often referred to as an 'interlayer state' due to a perceived analogy with graphite [1-5]. Our results for CVD-graphene synthesized on copper show a pronounced anisotropy for this state. We derive an excitation energy of 288.3 eV and a partial overlap with an isotropic contaminating resonance. After annealing and keeping the graphene in ultra-high vacuum, the NEXAFS signature of the 288.3 eV state only gradually appears and builds-up over several hours. This signature can be removed again by renewed annealing. The reversible phenomenon may thus relate to residual lattice mismatch between the graphene and the copper substrate. Associated stress may gradually be relaxed through the rippling of the graphene layer [6]. Tilting angles of $>20^{\circ}$ appear possible. The rippling is evidenced in our data by a correlated, reversible non-linearity of the cos-square-theta-dependence of the 285 eV π^* resonance of graphene.

[1] Fischer et al., *Phys. Rev. B.* **44**, 1427-1429 (1991)

[2] Pacile et al., *Phys. Rev. Lett.* **101**, 066806 (2008)

[3] Jeong et al.; *Phys. Rev. Lett.* **102** , 099701 (2009)

[4] Lee et al.; J. *Phys. Chem. Lett.* **1**, 1247-1253 (2010)

[5] Schultz et al.; *Nature Communications* **2**, 372 (2011)

[6] Paronyan et al., *ACS Nano* **5**(12), 9619 (2011)

TM4

Quest for zero loss: the materials selection problem in plasmonics

M. Cortie[1] and V. Keast[2]

[1] *School of Mathematical and Physical Sciences, University of Technology Sydney, Broadway 2007, NSW, Australia*

[2] *School of Mathematical and Physical Sciences, University of Newcastle, Callaghan, NSW 2308, Australia*

Under specific conditions incoming light can excite a wavelike oscillatory resonance in the free electrons of a conducting material. When this oscillation propagates along a surface it is usually termed a surface plasmon polariton; when confined to a discrete nanoparticle as a standing wave it is more correctly termed a localised surface plasmon resonance (LSPR). There is currently considerable interest in 'plasmonics'- the study of both kinds of plasmon- because applications as diverse as biosensors, optical computing, rectenna arrays, and meta-materials can make use of them. The strength of the plasmon resonance that can be excited depends on the geometric shape of the structure and, most importantly, its dielectric function at the wavelength of interest. The dielectric function, in turn, depends directly upon the electronic density-of-states of the relevant material. Here we consider how the dielectric function can be optimised for a desired type of plasmon resonance by selection of a suitable material. The metallic elements Au and Ag are well known material choices for these applications, Al and Cu are also possibilities, while Na and K have very suitable dielectric functions but rather unfavourable chemical properties. There are additional possibilities offered by alloying or compound formation and we present examples drawn from our own work on the Ag-Au, Cu-Au, Al-Au, Al-Pt, Au-Ni and Cu-Zn systems [1-6] as examples of what can be achieved. The most important strategy when matching material to desired plasmon resonance is that the energy range over which interband transitions occur must, in general, be avoided. Given the manner in which the Drude and interband components of the dielectric function interact, the region just below the absorption edge energy is particularly attractive. This can be accessed by suitable selection of material or by manipulation of the geometry or dielectric environment of the nanostructure of interest. In addition to metals, however, a range of semiconducting compounds are also of interest for plasmonic applications, although generally at somewhat longer wavelengths than for the metals. The diverse possibilities offered by these compounds are assessed.

[1] K. S. B. De Silva, A. Gentle, M. Arnold, V. J. Keast & M. B. Cortie, J. *Phys. D: Appl. Phys* **48**, 215304 (2015)

[2] V. Keast, K. Birt, C. Koch, S. Supansomboon & M. Cortie, *Applied Physics Letters* **99**, 111908 (2011)

[3] V. J. Keast, R. L. Barnett & M. B. Cortie, *J. Phys. Cond. Matter* **26**, 305501 (2014)

[4] V. J. Keast, J. Ewald, K. S. B. D. Silva, M. B. Cortie, B. Monnier, D. Cuskelly & E. H. Kisi, *J. Alloys & Compounds* **647**, 129-135 (2015)

[5] V. J. Keast, B. Zwan, S. Supansomboon, M. B. Cortie & P. O. Å. Persson, *J. Alloys & Compounds* **577**, 581-586 (2013)

[6] D. J. McPherson, S. Supansomboon, B. Zwan, V. J. Keast, D. L. Cortie, A. Gentle, A. Dowd & M. B. Cortie, *Thin Sol. Films* **551**, 200-204 (2014)

TM5

Preparation and Characterization of Poly Lactide and Poly (Butylene Adipate-co-Terephthalate) Nanocomposites Reinforced with Graphene Nanoplatelet

S. Kashi, R. Gupta, N. Kao and S. Bhattacharya V

School of Civil, Environmental and Chemical Engineering, RMIT University, Melbourne 3001, Australia

With excellent characteristics such as high mechanical properties and electrical conductivity, graphene nanoplatelets (GNPs) can be used for reinforcing polymers and developing novel materials. In the current study, different concentrations of GNPs (0-15 wt %) were embedded into poly lactide and poly (butylene adipate-co-terephthalate) which are among the leading biodegradable polymers. Morphology of the nanocomposites was studied via scanning electron microscopy and X-Ray diffraction. Effect of GNP loading on electrical conductivity and thermal stability of the two matrices were determined. Results showed significant enhancement in both conductivity and thermal stability of polymers with addition of GNPs.

TM6

Development of Hydrophilic Materials for Nanofiltration Membrane Achieving Dual Resistance to Fouling and Chlorine

Xi Quan Cheng[1,2], Y. Xu[2], X. Jiang[2], L. Shao[1], C. Lau[1]

[1] *School of Chemical Engineering and Technology, State Key Laboratory of Urban Water Resource and Environment (SKLUWRE), Harbin Institute of Technology, Harbin 150001, China*

[2] *Manufacturing Flagship, CSIRO, Private Bag 33, Clayton South, VIC 3169, Australia*

A hydrophilic thin-film-composite (TFC) nanofiltration (NF) membrane has been developed through the interfacial polymerization (IP) of amino-functional polyethylene glycol (PEG) and trimesoyl chloride. The selective layer is formed on a polyethersulfone (PES) support that is characterized using FTIR, XPS and SEM, and is dependent on monomer immersion duration, and the concentration of monomers and additives. The higher hydrophilicity alongside the larger pore size of the PEG-based selective layer is the key to a high water flux of 66.0 $Lm^{-2}h^{-1}$ at 5.0bar. With mean pore radius of 0.42 nm and narrow pore size distribution, the $MgSO_4$ rejections of the PEG based PA TFC NF membranes can reach up to 80.2%. The hydrophilic PEG based membranes shows positive charged since the isoelectric points range from pH = 8.9 to pH = 9.1 and the rejection rates for different salts of the novel membranes are in the order of R(MgCl2) > R(MgSO4) > R(NaCl) > R(Na2SO4). The pore sizes and water permeability of these membranes are tailored by varying the molecular weight and molecular architecture of amino-functional PEG. Due to the unique structure of the selective layer of the PEG based membranes consisting of saturated aliphatic construction unit (CH2-CH2-O), the membranes demonstrate dual resistance to fouling and chlorine. The membranes maintain good salt rejections and high water flux of PEG based membranes after treatment by 2000 ppm NaClO for 24 hours. Interestingly, the PEG based membranes exhibit excellent fouling resistance with a water flux recovery of 90.2% using BSA as a model molecule. More importantly, the hydrophilic PEG based NF membranes have been exploited to separate several water soluble antibiotics (such as tobramycin, an aminoglycoside antibiotic applied in the treatment of various types of bacterial infections), showing excellent performance in concentration or removal of antibiotics

TN1

Atomic-scale understanding of CO_2 adsorption processes in metal-organic framework (MOF) materials using neutron scattering and ab-initio calculations

J. Auckett[1], V. Peterson[1], S. Duyker[2]

[1]*ANSTO, Lucas Heights, NSW 2234, Australia*

[2] *School of Chemistry, University of Sydney, Sydney 2006, NSW, Australia*

The dependence of the industrialised world on fossil-fuel energy generation technologies and consequent increase in atmospheric CO_2 concentrations has been blamed for emerging adverse climate effects, including an increase in global mean temperatures [1]. Until renewable, carbon-free energy sources can be efficiently harnessed to meet the world's energy needs, interim measures are sought to suppress the atmospheric release of CO_2 from traditional coal and natural gas combustion processes. Microporous materials such as zeolites and metal-organic frameworks (MOFs) are therefore being investigated for the separation and capture of CO_2 at various stages of the combustion cycle. MOFs represent one of the most promising classes of materials for this application, offering unrivalled tunability of structural and chemical characteristics via the substitution of metals and choice and functionalisation of ligands [2]. In order for a MOF to be rationally tuned for improved performance, the nature of the interactions between the host framework and guest molecules must be well-understood at the atomic level. Our research targets this detailed understanding of MOFs using neutron scattering and computational methods. We are currently investigating several MOFs which display unexpected sorption properties such as "reverse sieving" – that is, selectively absorbing larger gas molecules while rejecting smaller ones – and unusual lattice expansion effects. Using in situ diffraction to locate the preferred binding sites of guest molecules in the framework, inelastic neutron scattering to probe system dynamics, and density functional theory-based molecular dynamics simulations to validate and interpret our experimental results, we are able to gain detailed information about the mechanisms of gas uptake and diffusion in these exciting new MOF materials.

[1] S. Solomon, G.K. Plattner et al., *Proc. Natl. Acad. Sci.* USA **106**, 1704-1709 (2009)

[2] G.J. Kearley & V.K. Peterson (eds.) *Neutron Applications in Materials*, Springer (2015)

TN2

Crystallographic and magnetic structure study in $SrCoO_{3-x}$ by high resolution x-Ray and neutron powder diffraction

F. Chang[1], M. Reehuis[2], J. Hester[3], M. Avdeev[3], F. Xiang[4], X. Wang[4], J. Seidel[5], C. Ulrich[1]

[1] *The School of Physics, University of New South Wales, NSW 2052, Australia*

[2] *Helmholtz-Zentrum Berlin für Materialien und Energie, D-140109 Berlin, Germany*

[3] *ANSTO, Lucas Heights, NSW 2234, Australia*

[4] *Institute for Superconducting and Electronic Materials, University of Wollongong, Wollongong, New South Wales 2522, Australia*

[5] *School of Materials Science and Engineering, The University of New South Wales, NSW 2052, Australia*

Transition metal oxides (TMOs) represent a wide set of materials with a broad range of functionalities, including superconductivity, magnetism, and ferroelectricity, which can be tuned by careful choice of parameters such as strain, oxygen content, and applied electric and magnetic fields [1-4]. This tunability makes TMO's ideal candidate materials for use in developing novel information and energy technologies and $SrCoO_3$ provides a particularly interesting system for investigation due to its propensity to form oxygen-vacancy-ordered structures as the oxygen content is decreased. The ties between structural and functional properties of this material are obvious as it undergoes simultaneously structural and magnetic phase transitions between two topotactic phases: from a ferromagnetic perovskite phase at $SrCoO_{3.0}$ to the antiferromagnetic brownmillerite $SrCoO_{2.5}$ [1,5]. In this study we have determined their crystallographic and magnetic structures of $SrCoO_{2.50}$, $SrCoO_{2.875}$, and cubic $SrCoO_{3.00}$ using high resolution X-ray and neutron powder diffraction from 4 K to 600 K. The correct structure of oxygen-deficient end-member $SrCoO_{2.5}$ was determined in space group of Imma, instead of Pnma or Ima2 proposed previously, with G-type antiferromagnetic order up to T_N = 570 K. In $SrCoO_{2.875}$, clear peak splitting was observed from (200) in cubic phase to (004) and (440) in tetragonal phase, indicating that the precise structure is I4/mmm with a = b = 10.829(9) Å and c = 7.684(2) Å at 95 K, and the corresponding magnetic structure is ferromagnetic with 1.86(4) μ_B per formula, in accordance to a spin configuration of cobalt ions with an intermediate spin state of both on Co^{3+} and on Co^{4+}. The end member $SrCoO_{3.00}$ possesses a simple cubic crystal structure with a = 3.817(2) Å at 95 K, and ferromagnetic order up to 280 K. The magnetic moment of 1.96(8) μB /Co^{4+} corresponds to an intermediate spin state of Co^{4+}.

[1] H. Jeen et al., *Nature Mater.* **12**, 1057 (2013)

[2] Yang et al., *Nature Mater* **8**, 485 (2009)

[3] J. Seidel et al., *Nature Com.* **3**, 799 (2011)

[4] T. Takeda, et al., *J. Phys. Soc. Jpn* **22**, 970 (1972)

[5] S. J. Callori, J. Seidel, C. Ulrich et al., *Phys. Rev. B* **91**, 140405 (2015)

TN3

Hydrates under pressure – new insights from sulfuric acid hydrates

H. Maynard-Casely[1], T. Hattori[2], S. Machida[3], A. Sano-Furukawa[2] and K. Komatsu[4]

[1]*ANSTO, Lucas Heights, NSW 2234, Australia*

[2] *J-PARC Center, Japan Atomic Energy Agency, Tokai, Japan*

[3] *Comprehensive Research Organization for Science and Society, Japan*

[4] *Geochemical Research Centre, University of Tokyo, Japan*

Hydrates are a rich and diverse class of materials that display a wide range of structures and properties – a feature that is only exaggerated when they are subjected to high-pressures. Consequently, these have implications on our understanding of many outer solar system bodies, where hydrates are amongst the dominant materials found there. For Europa and Ganymede, two moons under intense investigation from past and future space missions, their surfaces seen to be mostly water-ice and hydrates. Despite the apparent 'simplicity' of these materials, we still observe very complex geological formations on these moons – including subduction [1]. Hence, we need to understand the transformations of candidate surface materials under a range of pressure/temperature conditions in order to accurately explain the formations on these icy surfaces. One hydrate candidate material for the surfaces of these moons are sulfuric acid hydrates, formed from radolytic sulfur (from Io) reacting with the surface ice. Sulfuric acid hydrates have already been established to have a complex phase diagram with composition [2]. We have now used the Mito cell [3] at the PLANET instrument [4] to undertake the first investigation of the high-pressure behaviour of the water rich sulfuric acid hydrates. Compressing at 100 K and 180 K we see that the hemitriskaidekahydrate becomes the stable water-rich hydrate and observe some interesting relaxation behaviour in this material at pressure, which could have significant consequences for the interiors of Ganymede.

[1] Kattenhorn, S.A. and L.M. Prockter, "Evidence for subduction in the ice shell of Europa" *Nature Geosci* **7**(10), 762-767 (2014)

[2] Maynard-Casely, H.E., H.E.A. Brand, and K.S. Wallwork, "Phase relations between the water-rich sulfuric acid hydrates, potential markers of thermal history on Jupiter's icy moons" *Icarus* **238**(0), 59-65 (2014)

[3] Komatsu, K., et al., "Development of a new P–T controlling system for neutron-scattering experiments" *High Pressure Research* **33**(1), 208-213 (2013)

[4] Hattori, T., et al., "Design and performance of high-pressure PLANET beamline at pulsed neutron source at J-PARC. Nuclear Instruments and Methods in Physics Research Section A: Accelerators, Spectrometers, Detectors and Associated Equipment" **780**(0), 55-67 (2015)

TN4

Inelastic neutron scattering as a means for determining the magnetic exchange interactions in the frustrated quantum spin chain, Linarite

K. Rule[1], B. Willenberg[2], R. Mole[1], A. Wolter-Giraud[3], A. Tennant[4], G. Ehlers[4], A. Studer[1], J. Gardner[5] and S. Suellow[6]

[1] *The Bragg Institute, ANSTO, Lucas Heights, NSW 2234, Australia*

[2] *Helmholtz-Zentrum Berlin für Materialien und Energie, D-140109 Berlin, Germany*

[3] *IFW, Dresden, Germany*

[4] *Oak Ridge National Laboratories, Oak Ridge, Tennessee, USA*

[5] *National Synchrotron Radiation Research Centre, Hsinchu City, Taiwan 300*

[6] *Technische Universität Braunschweig, Germany*

One of the simplest models exhibiting one dimensional (1D) frustrated quantum interactions is the so called J1-J2 model. In this model competing ferromagnetic nearest-neighbour interactions (J1 > 0) and antiferromagnetic next-nearest-neighbours (J2 < 0) can give rise to novel phenomena such as multiferroicity for spiral spin states. Linarite, $PbCuSO_4(OH)_2$ is a natural mineral ideally suited to the study of frustration in J1-J2 systems due to an accessible saturation field and the availability of large single crystals well suited to neutron investigations. In this material the Cu^{2+} ions form spin S = 1/2 chains along the b direction with dominant nearest-neighbour FM interactions and a weaker next-nearest-neighbour AFM coupling, resulting in a magnetically frustrated topology [1, 2]. We present a neutron scattering study of linarite revealing a helical magnetic ground state structure with an incommensurate propagation vector of (0, 0.186, ½) below TN = 2.8K in zero magnetic field [3]. From detailed measurements in magnetic fields up to 12 T (B || b), a very rich magnetic phase diagram will be presented. In particular we will present new inelastic neutron scattering data and compare this with theoretical modelling of the spin Hamiltonian. These theoretical calculations imply that linarite possesses an xyz exchange anisotropy. Our data establish linarite as a model compound of the frustrated one-dimensional spin chain, with ferromagnetic nearest-neighbour and antiferromagnetic next-nearest-neighbour interactions.

[1] M. Baran et al., *Phys. Stat. Sol C.* **3**,220 (2006)

[2] Y. Yasui, M. Sato, and I. Terasaki, *J. Phys. Soc. Jpn*. **80**, 033707 (2011)

[3] B. Willenberg et al., *Phys. Rev. Lett.* **108**, 117202 (2012)

TA1

X-radiation in health and disease: Novel approaches to the study of disease processes and therapy

D. Myers

The University of Melbourne, Victoria 3010, Australia

Our current medical knowledge and understanding of human biology and physiology have been predicated by our capacity to image organs, body structures, different types of tissues and particular cell types. These imaging modalities range from advanced microscopy for imaging of cells and tissues through to 2D and 3D macroscopic techniques for imaging of tissues and organs. Soft tissues in particular are difficult to image, especially when surrounded by dense structures such as bone. Also, some regions, such as the brain, require special investigative techniques as they are closed tissue/organ structures with low contrast features. Medical diagnoses, monitoring of disease progression, efficacy of therapies and the recent advent of 'targeted imaging' rely upon techniques such as X-ray analysis, MRI, Positron Emission Tomography (PET) and more. In this seminar several recent adaptions of X-ray and synchrotron based X-ray science will be related. In particular, Phase-contrast X-ray imaging (PCXI), also termed microfocus imaging, X-ray Fluorescence Microscopy (XFM) and Microbeam X-ray Therapy (MRT) will be discussed. Since the discovery of X-rays and development of medical X-ray sources, X-ray imaging has accounted for approximately 60% of medical diagnostic procedures; X-ray imaging is still the predominant technology used in medicine. Over the past 30 years radioisotope-based imaging has expanded substantially with 3D positron emission tomography (PET) and combined PET/MRI being developed for simultaneous structural and functional imaging. More recently, advanced 3D imaging techniques have been aligned with targeted therapies and high resolution multi-modal imaging to improve our capabilities in definition of organ boundaries and particular tumours and organ abnormalities. Microbeam radiation therapy (MRT) is another capability and this is currently being developed at the Australian Synchrotron. Synchrotrons produce a broad range of electromagnetic radiation applicable for diverse analyses such protein crystallography, X-radiation for fluorescence spectroscopy, for mapping and quantification of trace metals, and for fast X-ray tomography for structural imaging. Access to synchrotron light sources has led to a renaissance in utilisation of X-rays for diverse imaging applications and novel radiation therapies. During this seminar the importance of advanced imaging techniques and synchrotron radiation to enable investigation of a range of diseases will be related. This presentation will include specific studies in which application of synchrotron radiation has aided investigations into bone disease and bone cancers, the study of brain abnormalities including epilepsy and traumatic brain injury and targeted therapy using MRT. Advanced medical imaging techniques have been central to our understanding of disease processes and have the potential to aid clinicians when considering

therapeutic interventions. The strong synergy that occurs in interdisciplinary research has been crucial to these developments. Project design and efficient implementation of advanced imaging techniques to achieve meaningful outcomes in science and medicine will also be discussed.

Acknowledgement: The contribution of the many scientists and organisations involved with this work will be related during delivery of this invited seminar.

TA2

Investigation of Targeting Capabilities of Peptide-conjugated Endocannabinoid-based lipid Nanoassemblies in the Treatment of Arthritis

N. Barrie[1], M. Moghaddam[1], N. Manolios[2], A. Marina[2]

[1] *CSIRO Materials Science and Engineering, CSIRO, North Ryde, NSW, Australia*

[2] *Department of Rheumatology, Westmead Hospital and University of Sydney*

Aims: To develop a novel drug delivery system using cannabinoid amphiphiles and evaluate the synovial homing capabilities of peptide-conjugated nanoparticles for the targeted treatment of arthritic conditions.

Background: Chronic inflammatory joint disease is a common problem that results in a great deal of pain, dysfunction and socio-economic hardship to those affected. We have developed and synthesized a series of endocannabinoid agonists that have the ability to self-assemble in the presence of a polar solvent to form a variety of nanoassembled particles governed by local constraints imposed by the effective shape of the molecule. The cannabinoid amphiphiles ability to self assemble makes them potentially useful vehicles for the encapsulation and controlled release of hydrophilic, hydrophobic and amphiphilic drugs. Furthermore, modification of pharmacokinetic properties through polymer conjugation allows the customisation and specific targeting of nanoparticles within a physiological system allowing a highly sophisticated drug delivery system. Together, the nanoparticles capacity for anti-arthritic drug deliver coupled with the targeting capability of peptides such as HAP-1, facilitates a selective accumulation of therapeutic agents in the inflamed synovium, potentially improving drug efficacy at the diseased site without compromise to healthy tissue. In addition to targeted drug delivery, the endogenous nature of cannabinoid amphiphiles further increases biocompatibility and may act in an analgesic capacity. Modulation of the endocannabinoid receptor system via interaction of amphiphiles endocannabinoid lipid constituents facilitates the potential for pain relief associated with rheumatoid arthritis via manipulation of the endocannabinoid system.

Methods: Lipid-based amphiphile components for nanoassemblies were synthesized in large scale. HPLC, LC/MS, Polarised optical microsopy (POM) and NMR were employed to examine the bulk phase of a variety of lipid mixtures at 25°C and 37°C. The synovium targeting peptide, HAP-1, and pegylated lipids were incorportated on the surface of these nanoassemblies and its physicochemical properties assessed using POM, particle sizing, and cryo-TEM. "Did" fluorochrome was incorporated into the nanoparticles lipid membrane and its bio-distribution was imaged in normal rat models via near-infrared fluorescence imaging system (NIRF).

Results and Discussion: Endogenous monoethanolamide lipids oleoylethanolamide (OEA) and linoleoylethanolamide (LEA) were synthesized and purified to greater than 98% purity. Both the monoethanolamide head group and the unsaturated hydrophobe are of key importance in dictating the self assembly behaviour of these molecules. The current study demonstrated the ability of endogenous fatty acid monoethanolamides with an increasing degree of hydrocarbon unsaturation to form cubic phases at 25°C and 37°C. 40% OEA/60%LEA was established as the threshold ratio for cubic stability at physiological temperatures and therefore the most physiologically relevant mixture. Functionalized 40% Oleoyl-PEG-2000 was synthesized, fluorescently tagged and either conjugated with or without HAP-1 peptide. HAP-1 conjugated nanoparticles demonstrated homing capacity, localising in the knee and hip joints in normal rats, whilst untagged nanoparticles exhibited no specific distribution.

TA3

Sodium for securing future renewable energy supply

M. Minakshi[1] and D. Appadoo[2]

[1] *Murdoch University, Murdoch, WA 6150, Australia*

[2] *Australian Synchrotron, Clayton 3168, Victoria, Australia*

The storage and recovery of electrical energy is widely recognized as one of the most important areas for energy research. Although renewable energy such as i.e. wind and solar generated electricity is becoming increasingly available in many countries including Australia, these sources provide only intermittent energy. Thus, energy storage systems are required for load levelling, allowing energy to be stored and used on demand. Energy storage in rechargeable batteries and supercapacitors is the most promising prospect for ensuring consistent energy supply [1-2] therefore allowing greater penetration of renewable energy into the electricity grid. Energy storage capability also has obvious benefits in terms of greenhouse emissions. Issues such as the environment, the rapid increase in fossil fuel prices, and the increased deployment of renewable energy sources, provide a greater need for the development of electrochemical energy storage, especially for large-scale applications. Thus, materials research and computational modelling play a key role in making further progress in the field of energy storage. Energy storage devices based on sodium have been considered as an alternative to traditional lithium based systems because of the natural abundance, cost effectiveness and low environmental impact of sodium. Phosphate materials such as $NaNiPO_4$, $NaMnPO_4$, $NaCoPO_4$ and $NaNi_{1/3}Mn_{1/3}Co_{1/3}PO_4$ will be discussed at the conference. Sodium transition metal phosphate has served as an active electrode material for an energy storage device [3-4]. The development of sodium transition metal phosphate with special emphasis on structural changes and novel synthetic approach can underpin technological advancements in small renewable energy harvesting and power generation technologies. The characteristics of the fabricated device such as improved storage capability, cycling stability, safety and economic life - cycle cost made this an attractive alternative to conventional charge storage devices using more expensive materials.

[1] J. Zhang, J. Jiang, H. Li, and X. S. Zhao, *Environ. Sci*. **4**, 4009 (2011)

[2] C. Liu, F. Li, L.-P. Ma, M.-M. Cheng, *Adv. Mater.* **22**, E28 (2010)

[3] M. Minakshi, D. Meyrick and D. Appadoo, *Energy & Fuels* **27**, 3516 (2013)

[4] M. Minakshi, T. Watcharatharapong, S. Chakraborty, R. Ahuja, S. Duraisamy, P. T. Rao and N. Munichandraiah, *Dalton Trans.* DOI 10.1039/c5dt03394b (2015)

TA4

Bi(III)-containing lanthanum germanium apatite-type oxide ion conductors and their structure-property relationships

M. Tate[1], G. McIntyre[1] and I. Evans[2]

[1] *The Bragg Institute, ANSTO, Lucas Heights, NSW 2234, Australia*

[2] *Durham University, Durham, United Kingdom*

Oxide ion conductors are used in a wide variety of applications, including oxygen sensors and separation membranes, but are undergoing significant study for their use in solid oxide fuel cells (SOFCs), which allow for the direct conversion of chemical to electrical energy. Apatite-type silicates and germanates, $La_{9.33+x}(TO_4)_6O_{2+3x/2}$ (T = Si, Ge), have exhibited high oxide ion conductivities, potentially allowing for their use in SOFCs. Apatite-type compounds have the general formula, $[A^I_4][A^{II}_6][TO_4]_6X_{2\pm\delta}$, (A = alkaline or rare earth metal, or Pb; T = Ge, Si, P, V; X = O, OH, halides) and can be thought of as comprised of a framework of $A^I_4(TO_4)_6$ with flexible cavities containing $A^{II}_6X_2$ units. The structures of apatite-type materials are primarily hexagonal, with the remainder being monoclinic, with several triclinic examples known. The origin of the triclinic structure is thought to be partly due to the size differences between the units comprising the framework and those within the cavities. The inclusion of interstitial oxide ions have been shown to promote the triclinic distortion, potentially caused by further expansion of the framework. Three novel Bi(III)-containing lanthanum germanium apatite compounds ($Bi_2La_8[(GeO_4)_6]O_3$, $Bi_4Ca_4La_2[(VO_4)_2(GeO_4)_4]O_2$, and $Bi_4Ca_2La_4[(GeO_4)_6]O_2$) were synthesised by a solid state synthetic method, before undergoing AC impedance spectroscopy experiments to study their electrical properties. The $Bi_2La_8[(GeO_4)_6]O_3$ compound has been identified as being the first bismuth containing apatite with a triclinic structure, whilst the Bi_4-containing compounds possess hexagonal structures. All samples show high levels of conductivity, with the triclinic sample possessing higher conductivity values than the hexagonal samples at high temperature.

.

TA5

Low temperature effect of lithium diffusion in 18650-type MNC battery

C. Wu[1], M.Avdeev[2], C. Chang[3] and P. Pan[3]

[1] *National Synchrotron Radiation Research Centre, Hsinchu City, Taiwan 300*

[2] *ANSTO, Lucas Heights, NSW 2234, Australia*

[3] *National University of Tainan, Tainan City, Taiwan 700*

Investigations of the phenomena in atomic scale are essential for fully understandings of the activities in battery operation. The battery is known to be operated in a broad temperature range below and above the ambient temperature. Temperature change could affect the performance, and might even raise safety issue. Li-plating, where metallic Li-ions accumulate onto the graphite anode, is a recently realized atomic pheromone that severely degrades the performance of the battery. These including capacity loss, impedance raise, activity slowing down and aging speeding up. It is now known that intercalation into the graphite and platting onto the graphite surface can both occur when Li-ions return to the graphite anode upon charging. Li-plating will partially block the insertion of Li-ions onto the graphite electrode in some extent, which reduces the migration of Li-ions during discharging and charging. Clearly, local environment, such as temperature or electric field, could affect the insertion rate, but experimental study or theoretical modeling concerning these effects are still limited.

Here, we report on the results of studies made, using cold neutron triple-axis spectrometer – SIKA's elastic mode, on the Li^+ diffusion rate of an 18650-type Li-ion battery in discharging-charging operations, carried out at and below the ambient temperature. Sizable in-situ neutron diffraction intensities for the {001} reflection of LiC_6, for the {002} reflection of LiC_{12}, as well as for the {004} reflection of LiC_{54} were clearly detected in very 5 minute interval during a discharging-charging operation, which were then used to extract the Li^+ diffusion rate during operation. Interestingly, operation with a C/5 discharging rate performed at -20 ℃ causes a dramatically 25% reduction in the Li^+ diffusion rate and even more surprisingly the discharge transfers only 35% of the Li out of the graphite anode since the diffusion essentially stop in the early stage (~1/3) of the discharge period. The reduction and stopping of Li^+ diffusion can effectively corrected by employing a lower discharging rate in the operation

FM1

A Morphotropic Phase Boundary in Samarium-modified Bismuth Ferrite Thin Films

N. Valanoor

School of Materials Science and Engineering, The University of New South Wales, NSW 2052, Australia

Interfacial control of a polar (rhombohedral)-to-non-polar (orthorhombic) phase transition in (001) oriented epitaxial $BiFeO_3/(Bi_{1-x}Sm_x)FeO_3$ superlattices is presented. We demonstrate controlling the composition at which a polar phase transformation takes place by tuning the strength of the interlayer interactions while holding the average composition constant. It is shown that the thickness of the superlattice layers have a strong influence on the interlayer polar coupling, which in turn changes the phase transition. For shortest periods studied (layers 5 and 10 nm thick) the onset of the phase transition is suppressed along with a significant broadening (as a function of Sm^{3+} concentration) of an incommensurately modulated phase, determined by two-dimensional x-ray diffraction mapping. Consequently, ferroelectric character with robust polarization hysteresis and enhanced dielectric constant, is observed even for substitution concentration of Sm^{3+} which would otherwise lead to a leaky paraelectric in single-layer $(Bi_{1-x}Sm_x)FeO_3$ films. The experimental results are fully consistent with a mean-field thermodynamic theory which reveals that the strength of the interlayer coupling is strongly affected by the polar-polar interaction across the interface.

Part of this work appears in *Phys. Rev. B* **90**, 245131 (2014)

FM2

Reversible electrochromism, elasto-optic and thermo-optic effects in $BiFeO_3$ films

D. Sando

School of Materials Science and Engineering, The University of New South Wales, NSW 2052, Australia

Chromism refers to a change in optical absorption of a material upon application of stimulus; e.g. photochromism – light; thermochromism – heat; electrochromism – electric charge; magnetochromism – magnetic field. This phenomenon has wide applications, in for example so-called 'smart glass' which can be switched from a transparent to opaque state through the application of voltage, heat, or light. Bismuth ferrite ($BiFeO_3$ – BFO) is the only known single-phase multiferroic material whose ordering temperatures are above ambient (ferroelectric TC = 1200 K; antiferromagnetic TN = 640 K) [1]. As a consequence, this material has attracted enormous research interest, on both a fundamental level and for its promise in room-temperature spintronics. In addition to its outstanding ferroelectric properties and rich spin physics, BFO has rather striking optical properties: a band gap in the visible range (attractive for light harvesting applications); a bulk photovoltaic effect with open-circuit voltages much higher than the band gap, very large birefringence, and a significant electro-optic response [2]. Epitaxial strain has been shown to be a powerful means of modifying the physical properties of BFO films [3]. By depositing strained thin films on substrates with different lattice parameters, the effects of both compressive and tensile strain can be explored. Important phenomena revealed using this technique are the drastic modification of the ferroelectric ordering temperature [4], and the spin order [5]. In addition, large compressive strains can stabilize a highly-distorted polymorph (T-like phase BFO) which shows distinctly modified physical properties when compared to the R (bulk-like) phase. Of particular relevance to this work is the larger optical band gap and the related modulation of optical absorption for photon energies near the band edge. In this presentation we first describe the effect of epitaxial strain on the optical band gap and refractive index of strained BFO films. Via strain engineering techniques we uncover a large elasto-optic effect (change in refractive index with strain) that surpasses that of the best acousto-optic materials (such as quartz or TeO_2). More importantly, through dynamic switching between the different phases, we demonstrate a time-stable, reversible, and intrinsic electrochromic effect. Furthermore, through temperature dependent optical measurements, we reveal a large thermo-optic effect (change in index with temperature), a phenomenon which could be attractive for optical modulators or switches. Our results constitute an important first step in the development of integrated multifunctional thin film optical devices based on complex oxides. Indeed the coupling of optical,

magnetic, and piezoelectric orders possible in this class of materials suggests new device opportunities based on ferroelectric and multiferroic thin films.

[1] G. Catalan and J.F. Scott, *Adv. Mater*. **21**, 2463 (2009)

[2] D. Sando et al, *Phys Rev. B* **89**, 195106 (2014)

[3] D. Sando et al, *J. Phys. Cond. Mat*. **26**, 473201 (2014)

[4] I.C. Infante et al, *Phys. Rev. Lett.* **105**, 057601 (2010)

[5] D. Sando et al, *Nat. Mater*. **12**, 641 (2013)

FM3

Effects of ^{18}O isotope substitution in multiferroic $RMnO_3$ (R = Tb, Dy)

P. Graham[1], N. Narayanan[2], G. McIntyre[3], W. Hutchison[2], C. Ulrich[4], N. Reynolds[4]
P. Rovillain[4], J. Hester[3], J. Kimpton[5], M. Yethiraj[3], E. Pomjakushina[6], K. Conder[6]
and M. Kenzelmann[6]

[1] *University of New South Wales, NSW 2052, Australia*
[2] *School of PEMS, UNSW Canberra, Canberra, ACT 2600, Australia*
[3] *The Bragg Institute, ANSTO, Lucas Heights, NSW 2234, Australia*
[4] *School of Physics, University of New South Wales, NSW 2052, Australia*
[5] *Australian Synchrotron, Clayton 3168, Victoria, Australia*
[6] *Paul Scherrer Institute, CH-5232 Villigen, Switzerland*

Multiferroic materials demonstrate desirable attributes for next-generation multifunctional devices as they exhibit coexisting ferroelectric and magnetic orders. In type-II multiferroics, coupling exists that allows ferroelectricity to be manipulated via magnetic order and vice versa, offering potential in high-density information storage and sensor applications. Despite extensive investigations into the subject, questions of the physics of magnetoelectric coupling in multiferroics remain, and competing theories propose different mechanisms. The aim of this investigation was to study changes in the statics and dynamics of structural, ferroelectric and magnetic orders with oxygen-18 isotope substitution to shine light into the coupling mechanism in multiferroic $RMnO_3$ (R=Tb, Dy) systems.

We have performed Raman spectroscopy on ^{16}O and ^{18}O-substituted $TbMnO_3$ single crystals. Oxygen-18 isotope substitution reduces all phonon frequencies significantly. However, specific heat measurements determine no changes in Mn^{3+} (28 and 41 K) magnetic phase transition temperatures. Pronounced anomalies in peak position and linewidth at the magnetic and ferroelectric phase transitions. While the anomalies at the sinusoidal magnetic phase transition (41 K) are in accordance to the theory of spin-phonon coupling, further deviations develop upon entering the ferroelectric phase (28 K). Furthermore, neutron diffraction measurements on ^{16}O and ^{18}O-substituted $DyMnO_3$ powders show structural deviations at the ferroelectric phase transition (17 K) in the order of 100 fm in the b direction. The *Pbnm* space group is centrosymmetric and therefore does not allow ferroelectricity via atomic displacements, however our Reitveld analysis for the subgroup $P2_1$ shows significant displacements and polarisation along b that is comparable to the experimental value, making it the most promising candidate for ionic displacement induced polarisation in $DyMnO_3$. These combined results demonstrate that structure is an important consideration in the emergence of ferroelectricity in these materials.

FM4

Growth and Properties of Strain-tuned $SrCoO_x$ ($2.5 \leq x < 3$) Thin Films

Songbai Hu[1], J. Seidel[1] and F. Klose[2]

[1]*The University of New South Wales, NSW 2052, Australia*

[2]*ANSTO, Lucas Heights, NSW 2234, Australia*

Controlling material properties by strain is one of the main concepts of thin film growth technology. By altering the order parameter in ferroic materials with which the lattice is coupled, new properties can be achieved, e.g. in perovskite $SrCoO_x$ which was identified as a parent phase of strong spin-phonon coupling materials. Here, we present results on a strain-induced antiferromagnetic-ferromagnetic phase transition in high quality epitaxial $SrCoO_x$ ($2.5 \leq x < 3$) (oxygen deficient $SrCoO_3$) thin films grown on (001) $SrTiO_3$, (110) $DyScO_3$ and (001) $LaAlO_3$ substrates by pulsed laser deposition. Electronic and magnetic properties of the samples were characterized by XAS, XPS, neutron scattering and magnetometry measurements. Our results demonstrate that the ferromagnetism observed in $SrCoO_x/SrTiO_3$ can be suppressed and changed to antiferromagnetism in $SrCoO_x/DyScO_3$ through tensile strain. Further measurements on $SrCoO_x/LaAlO_3$ are currently on-going.

FM5

Experimental observations of grain-scale property coupling in electroceramics

J. Daniels

The University of New South Wales, NSW 2052, Australia

Fundamental understanding of electro-mechanical properties of ceramics requires detailed multilength-scale analysis methods. Previously, information of the grain-scale property coupling of elastic strain and domain switching behaviour under electric fields has been unobtainable from the bulk of an electro-ceramic material. Here, grain resolved scattering methods have been used to investigate the phase and domain structure of individual grains within bulk polycrystalline electroceramic samples under electric field. Example materials are chosen which undergo contrasting strain mechanisms including field-induced phase transformations, and ferroelectric/ferroelastic domain switching. The data obtained show that the grain orientation with respect to the applied electric field vector dictates both the induced phase and degree of domain texturing observed within a given grain. Such knowledge will be of potential benefit to the future engineering of high-strain actuators, but also has implications for all polycrystalline ferroic materials.

FM6

Gamma irradiation effect on optical and laser damage performance of KDP crystals

X. Yuan, W. Zheng

Research Center of Laser Fusion, China Academy of Engineering Physics, Sichuan, China

KDP (KH_2PO_4) is a nonlinear transparent dielectric crystalline material used in various laser systems for harmonic generation. It has been used for inertial confinement fusion in the National Ignition Facility, USA. However, the physical and chemical properties of the KDP crystals may degrade under γ and neutron radiations. Therefore, it is important to understand the effects of radiations on the optical properties especially laser induced damage performance during subsequent laser irradiation. In this work, the effect of Co60 gamma-ray irradiation on KDP crystal with the dose in a range from 1 kGy to 100 kGy is investigated using UV-Vis absorption, fluorescence, DC electrical conductivity, positron annihilation lifetime, and laser induced damage threshold (LIDT). A wide absorption band between 250 and 400 nm appears after γ-irradiation and its intensity increases with the increasing irradiation dose. The dc electrical conductivity of γ-irradiated KDP crystals increases with the increasing irradiation dose when the dose is less than 10 kGy while it remains constantly with the irradiation dose beyond 100 kGy. The increase of electrical conductivity is associated with the increase of proton defect concentration in the crystal and the related mechanism is discussed. The positron annihilation lifetime spectroscopy is also used to reveal the evolution of vacancy-type defects in KDP crystal. The decrease of LIDT and size of vacancy-type clusters with the increasing irradiation dose is also investigated.

FN1

Two-dimensional Coulomb gas at negative temperature

T. Simula

Monash University, Victoria 3800, Australia

Lars Onsager is perhaps best known as the recipient of 1968 Nobel Prize in chemistry and by his tour de force solution to the two-dimensional Ising model. However, his remarkable insight predicting the quantisation of vorticity in superfluid helium and the statistical mechanics description of two-dimensional turbulence have received much less attention. In this talk, I will briefly review certain aspects of the problem of two-dimensional turbulence with a particular emphasis on Onsager's statistical hydrodynamics model. I will then apply this model to turbulent superfluid Bose—Einstein condensates in which the quantised vortices have a long-range effective interaction and can be mapped to a two-dimensional Coulomb gas of positive and negative charged particles. By observing the dynamics of such vortex charges in numerical simulations we have found them to spontaneously arrange to large scale vortex clusters, coined Onsager vortices, that correspond to absolute negative Boltzmann temperatures [1]. I will discuss the microscopic mechanism leading to the emergence of such novel states of matter. Finally, I will outline the recent progress in Australia and elsewhere toward experimentally observing such states [2] with the prospect of realising Onsager's prediction of super vortices in two-dimensional fluid turbulence.

[1] "Emergence of Order from Turbulence in an Isolated Planar Superfluid", Tapio Simula, Matthew J. Davis, and Kristian Helmerson, *Physical Review Letters* **113**, 165302 (2014)

[2] "Vortex Gyroscope Imaging of Planar Superfluids", A. T. Powis, S. J. Sammut, and T. P. Simula, *Physical Review Letters* **113**, 165303 (2014)

FN2

Multimode photon-assisted tunnelling in superconducting quantum circuits

M. Woolley

The University of New South Wales, UNSW Canberra, Canberra, ACT 2600, Australia

Among the most exciting recent advances in the field of superconducting quantum circuits is the ability to coherently couple microwave photons in low-loss cavities to quantum electronic conductors [1]. These hybrid quantum systems hold great promise for quantum information processing applications, and they enable the exploration of new physical regimes of light-matter interactions. The physics of a tunnel junction illuminated by a purely classical microwave field has been understood since the 1960's with the classic work of Tien and Gordon [2]. This situation is equivalent to simply having an ac bias voltage across the conductor, and the resulting modification of the current is known as photon-assisted tunneling. Despite the word "photon" in the effect's name, in this standard formulation there is nothing quantum in the treatment of the applied microwave field. If the cavity is not driven, the cavity-plus-conductor setup realizes another well-studied quantum transport problem: dynamical Coulomb blockade (DCB) [3,4]. Here, the cavity acts as a structured electromagnetic environment for the junction, one that can absorb (and at non-zero temperature, emit) energy from tunnelling electrons. In stark contrast to standard DCB, in Ref. 5 we considered a non-equilibrium environment produced by preparing a microwave cavity in a non-classical ("quantum") state. The cavity effectively acts as an ac voltage bias across the conductor; by maintaining the cavity in a non-classical state, the junction is exposed to a non-trivial microwave field. We considered stationary, single-mode non-classical microwaves (e.g. squeezed states, Fock states), in the experimentally-relevant situation where a superconducting microwave cavity is coupled to a conductor in the single electron tunneling regime. We found that the conductor functions as a non-trivial probe of the microwave state: the emission and absorption of photons by the conductor is characterized by a non-positive definite quasi-probability distribution which is related to the Glauber-Sudarshan P-function of quantum optics. These negative quasi-probabilities have a direct influence on the conductance of the conductor, and the non-classicality of the microwave field may be inferred directly from features in the current-voltage characteristic. Here we consider the behaviour of a quantum conductor in the presence of stationary, but multimode, structured microwave field environments. We show how the statistics of these microwave fields, including their correlations and entanglement, impact the current and current noise of the coupled conductor. We describe how the statistics of the multimode microwave fields can be inferred through transport measurements alone.

[1] K. D. Petersson et al., *Nature* **490**, 380 (2012)

[2] P. K. Tien and J. P. Gordon, *Phys. Rev.* **129**, 647 (1963)

[3] M. H. Devoret et al., *Phys. Rev. Lett.* **64**, 1824 (1990)

[4] S. M. Girvin et al., *Phys. Rev. Lett.* **64**, 3183 (1990)

[5] J.-R. Souquet, M. J. Woolley, J. Gabelli, P. Simon, and A. A. Clerk, *Nat. Comm.* **5**, 5562 (2014)

FN3

Focusing of electrons and holes in semiconductors: from semi-classical dynamics to spintronics

S. Bladwell and O. Sushkov

The University of New South Wales, NSW 2052, Australia

The dynamics of charge carriers in spin-orbit coupled systems is a vital area of investigation for the extremely active field of spintronics. Controlling and manipulating the flow of electrons and holes serves as the foundation of an entire class of spintronic devices, most notably the Datta-Das spin transistor [1]. In this talk, I give an overview of the dynamics of charge carriers in such semiconductor systems, subject to external fields, in the context of magnetic focusing experiments. This experimental technique involves the coherent focusing of charge carriers over a scale of micrometers by a weak magnetic field, from an injector to a collector quantum point contact (QPC) [2][3]. I will present a detailed semi-classical theory for the focusing of both electrons and holes for general spin orbit interactions, and show that for the experimentally interesting case of polarization inducing in-plane magnetic fields, a significant change in the magnetic focusing spectrum is possible.

[1] S. Datta, and B. Das, *Appl. Phys. Lett*. **65**, 665 (1990)

[2] H. Van Houten}, C. W. J. Beenakker, J. G. Williamson, M. E I Broekaart, P. H. M . Van Loosdrecht, B. J. Van Wees, J. E. Mooij, C. T. Foxon, and J. J. Harris, *Phys. Rev. B* **39**, 8556 (1989)

[3] L. P. Rokhinson, V Larkina, Y. B. Lyanda-Geller, L. N. Pfeiffer, K. W. West, *Phys. Rev. Lett.* **93**, 146601 (2004)

FN4

Amplitude of charge density wave in cuprates

Y. Kharkov and O. Sushkov

The University of New South Wales, NSW 2052, Australia

Discovery of charge density wave (CDW) in the pseudogap phase is the most significant breakthrough in physics of cuprates in the past few years. The CDW has been reported in YBCO [1,2] and other cuprates [3,4] by several experimental groups. Even though the microscopic mechanism of CDW and its relation to superconductivity remains a puzzle, it is firmly established that CDW is incommensurate with ordering wave-vector laying in the Cu-O plane. Value of CDW wave-vector has been measured by X-ray diffraction and by RIXS. In YBCO CDW exist in the doping interval $0.09 \leq p \leq 0.13$ and the wave vector, $\boldsymbol{q}_{CDW} \approx (0,\ 0,\ 31)$ r.l.u., only very weakly depends on doping. The amplitude and the pattern ("s-wave" CDW versus "d-wave" CDW) of the CDW modulation is unknown and highly disputable in literature. The amplitude/pattern is the very important missing piece of information. In the present work we point out that the most recent data on nuclear quadrupole resonance [5] and on phonon dispersion anomalies [6] allow to determine the amplitude and also shed light on the pattern. We perform the corresponding analysis of the data and for the first time determine the amplitude of CDW. In the proposed talk we overview CDW experiments, explain the idea of our analysis, and for the first time report the value of the CDW amplitude.

2016

ABSTRACTS FOR POSTER SESSIONS

WP1

Porosity in Ge and $Si_{1-x}Ge_x$ Alloys Induced by Ion Implantation

H. Alkhaldi[a,b], F. Kremer[c], T. Bierschenk[a], J.L. Hansen[d], A. Nylandsted-Larsen[d], J.S. Williams[a] and M.C. Ridgway[a]

[a] *Department of Electronic Materials Engineering, Australian National University, ACT 2601, Australia.*
[b] *Physics Department, University of Dammam, Saudi Arabia.*
[c] *Centre for Advanced Microscopy, Australian National University, ACT 2601, Australia.*
[d] *Department of Physics and Astronomy, Aarhus University, DK-8000 Aarhus C, Denmark.*

Over the past two decades, nanoporous semiconductors such as Si, Ge and Si_xGe_{1-x} alloys have attracted remarkable interest in both fundamental research and industrial applications. Such materials can be used as filters [1], sensors [2], and as anodes for electric batteries [3]. Much research has focused on studying porosity in Ge, dating back to 1982 [4], where it was reported that irradiation-induced macroscopic swelling occurred in amorphous materials. A porous structure can be formed by using several ions species. A low fluence of 1015 ion/cm^2 can drastically change the surface morphology. Nanoporous structure is also sensitive to the temperature as reported by Stritzker [5] where a porous structure in Ge can be formed between -80°C to 200°C. Out of this range, there is no pore formation. However, the only study which investigated porosity in $Si_{1-x}Ge_x$ alloys is by Romano *et. al* [6] they found a porous structure at 90% of Ge, no porosity at lower Ge content. On the other hand this current research has observed a porous structure in $Si_{1-x}Ge_x$ alloys for $x \geq 0.77$ irradiation at room temperature. In the current work, we characterize the pore formation with respect to the implantation temperature and the alloy compositions. Multi characterization techniques have used including electron microscopy (TEM, and SEM), and optical profilometry.

[1] H. Föll, J. Carstensen, and S. Frey, "Porous and Nanoporous Semiconductors and Emerging Applications," *J. Nanomater*, 1-10 (2006)

[2] G. Kaltsas, A. Nassiopoulos, and A. G. Nassiopoulou, "Characterization of a silicon thermal gas-flow sensor with porous silicon thermal isolation," *Sens. J, IEEE*, **2**, 463-475 (2002)

[3] N. G. Rudawski, B. L. Darby, B. R. Yates, K. S. Jones, R. G. Elliman, and A. A. Volinsky, "Nanostructured ion beam-modified Ge films for high capacity Li ion battery anodes," *Appl. Phys.Lett*, **100**, 083111 (2012)

[4] B. R. Appleton, O. W. Holland, J. Narayan, O. E. Schow, J. S. Williams, K. T. Short, et al., "Characterization Of Damage In Ion-Implanted Ge," *Appl. Phys. Lett*, **41**, 711-712 (1982)

[5] B. Stritzker, R. G. Elliman, and J. Zou, "Self-ion-induced swelling of germanium," *Nucl. Instrum. Methods Phys. Res., Sect. B.* **175**, 193-196 (2001)

[6] L. Romano, G. Impellizzeri, L. Bosco, F. Ruffino, M. Miritello, and M. G. Grimaldi, "Nanoporosity induced by ion implantation in deposited amorphous Ge thin films," *J. Appl. Phys.* **111**, 5 (2012)

WP2

Synthesis and characterisation of $CoMoO_4$ nanospheres with improved supercapacitive performance

M. Barmi and M. Minakshi

Murdoch University, Murdoch, WA 6150, Australia

Electrochemical energy storage has been the main topic of interest in the recent years. The important features of electrochemical energy storage include low maintenance, excellent efficiency, cycling stability and environmental friendliness. There are ranges of candidates that can be employed as electrodes for supercapacitors [1-3]. Metal molybdate has attracted interest due to its electrochemical properties of the active metal ions in the chemically stable molybdate structure, and the pseudocapacitive and semiconducting nature of the material. In this work, $CoMoO_4$ materials were synthesised via a simple chemical synthetic route at 300^oC. The pure $CoMoO_4$ material showed rod shaped particles with weak redox reaction exhibiting specific capacitance of 23 Fg^{-1}. To enhance the supercapacitive behaviour of the pure material, urea and Pluronic F127 surfactant were added to the synthesis bath in separate attempts. Results showed that the addition of urea as a fuel can change the morphology from rod to nanosheet shape and as a result increase the capacitance to 47 Fg^{-1}. However, it was not suitable for cyclability. To further improve the specific capacitance and cyclability of $CoMoO_4$, urea was replaced by F127 surfactant, and significant change in morphology of the synthesised material was observed by obtaining nano sphere like particles. The specific capacitance of surfactant assisted $CoMoO_4$ resulted in 77 Fg^{-1}. Detailed results will be presented at the conference.

[1] Bao. F., Z.Z., Guo. W., Liu. X., *Electrochimica Acta*, **157**, 31-40 (2015)

[2] Liu. m. C., K.L.B., Ma. X. J., Lu. C., Li. X. M., Luo. Y. C., Kang. L., *New J. Chem.*, **36**, 1713-1716 (2012)

[3] Xu. K., L.W., Liu. Q., Li. B., Liu. X., An. L., Chen. Z., Zou. R., Hu. J., *J. Mater. Chem. A*, **2,** 4795-4802 (2014)

WP3

Electrolytic manganese dioxide from secondary sources for energy storage

A. Biswal[1], M. Minakshi[1] and B. Tripathy[2]

[1] *Murdoch University, Murdoch, WA 6150, Australia*

[2] *CSIR - Institute of Minerals and Materials Technology, Odisha 751013, India*

Recycling of material from secondary/spent catalysts is utmost essential in the present day [1]. A novel approach has been made to synthesize electrolytic manganese dioxides (EMD) from secondary sources2, such as manganese cake (EMDCake), manganese leach residue (EMDLR) and cobalt manganese bromide spent catalyst sludge (EMDCMBS). The synthesized materials were characterised using various physico-chemical techniques. X-ray diffraction pattern confirmed the presence of γ-phase in all the cases. TEM analysis suggests the presence of needle like grains within the range of 20 - 40 nm. Electrochemical characterisation carried out by galvanostatic charge-discharge technique revealed that the initial discharge capacity of EMDCake, EMDLR and EMDCMBS were 280, 267 and 240 $mAhg^{-1}$ respectively in 9M KOH in Zn/MnO_2 system. The chemical composition of the EMDs were determined and compared with the BIS standard3 (Bureau of Indian standard, 1996). All the materials found to be suitable for alkaline primary battery applications. The synthesized EMDs are quasi-reversible with continuous charge/discharge cycling.

[1] W. Zhang and Y. C. Chu, *Hydrometallurgy* **89**,137 (2007)

[2] A. Biswal, B. C. Tripathy, K. Sanjay, T. Subbaiah, and M. Minakshi, *RSC Adv*. **5** , 58255 (2015)

[3] Bureau of Indian Standard 1996, "Manganese dioxide for dry batteries", IS-11153

WP4

Do porosity templates improve the performance of supercapacitor electrode materials?

S. Albohani[1], D. Laird[2] and M. Minakshi[2]

[1] *Chemical Engineering and Chemistry, Murdoch University, Murdoch, WA 6150, Australia*

[2] *Murdoch University, Murdoch, WA 6150, Australia*

It is well recognised that to fully harness the potential of renewable energy generation, advances in materials to store and release that captured energy are required. Supercapacitors, with their fast charge-discharge rates, long life span, and high power density are one of the most promising targets for such applications. In order to maximise the performance of supercapacitors, electrode materials optimised to deliver high and stable capacitance as well as high conductivity over many charge-discharge cycles need to be developed. Recently mixed metal oxides have been investigated for this purpose as pristine transition metal oxides tend to be poor conductors. Binary transition metal oxides (BTMOs) are emerging as particularly intriguing novel material for the electrodes in these supercapcitors due to their wide potential window, superior conductivity, and improved stability [1,2]. One of the main issues with these materials is a relatively low surface area and physical deformations that can occur during the charge-discharge cycle. This could be alleviated by making these materials more porous and the actual pore size and distribution may be controllable using a template during the synthesis of the electrode material. We have investigated the use of nickel molybdate ($NiMoO_4$) and two different soft-templating agents - naturally sourced eggshell membranes and fully synthetic polymethylmethacrylate (PMMA) – as electrode materials for supercapacitor applications. The egg shell membrane provides a fibrous random template while the PMMA is considered a more regular arrangement which we postulated would lead to differences in pore size and distribution throughout the synthesised material. $NiMoO_4$ electrode material with and without a pore template was synthesised from simple salts by a solvothermal combustion synthesis method. The electrochemical properties of the resulting materials revealed that $NiMoO_4$ synthesised with eggshell membrane as a template showed superior performance to both non-templated material and that using a PMMA template. The best performing material had a specific capacitance of 260 Fg^{-1}, four times greater than that of non-templated material, when tested with a two electrode cell configuration in 2M NaOH electrolyte. The superior electrochemical performance of the eggshell templated material will be discussed with respect to differences in the surface chemistry and mesoporosity of the templated material.

[1] Senthilkumar *et al RSC Advances* **3**,352 (2013)

[2] Zhang *et al. J. Mater. Chem. A*, **3**,43 (2015)

WP5

Multigelator organogels-mixture of gelators assembled by different driving forces

J. Chen[1] and J. Li[2]

[1] *Institute for Frontier Materials, Deakin University, Geelong, Victoria 3220, Australia*

[2] *Deakin University, Geelong, Victoria 3220, Australia*

In this study, an organogel composed of two low molecular weight gelators with distinct structures has been studied. One of the gelators is the derivative of anthracene with fluorescence, the other is based on glutamic acid. The gelation process and the structure of the self-assembled fibres have been studied with optical microscopes, differential scanning calorimeter (DSC), and rheometer. The two gelators form gel in dimethyl sulfoxide (DMSO) individually, meanwhile the composite gels exhibit unique feature both in structure and in properties. With NMR spectroscopy and FTIR, the interaction between the molecules has been investigated in detail. All the results show that the two gelators self-sort during the gelation. The great contrast in structure of the two gelators demonstrated that their self-assemble was bonded by different intermolecular forces.

WP6

In situ characterisation of calcium carbonate prenucleation clusters around the solubility limit using Small Angle X-ray Scattering technique

J. Avaro and A. Rose

Southern Cross University, East Lismore, NSW 2480 Australia

In the classical nucleation theory, a mineral will form in supersaturated solution by the random collision of dissolved ions to yield transient clusters through a dynamic and reversible process. Random addition of dissolved ions eventually causes a "critical cluster" size to be reached, at which point the process becomes essentially irreversible and the first mineral crystal is considered to have formed. Nevertheless, it has been proven that calcium carbonates don't follow this theory. Instead, its abiotic precipitation proceeds by a novel mechanism involving formation of nanoparticle, between 1 and 250 nm in size and thermodynamically stable in under and supersaturated solution ($\Omega < 1$ and $\Omega > 1$). However, in situ studies aiming to characterise these nanoparticles have always been undertaken in highly oversaturated and simplistic conditions. Moreover, the exact role as well as their physical and chemical characteristics remains poorly understood. Here we've combined SAXS technics with an ultra-fast mixing device in order to acquire high quality data at extremely short reaction times (estimated < 1ms) representing the very early stage of calcium carbonate nanoparticles formation. With these technics we've been able to characterise the size and shape of these nanoparticles around the solubility limit ($\Omega < 1$ and $\Omega > 1$), varying pH.

WP7

Terahertz Characterisation of 3D Printed Plastics

J. Colla, A. Squires and R. Lewis

University of Wollongong, Wollongong, New South Wales 2522, Australia

Spectra of 3D printed plastics are presented. The recent surges forward in 3D printing technology has seen its application to a wide variety of fields from healthcare to art. Typically users are interested in the mechanical properties and uses of 3D printed objects however we explore the potential of optical properties and uses. In this work 20 commercially available plastics have been characterised. These include five Nylon samples, three PET based samples, two polycarbonate samples, two metallised plastics, polystyrene, polypropylene and six other common commercial 3D printing plastics. The samples were created with a commercial 3D printer (Makerbot Replicator 2X). Samples have been analysed by Time Domain Spectroscopy (TDS) and Fourier Transform Spectroscopy (FTS). The combination of equipment used allowed us to observe the transmission of each plastic from 0.2 to 180THz. This region typically referred to as terahertz (THz) is of particular interest to us. THz has many applications including non-destructive material characterisation, product monitoring in industry and security imaging [1]. Some characterisation of 3D printed plastics has been undertaken and shows room for exploration in the area [2]. 3D printing allows a laboratory to have a method to very quickly and cheaply fabricate optics for various uses. Previously it has been demonstrated that 3D printed plastics are suitable for use when creating aspherical THz lenses and diffraction gratings [3]. Other applications in the THz region that hold great potential include waveguides and polarisers, which rely on the reflectivity of the materials used. Many plastics present a usable transmission window in the 0.2 – 1 THz range. In particular, the nylon based samples and polyethylene based samples displayed very consistent spectra across manufacturers, despite the various additions made to facilitate printing. Polypropylene was very transmissive however very difficult to print with. The polycarbonate samples were found not only to be the best to print with, but also had a consistently low absorption coefficient, less than 10 cm^{-1}. We observe good agreement when comparing overlapping regions of spectra obtained from different equipment. As expected, most plastics displayed a very low (<1%) transmission through the 2 – 20 THz range. Noteworthy are the conductive plastics, which have an extremely low transmission; however, they may present a viable alternative to metal plating 3D printed optics in order to obtain usable reflectivities. Reflection data is also presented for this range. We aim to understand the physical properties of these materials and further explore the practical capabilities. 3D printing of THz optics is certainly viable and will continue to become more so as 3D printing technology continues to advance.

[1] R. A. Lewis, *Terahertz Physics*, (Cambridge: Cambridge University Press, 2012)

[2] Busch, S. F., Weidenbach et. al "Optical Properties of 3D Printable Plastics in the THz Regime and their Application for 3D Printed THz Optics" *Journal of Infrared, Millimeter, and Terahertz Waves* **35**(12) 993-997 (2014)

[3] Squires, A. D., Constable, E. & Lewis, R. A. "3D printed terahertz diffraction gratings and lenses" *Journal of Infrared, Millimeter, and Terahertz Waves*, **36**(1), 72-80 (2015)

WP8

THz Spectroscopy of Artists' Pigments, Binders and Canvas

A. Squires[1], M. Kelly and R. Lewis

University of Wollongong, Wollongong, New South Wales 2522, Australia

Recent developments in Terahertz (THz) radiation open up applications in non-destructive and non-invasive analysis of artworks of cultural significance. This spearheads large interest in areas such as conservation science [1]. This arises due to favourable THz characteristics, which show large transmission for materials such as paints and plastics, as well as biological materials such as wood [2]. We present data using THz radiation to analyse a series of canvas substrates, binders and paint pigments used in artistic paintings with cultural significance. These were acquired using z-omega Z2 and Advantest TAS7500 Spectrometers utilising Time Domain Spectroscopy (TDS). Our studies cover a 0.1 – 7 THz range. We investigate canvas including polyester, cotton and linen with raw material and preparation mediums such as priming agents present in the canvas weave. The binders cover multiple constituents including oils (linseed, poppy, walnut and safflower), varnishes, fat, acrylics and waxes. We explore 47 pigment samples consisting of organic and metallic based grounds including iron, carbon, cadmium and zinc. Canvas samples exhibit a large number of features, most likely of phonon origin, in the 0.1 – 7 THz range. Polyester canvas shows an absorption at 3.4THz. Coarse Linen exhibits a sharp absorption at 2.4THz in conjunction with a broad absorption at 1.6THz. Cotton Duct canvas displays two broad absorptions at 1.2 and 2THz. Belgian Linen primed with oil was featureless, however, when primed with clear glue two broad absorptions develop at 1.6 and 2.8THz. Thus different canvas and preparation processes are distinguishable by THz radiation. Binders were likewise found to show unique spectra. The natural oil binders presented broad features in one of (or both) a 2 - 2.3 THz region and 3.1 - 3.3 THz region. Despite this, relative shifts between the features and the absence of some features conserve distinctiveness to individual spectra. Two wax binders measured were indistinguishable with no appreciable features. Acrylics, fats and varnishes showed combinations of sharp features at 2THz and near 3THz with various broad absorptions across the range, all of which are unique. Pigment samples investigated in the 0.1 – 1 THz region illustrate identification capabilities between optically identical pigment colour obtained from different suppliers, for example, the Blauw extra, Blauw Donker and Hollands Blauw pigments. Pigments of different raw constituents, such as zinc, cadmium, carbon and iron are also identifiable. Our results show unique and distinguishable spectra, especially for canvas materials and binding agents. This 'finger print' for each spectrum is desirable as it validates applications of THz radiation in identifying constituent materials used in paintings. This is especially relevant to older pieces where information about the painting materials and process have been lost over time.

We thank the Australian Research Council and the UOW Global Challenges program for support.

[1]. J. B. Jackson *et. al*, "A Survey of Terahertz Applications in Cultural Heritage Conservation Science," *Terahertz Science and Technology, IEEE Transactions on*, **1**, 220-231 (2011)
[2]. R.A. Lewis, "Terahertz Physics" (Cambridge: Cambridge University Press, 2012)

WP9

Steels and intermetallics under extreme conditions

K. Liss[1], A. Shiro[2], R. J. Dippenaar[3], K. Akita[4], K. Funakoshi[5], M. Reid[1], H. Suzuki[2]
T. Shobu[2], Y. Higo[5], H. Saitoh[2], S. Zhang[4] and Y. Tomota[6]

[1]*ANSTO, Lucas Heights, NSW 2234, Australia*

[2] *QuBS, Japan Atomic Energy Agency, Japan*

[3] *University of Wollongong, Wollongong, NSW 2522, Australia*

[4] *CROSS-Tokai, Research Centre for Neutron Science and Technology, Japan*

[5] *SPring-8, Hyogo Prefecture 679-5148, Japan*

[6] *Department of Materials Science and Engineering, Ibaraki University, Ibaraki Prefecture 310-0056, Japan*

Materials are being designed and engineered for ever superior mechanical and operational properties, such as steels for lighter cars and energy-absorbing behaviour in an accident, and titanium aluminides for lighter airplane turbine blades. The manufacturing of such materials may involve processes at extreme conditions, under high pressure or high temperature. Examples are high-pressure torsion and near net-shape forging. Therefore, it becomes eminently important to know and understand the phase diagrams of such materials at extreme conditions. Structural changes may open processing windows, while elevated mechanical properties are conserved under less extreme conditions. Here, we present first phase diagram studies on high-manganese steels and on titanium aluminides by in-situ synchrotron X-ray diffraction in a large-volume cell.

WP10

Improved Micro-CT of SiC/SiC Ceramic Matrix Composites

J. Thornton[1], M. Zonneveldt[1], B. Arhatari[2], J. Kimpton[3], M. Sesso[4], S. Kim[4], C. Hall[3]

[1]*DST Group, Fishermans Bend, Victoria 320, Australia*

[2] *La Trobe University, Victoria 3086, Australia*

[4] *Australian Synchrotron, Clayton 3168, Victoria, Australia*

[5] *Swinburne University of Technology, Hawthorn, Victoria 3122, Australia*

Ceramic matrix composites composed of silicon carbide fibres in a silicon carbide matrix (SiC/SiC) are being introduced into gas turbine engines. Their introduction will increase engine thrust by allowing high operating temperatures and also reduce weight. Unlike monolithic ceramics they are effectively tough with elastic energy being consumed in fibre pull-out during crack propagation. However, much work still needs to be done before these materials are fully understood. The authors have been mapping the crack propagation in SiC/SiC using micro-CT and in-situ mechanical loading. Bright synchrotron X-ray sources were used to provide the intensity to map the crack propagation in practical times. One run was performed using the IMBL using 25 keV X-rays, and a second using the powder diffraction beam line at 15 keV. The first run showed fibre pull-out but failed to resolve the effects of the fibre coatings. The use of 15 keV improved the image quality and enabled fibre coatings to be resolved. The poster will compare the two experimental set-ups and the two sets of images and discuss what factors contributed to the improvement in image quality. Ideas for further improvements will also be presented.

WP11

Mechanical meta-materials: beyond conventional property limits

L. Wang and J. Daniels

The University of New South Wales, NSW 2052, Australia

Meta-materials have attracted significant interests over the past decades due to their unique properties for industrial applications. Some meta-materials, such as Sn-$BaTiO_3$ (BT)[1, 2], ZnAl-$BaTiO_3$ [3, 4] (Metal matrix composites), are classed as metal matrix composites (MMCs) and have been demonstrated to have ultra-high stiffness due to the inclusion of BT particulates which undergoes a volume-change phase transformation. The mechanism responsible for this is derived from a constraint caused by the metal phase that surrounds the BT particulates in MMCs. The stress state of the two phases and their interaction under the combination of stress and thermal sources have also been revealed based on high energy X-ray diffraction measurement of bulk samples [5]. By using thermally mismatched materials, the two phases will behave differently during cooling process, resulting in a constraint on the ceramic particulates. Under this condition, the ceramic particulates will as expected store elastic energy at an equilibrium state. When non-equilibrium state presents during phase transformation, the stored energy will be released and this state will also be stabilized by the constraint from surrounding metals. Given the sufficient large energy stored in the inclusion, it may drive the composite to display ultra-high or even negative stiffness when an external stress is applied. However, restrictions remain in MMCs due to the limited temperature range over the stress-induced phase transition in BT inclusion. Our work will try to explore the mechanism of the structural coupling between the two phases based on BT encapsulated MMCs and provide an insight for broadening this limited temperature range by changing the negative stiffness inclusion. Ex-situ mechanical measurements on BT have been performed at various frequencies. By doing this, the mechanical behaviour of BT will be directly observed and confirmed and is essential for identifying the related elastic properties in MMCs.

[1] Jaglinski, T., et al., "Composite materials with viscoelastic stiffness greater than diamond" *Science* **315**, 620 (2007)

[2] Jaglinski, T.M.L., R. S.,"Negative stiffness and negative poisson's ratio in materials which undergo a phase transformation" Adaptive Structures: Engineering Applications, Wiley **(**2007)

[3] Dong, L., D.S. Stone, and R.S. Lakes, "Extreme anelastic responses in $Zn_{80}Al_{20}$ matrix composite materials containing $BaTiO_3$ inclusion" *Scripta Materialia* **65**(4), 288-291 (2011)

[4] Jaglinski, T. and R.S. Lakes, "Zn-Al-based metal-matrix composites with high stiffness and high viscoelastic damping" *Journal of Composite Materials*, **46**(7), 755-763 (2012)

[5] Daniels, J.E., et al., "Phase transformation of constrained $BaTiO_3$ particles in a Sn matrix" *Scripta Materialia*, **61**(4), 391-394 (2009)

WP12

Curing of large size construction for space exploitation

A. Kondyurin

School of Physics, The University of Sydney, Sydney, NSW 2006 Australia

Space exploitation is impossible without large space structures. We need to make sufficient large volume of pressurized protecting frames for crew, passengers, space processing equipment, & etc. We have to be unlimited in space. Now the size and mass of space constructions are limited by possibility of a launch vehicle. It limits our future in exploitation of space by humans and in development of space industry. Large-size space construction can be made with using of the curing technology of the fibers-filled composites and a reactionable matrix applied directly in free space. For curing the fabric impregnated with a liquid matrix (prepreg) is prepared in terrestrial conditions and shipped in a container to orbit. In due time the prepreg is unfolded by inflating. After polymerization reaction, the durable construction can be fitted out with air, apparatus and life support systems. Our experimental studies of the curing processes in the simulated free space environment showed that the curing of composite in free space is possible. The large-size space construction can be developed. A project of space station, Moon base, Mars base, mining station, interplanet space ship, telecommunication station, space observatory, space factory, antenna dish, radiation shield, solar sail is proposed and overviewed.

The study was supported by Humboldt Foundation, ESA (contract 17083/03/NL/SFe), NASA program of the stratospheric balloons and RFBR grants (05-08-18277, 12-08-00970 and 14-08-96011)

WP13

Polyurethane medical implants improved by plasma immersion ion implantation

I. Kondyurina[1], B. Bao[1], A. Kondyurin[2] and M. Bilek[2]

[1] *School of Medicine, The University of Sydney, Sydney, NSW 2006 Australia*

[2] *School of Physics, The University of Sydney, Sydney, NSW 2006 Australia*

Polyurethane is used in medicine for permanently implanted devices due to its elasticity, mechanical strength, biostability, biocompatibility and hemocompatibility. However, the immune system recognises polyurethane as foreign and initiates an immune response that can result in a range of negative consequences as foreign body rejection, inflammation, pain and dysfunction of the implant. We use plasma immersion ion implantation for activation of the polyurethane surface to facilitate covalent binding of a biologically active protein layer and report on the results in application relevant assays. A polyurethane composition with mechanical properties adjusted to soft tissue was developed to match the mechanical properties of the vasculature and ensure suitability for surgical suture. Plasma immersion ion implantation was performed to active the surface. Mechanical properties of the structures were characterised with tensile testing whilst the chemistry and morphology of the surfaces were characterised by AFM, FTIR and XPS spectroscopy. The activated surface was then used to covalently immobilise bioactive protein molecules directly from solution. The immobilised protein layers were characterised with ELISA. The effects on cell adhesion in-vitro and on cellular responses in a mouse model of the ion treated materials both with and without protein immobilised will be reported.

WP14

In-situ diffuse scattering experiment on stress-induced ferroelastic transformation in Ti-15Nb-2.5Zr-4Sn

E. Obbard[1], R. Burkovsky[2], H. Wang[3] and Y. Hao[3]

[1] *Department of Electrical Engineering and Telecommunications, The University of New South Wales, NSW 2052, Australia*

[2] *St. Petersburg State Polytechnical University, St. Petersburg, Russia*

[3] *Shenyang National Laboratory for Materials Science*

Research to optimize the biocompatibility of titanium alloys for orthopaedic applications focusses on minimizing the Young's modulus of quenched, β-phase (Im-3m) titanium by adjusting the concentration of β-stabilizing elements. Ti-15Nb-2.5Zr-4Sn has the lowest Young's modulus yet measured in any forged titanium alloy of less than 50 GPa. This composition also possesses a controllable thermal expansion coefficient that is influenced by prior plastic deformation and it is superelastic over a very wide temperature range. There is pronounced non-linear elasticity and asymmetric response to strain, associated with the stress induced, ferroelastic transition between the bcc β-phase and α" (Cmcm) martensite phase. The potential to tailor these remarkable properties to specific applications, as well as further progress in superelastic alloy development require a clear microscopic understanding of the underlying physical effects. Therefore, to investigate these "pre-martensitic" phenomena and quantitatively explain the non-linear elastic responses we carried out in-situ measurement of β-phase Ti-15Nb-2.5Zr-4Sn single crystals on ESRF beamline ID15B, equipped with a large position-sensitive detector and rotating load rig, that allows single-crystal x-ray scattering measurements with crystals as thick as several millimetres with simultaneous application of compressive or tensile stress. The results give a detailed picture of the large bcc crystal as it approaches and progresses through the structural transformation. Domains of ferroelastic α" and also ω instabilities form in response to the temperature and the direction and magnitude of the applied stress. We present these results and discuss some of the challenges of developing a quantitative interpretation of the data, an important one being how to properly treat coupling between elastic deformation and correlated structural distortions.

WP15

Prodrug Amphiphile Nanoparticles of Gemcitabine and 5- Fluorouracil

J. Bulanadi[1], M. Moghaddam[1], A. Xue[2], S. Julovi[2], S. Bal[1], X. Gong[1], R. Smith[2]

[1] *CSIRO Materials Science and Engineering, CSIRO, North Ryde, NSW, Australia*

[2] *Kolling Institute of Medical Research, University of Sydney, Sydney, NSW 2006 Australia*

Prodrug analogues of the chemotherapeutic drugs gemcitabine and 5-fluorouracil have been developed in order to overcome the severe systemic toxicity and limitations often associated with these types of drugs such as lack of selectivity, high toxicity, low bioavailability, poor pharmacokinetic profiles, and low stability. Prodrug modification was achieved through the covalent attachment of hydrophobic chains to the hydrophilic drugs which conferred amphiphilic properties onto the prodrugs. The amphiphilic nature of the prodrugs allows for the self-assembly into nanostructured particles when dispersed in water. This effectively fuses the concept of the prodrug and sustained targeted delivery systems into high payload prodrug nanoparticles. A series of gemcitabine prodrug amphiphiles with varying hydrophobic chains were synthesized and characterized for their molecular structure and purity, using 1H – NMR, ESI – MS and HPLC. The thermal stability profiles of the prodrug amphiphiles were determined using TGA and DSC analysis. The gemcitabine prodrugs were incorporated within the membrane of a synthetic high density lipoprotein constructed from a combination of phospholipids and cholesterol due to its inability to self-assemble into stable lyotropic liquid crystalline nanostructures without the assistance of a matrix lipid. The physicochemical properties of the gemcitabine high density lipoproteins have been assessed using cryo-TEM, dynamic light scattering and synchrotron SAXS, indicating that these high density lipoproteins formed liposomal particles and of ~120 nm in size. The prodrug nanoparticles efficacy in vitro have been assessed through cell proliferation assays which have shown superior cytotoxicity compared to the naked drug alone. Preliminary in vivo experiments to evaluate localization of the nanoparticle and antitumour efficacy on a pancreatic cancer cell-derived animal model in NOD/SCID mice have also been conducted and have shown superior efficacy compared to gemcitabine. In order to enhance the efficacy of the nanoparticle treatment and utilize the benefits of multidrug treatments, the gemcitabine prodrug amphiphile has also been combined with a 5-fluorouracil prodrug amphiphile, resulting in a dual drug nanoparticle. The physicochemical properties of this nanoparticle were also determined using the same techniques, as well as their efficacy assessed in vitro and in vivo. The results thus far indicate the potential of the gemcitabine and 5-fluorouracil prodrug amphiphiles as promising nanomedicinal chemotherapeutics.

WP16

Spin-polarized single and double electron spectroscopies

J. Williams and S. Samarin

Department of Physics, University of Western Australia, Crawley, WA 600, Australia

Spin-polarized single- and two-electron reflection spectroscopies with various kinematics for W(110) and W(100) crystals, with deposited thin films of Co, Fe, and/or Ag, reveal many aspects of structure and scattering asymmetries [1-5]. The experimental apparatus and methodology are a subset of the time-coincidence pulsed two electron scattering approach [2] in which the experimental variables include the incident electron energy and spin, the outgoing electron momenta and single or multilayered film structures.

Discussions will include extensive recent results which highlight electron correlations in exchange and spin-orbit interactions with spin and scattering dynamical asymmetries. For example, the emission of correlated electron pairs from Au(111) and Cu(111) surfaces with incident low-energy electrons indicates the contributions of surface states, d-states and spin effects [3]. The controlling spin-orbit interaction in a ferromagnetic Fe/Au double layer has been characterized [4]. Spin-dependent elastic electron scattering, from W(110) modified by irradiation with 200 eV argon ions to induce lattice defects, indicates a possible way to construct a spin-active interface with prescribed properties [5]. Further, a spin-dependence of plasmon excitations in Ag/W and Ag/Fe layers may be attributed to spin-active Ag/W or Ag/Fe interfaces.

The experimental measurements and their interpretations are guided by the following specific fundamental features of electron scattering from clean surfaces. The presence of the crystalline surface implies that the parallel-to-the-surface electron momentum is conserved. Refraction of the electron trajectories at the surface potential barrier occurs while passing through the interface. An ordered distribution of scattering centres at the surface implies that electrons (or electron pairs) undergo a diffraction. Imbalance of spin-up and spin-down electrons in the valence band in a ferromagnetic surface leads to the intensity asymmetry of spectra. The spin effects depend strongly on kinematics of scattering. The measurements are characterized geometrically by fixed angles between the incident electron beam and the axis of the detectors (analyzers) and the sample rotated around the axis perpendicular to the scattering plane containing the electron beam and detectors. Then the angles of incidence and detection can be varied conveniently.

Generally the SPEELS measurements are made with (i) specular geometry, when the incidence angle is equal to the detection angle; and (ii) off-specular geometry when the incident angle is not equal to

the detection angle. It is assumed that in the specular geometry the mechanism of the electron energy loss is of dipole type, i.e. the energy loss does not involve a large momentum transfer and the interaction of the incident electron with the surface occurs through the electromagnetic field generated by the electron. In the second case, the off-specular geometry, the electron-electron encounter occurs with substantial momentum transfer from the incident electron to the valence electron of the target. It is also assumed that in the dipole-type of scattering no exchange effects can be observed.

WP17

Structures of Silane SAMs on Oxide Surfaces

A. Magerl[1], H. Steinrück[2], M. Deutsch[3], B. Ocko[4]

[1] *University Erlangen-Nürnberg, Staudtstrasse 3, 91058 Erlangen, Germany*

[2] *SLAC National Accelerator Laboratory, Menlo Park, California 94025, USA*

[3] *Bar-Ilan University, Ramat Gan 5290002, Israel*

[4] *Brookhaven National Laboratory, Upton, New York, USA*

While the structure of thiols on crystalline gold is dominated by the strong covalent bond between gold and sulfur atoms promoting an epitaxial coverage, the situation is much more delicate for silanes on crystalline or amorphous oxide surfaces due to the complex headgroup-surface interaction competing with the chain-chain interaction. By synchrotron X-ray reflectivity and grazing incidence diffraction we have obtained a hitherto unknown detailed picture of the structural relations between SAMs and substrate. These feature a novel rotational epitaxial relationship in case of a crystalline oxide surface. A full account of the structure in case of the amorphous native oxide of silicon calls for an oxygen depleted layer at the Si/SiO_2 junction. In both cases cross-linking between the head groups is a salient structural feature.

WP18

Biocompatible magnesium based ultrastable metallic glass (SMG) thin films

S. Gleason[1], K. Laws[1], J. Jiang[2] and M. Ferry[1]

[1] *School of Materials Science and Engineering, The University of New South Wales, NSW 2052, Australia*

[2] *Zhejiang University, Hangzhou, Zhejiang, 310027, China*

Ultrastable metallic glass (SMG) thin films of magnesium based biocompatible alloys are produced via physical vapour deposition (PVD) techniques. SMG thin films are achieved via refinement of PVD power, pressure, and substrate temperatures. The SMG thin films display improved thermal and kinetic properties differentiating them from similar tradition bulk quenched or vapour deposited alloys. Other material properties are also enhanced or modified.

WP19

Epitaxial Growth of Spinel Iron Vanadate Thin Films on Perovskite Substrate

D. Zhou[1], Y. Zhou[1], N. Valanoor[1], Q. He[2] and Y. Chu[2]

[1] *School of Materials Science and Engineering, The University of New South Wales, NSW 2052, Australia*

[2] *Department of Materials Science and Engineering, National Chiao Tung University, Hsinchu City, Taiwan 300*

Epitaxial spinel FeV_2O_4 (FVO) films of ~ 80 nm thickness were grown on (001) $SrTiO_3$ (STO(001)) substrates by pulsed laser deposition (PLD) technique. By using in-situ RHEED, we find that FVO grows in an island growth mode with a spot-like RHEED pattern observed. Both the X-ray diffraction (XRD) and transmission electron microscopy (TEM) analysis showed that the FVO film have a single-phase spinel structure and is epitaxially cubic on cubic grown on STO(001) substrate. With a 7% lattice mismatch between bulk FVO and STO, Moire fringes along the interface were observed from the film cross-section TEM images, which indicates that the FVO/STO film have a semicoherent-type interface. The NT1 (~120 K) and NT2 (~45 K) were observed in the magnetization-temperature measurement via superconducting quantum interference device (SQUID). The X-ray magnetic circular dichroism (XMCD) and X-ray absorption spectroscopy (XAS) analysis confirmed that the valance status of the Fe and V ions of the spinel oxide FVO film are divalent and trivalent, respectively, as well as the antiparallel arrangement of the Fe and V spins below the NT1 (~120K).

WP20

Fingering instability in solid state dewetting of single crystal Ni films

S. Jahangir[1], N. Valanoor[1], C. Thompson[2] and G. Kim[2]

[1] *School of Materials Science and Engineering, The University of New South Wales, NSW 2052, Australia*

[2] *Massachusetts Institute of Technology, Cambridge, Massachusetts, United States*

Metallic thin films have high surface to volume ratio, which makes them thermodynamically unstable. By annealing the film to reduce this extra surface energy capillary forces drive the film to undergo dewetting and alters the 2D structure of the film to 3D micro/nano-islands depending on the initial film thickness. In case of single crystal films dewetting results into formation of more regular 3D structures such as arrays of nano/micro wires or islands. Dewetting from an artificial edge begins with formation of a rim which is thicker than the original film, due to pile up of atoms from triple line to top of the film edge. The rim height may change in time due to combination of a few mechanisms such as Rayleigh-like instability, these local height differences can promote different retraction velocity that leads to formation of a specific morphology, called "fingering instability". We have studied fingering instability in patterned single crystal Ni films grown on MgO substrate, to do so we have used in-situ high temperature confocal laser microscope which provides real time observation of dewetting process, in addition to ex-situ microscopy techniques such as SEM and AFM. We report anisotropic behaviour of fingering in (110) Ni film, as they just form along kinetically unstable edges. The retraction rate of fingers and periodic finger spacing are both function of the temperature, however retraction rate has stronger dependency to the temperature. Fingers propagating from an initially flat film edge have a characteristic spacing of what we call "natural finger spacing"; however by pre-patterning the flat edge, fingers will follow the wavelength of the induced pattern if the wavelength is close enough to the natural fingering spacing.

This work was supported by ACS Petroleum Research Fund. N.V thanks support from ARC Discovery Project. S.J acknowledges support from Australian Postgraduate Award as well as Baxter Family Scholarship.

WP21

Modelling TiO_2 supported Au cluster photocatalyst using DFT and SCC-DFTB approaches

L. Junda[1], G. Metha[1] and S. Irle[2]

[1] *The University of Adelaide, Adelaide, SA 5005, Australia*

[2] *Nagoya University, Japan*

Photocatalysis, which exploits the use of clean and infinite solar energy, has the potential to be one of the most influential solutions to green and sustainable chemistry. Titanium dioxide-based catalysts have shown great capability in photocatalysis due to its non-toxic, stable and highly active properties. However, the reaction efficiency is still too low for practical applications. To address this issue, co-catalysts can be introduced to the photocatalysis system. Nobel metal nanoparticles supported on semiconductors can provide reaction sites, take part in charge separation and transportation thus significantly improving the photo-reactivity. Metal clusters have recently been shown to also act as co-catalysts in photocatalytic systems. Metal clusters can have completely different physical and chemical properties due to their size effects; they have higher surface-area-to-volume ratio than normal metal materials and have demonstrated ability to lower activation barriers by enabling new reaction pathways for reaction. Thus, metal clusters have great potential as co-catalysts in photocatalytic systems. Density Functional Theory (DFT) is used to investigate the structure and photocatalytic activities of binary photocatalysts made up of Au clusters supported on TiO_2. Compared to ab initio quantum mechanical methods, DFT is more effective when performed carefully with proper benchmarking. However, in order to simulate realistic Au cluster-TiO_2- photocatalysts, an extraordinary large model, which is beyond the capability of DFT needs to be simulated. This poster will present early results work utilizing Self-Consistent Charge Density Functional Tight-Binding (SCC-DFTB) calculations. DFTB parameters are developed for the Au-TiO_2 photocatalytic system using automatic DFTB parameterization code. A comparison will be made between DFT calculation and DFTB of structural and energy properties.

WP22

Photoconductivity of nanoscale grain boundaries in two dimensional ZnO platelets

N. Faraji Ouch Hesar

The University of New South Wales, NSW 2052, Australia

The response of individual grain boundaries in polycrystalline ZnO platelets to light illumination on the nanoscale is studied using scanning probe based techniques. While many previous studies show the UV responses of ZnO, we find that even in the visible light range below the bandgap grain boundaries are sensitive to light, which is attributed to defect accumulation and local changes of the band structure at the grain boundaries.

WP23

A novel method for the preparation of a monolithic alumina catalyst support

M. H Amin[1], S. K. Bhargava[1], J. Patel[2] and M. Mazur[3]

[1] *CAMIC, RMIT University, Melbourne, VIC 3001, Australia*

[2] *CSIRO Energy, Clayton, Melbourne, VIC 3169, Australia*

[3] *RCAM, RMIT University, Melbourne, VIC 3001, Australia*

First used to facilitate oxidation reactions in 1800s, heterogeneous catalysts now play important roles in many other catalytic processes, such as hydrocarbon reforming, polymerization, hydrogenation, dehydrogenation, long-chain hydrocarbons cracking and isomerization reactions. Nowadays, heterogeneous catalysis is the core of most modern conversion processes in the natural gas reforming, petrochemicals manufacture and oil refining sectors. Recently, there has been considerable interest in the development of more efficient catalysts able to operate efficiently under severe reaction conditions. Catalyst stability is a key challenge in this area. One of the main components of many heterogeneous catalyst systems is an inorganic support. Such supports often play a key role in the performance of the catalysts. Alumina is one of the most frequently used catalyst supports, due to its thermal stability and high specific surface area. Enhancing the catalytic performance of catalysts by modification of the micro and macro structure of the alumina support has been the focus of numerous studies. Alumina monoliths represent an attractive alternative to conventional supports in some applications, in particular, those which involve high flow rates. Monolithic ceramic supports are typically produced by injection moulding techniques; however such processes are not suited to materials with low plasticity, such as alumina. In this study, a novel process was developed to enable the manufacture of a monolithic alumina support by combining 3D printing with an aqueous gelcasting method. A sacrificial resin mold, produced by 3D printing and gelcasting was employed to form a green body through polymerization of an aqueous slurry. The slurry was prepared using acrylamide as an organic monomer, N, N ‘- methylenebisacrylamide as a cross-linking agent, ammonium persulfate as initiator, sodium silicate as dispersant and N,N,N,N-tetramethyl ethylenediamine ($C_6H_{16}N_2$,TEMED) as the catalyst. The optimum amounts of monomer, initiator, catalyst, cross-linking agent and dispersant was identified and the effect of various operating variables, such as the milling time and the drying method, were studied.

WP24

Refractive index of graphite and graphene at wavelengths spanning the carbon K edge

H. Wahab[a], C. Jansing[b], H.-Ch. Mertins[b], S.-H. Choi[c] and H. Timmers[a]

[a] *School of Physical, Environmental and Mathematical Sciences, University of New South Wales in Canberra, PO Box 7916, Canberra BC 2610, Australia.*

[b] *Department of Engineering Physics, Münster University of Applied Science, Stegerwaldstraße 39, Steinfurt, Germany.*

[c] *Department of Applied Physics and Institute of Natural Sciences, Kyung Hee University, Yongin 446-701, Korea.*

Due to the resonantly enhanced birefringence of graphite and graphene across the carbon 1s absorption edge, these materials may open up new avenues for optical devices such as x-ray halfor quarter-wave plates. Such applications, however, require the knowledge of the refractive index across the carbon 1s absorption edge which is near 285 eV. Data for graphite are uncertain and the respective data for graphene have not been determined. Furthermore, the electronic structure of graphene is known to depend on its substrate, which may also affect the refractive index. Based on measurements at the Australian Synchrotron the optical constants defining the refractive index at energies spanning the carbon 1s edge of both, highly oriented pyrolitic graphite (HOPG) and graphene, have been determined. The graphene was CVD-deposited and supported by copper foil. The refractive index was extracted from the data via the piecewise Kramers - Kronig transformation of NEXAFS spectra. It has been found that with the associated optical constants successful simulations of reflection spectra for both materials are possible. The simulated spectra have been compared with results from recent experiments at the BESSY synchrotron in Berlin.

WP25

Terahertz Spectroscopic Characterizations for Graphite Nanofibers and Graphite

H. Zhang, J Horvat and R. Lewis

School of Physics and Institute for Superconducting & Electronic Materials, University of Wollongong, NSW 2522, Australia

Terahertz (THz) time-domain spectroscopy (THz-TDS) is a powerful technique to study materials properties such as complex dielectric response and conductivity in the far-infrared spectral region, with the advantages of high signal-to-noise ratio (SNR), noncontact optical probe, and measuring the amplitude and phase of electric field simultaneously thus not requiring Kramers-Kronig (K-K) transformation. Graphite is an allotrope of carbon, classified as a semimetal, which is characterized by a high anisotropic three-dimensional (3D) band structure [1]. The research for electrical, magnetic and optical properties of graphite have been triggered by the single layer graphene [2], and other two-dimensional materials (e.g. Hexagonal Boron Nitride-hBN, MoS^2 and Black phosphorus) [3]. The generation of THz pulses from highly oriented pyrolytic graphite (HOPG) samples illuminated with femtosecond laser pulses has also been reported [4]. Graphite nanofiber is produced by the metal catalyzed decomposition of certain hydrocarbons at temperatures from 400 - 800°C [5]. One of the outstanding features of these structures is the presence of a large number of edges, which in turn constitute sites readily available for chemical or physical interaction, particularly adsorption. These properties are likely to be derived from the intermolecular bonds in graphite nanofiber, which may have different characteristics than for standard graphite [6]. THz spectroscopy is a technique of choice for studying these characteristics, as the energy of THz radiation corresponds to the weak intermolecular bonds between graphite sheets and in the same time intra-molecular vibrations of the graphite rings can be excited. We concentrate on the seldom used frequency range of 0.1 – 7 THz, which cannot be accessed by standard far-infrared spectrometers. THz spectra of graphite nanofibers are compared to other forms of graphite, such as pencil lead (B, HB, and 2H) drawing on paper, absorption modes identified and conclusions have drawn on specific characteristics of graphite nanofiber.

[1] Seibert, K. et al. "Femtosecond carrier dynamics in graphite" *Phys. Rev. B* **42**(5), 2842–2851 (1990)

[2] Mak, K. F. et al. "Measurement of the optical conductivity of graphene" *Phys. Rev. Lett.* **101**, 196405 (2008)

[3] Fengnian Xia, Han Wang, Di Xiao, Madan Dubey and Ashwin Ramasubramaniam, "Two-dimensional material nanophotonics" *Nature Photonics* **8**, 899-907 (2014)

[4] Gopakumar Ramakrishnan, Reshmi Chakkittakandy, and Paul C. M. Planken, "Terahertz generation from graphite" *Opt. Express* **17**, 16092-16099 (2009)

[5] Nelly M. Rodriguez, Alan Chambers, and R. Terry K. Baker "Catalytic Engineering of Carbon Nanostructures" *Langmuir* **11**(10), 3862-3866 (1995)

[6] James Lloyd-Hughes, "Terahertz spectroscopy of quantum 2D electron systems" *J. Phys. D: Appl. Phys.* **47**, 374006 (2014)

WP26

Optical bistability due to nonlinear surface plasmon polaritons in graphene

M. Sanderson, Y. Sing Ang and C Zhang

University of Wollongong, Wollongong, New South Wales 2522, Australia

Optical bistability is found to occur under reasonable fields in a prism-air-graphene-dielectric structure. Due to this field, the reflection characteristics of the structure are modified such that the absorption peak which results in surface plasmon polariton (SPP) excitation is shifted such that bistability arises. This effect is due to the nature of the nonlinear SPP's which have their energy and frequency as a function of the incident field 1 as well as the strong nonlinear response of graphene [2]. This nonlinear effect is determined by solving the Boltzmann transport equation and expanding the Fermi-Dirac distribution out into higher order terms [3]. A hysteresis-like curve is found when considering the optical bistability at a fixed frequency and the minimum required field and the frequency for bistability to occur has been determined.

[1] S. Gong, T. Zhao, M. Sanderson, M. Hu, X. Chen, P. Zhang, R. Zhong, C. Zhang and S. G. Liu, *Appl. Phys. Lett*. **106**, 223107 (2015)

[2] - A. R. Wright, X. G. Xu, J. C. Cao, and C. Zhang, *Appl. Phys. Lett.* **95**, 072101 (2009) [3] - N. M. R. Peres, Y. V. Bludov, J. E. Santos, A. Jauho and M. I. Vasilevskiy, *Phys. Rev. B* **90**, 125425 (2014)

WP27

Quantitative 3D Strain Mapping in Nanodiamonds using Bragg Coherent Diffractive Imaging (BCDI)

M. S. Maqbool[1] , D. Hoxley[2] , N. Phillips[1] , A. Stacey[4] , J. N. Clark[5] , B. Chen[2] , D. Langley[2] , R. Harder[6] , E. Balaur[2] and B. Abbey[2]

[1] ARC CoE for Advanced Molecular Imaging, La Trobe University, Victoria 3086, Australia

[2] La Trobe University, Victoria 3086, Australia

[4] Centre of Excellence for Quantum Computation and Communication Technology, University of Melbourne, Victoria 3010, Australia

[5] Stanford University, Stanford, CA 94305, United States

[6] Argonne National Laboratory, Illinois 60439, United States

Nanodiamonds (NDs) with nitrogen vacancy (NV) centres have been shown to be useful for applications involving cellular tracking in vivo at the molecular level. The sustained fluorescence of these nanodiamonds is related to their structure, and is supposed to be influenced by the strain distribution inside the crystals. In nanocrystals even relatively small amounts of strain can induce large changes in the mechanical, optical and electronic properties of nanocrystals. The current work elaborates first application of Bragg coherent diffractive imaging (BCDI) for mapping the three-dimensional (3D) strain fields within the crystalline nanodiamonds. For reference, a control sample (as-grown crystals) has been compared with a strain-induced (implanted with 10^{12} ions per cm^2) sample. The comparison of control and strain-induced samples will help to optimise their application for tracking the processes at molecular level.

WP28

The role of dielectric function for the control of coupled dipole resonances in dimers of dissimilar metallic nanorods

G. Fletcher, M. Cortie and M. Arnold

School of Mathematical and Physical Sciences, University of Technology Sydney, Broadway 2007, NSW, Australia

The position and intensity of plasmon resonances in metallic nanostructures depends acutely on the complex dielectric function of the materials used and, of course, on the geometry, e.g. [1]. Ideally, the material or materials should possess a high DC conductivity and an absence of interband transitions in the visible part of the spectrum. Materials available vary from low-loss (Ag or K) to 'lossy' (Ni or Pt, for example). In general, inclusion of a lossy material in a composite nanostructure would be expected to attenuate any localised plasmon resonances. We have been exploring the effect of dielectric function on the optical properties of dimers of dissimilar metal nanorods and discovered surprising effects when a lossy material is paired with a low loss material: the geometry of the high loss material exerts a controlling influence over the resonance, in particular its frequency. In contrast, variation of the dimensions of the low loss rod for a given length of high loss rod has far less effect. We use calculations based on the Boundary Elements Methods to examine this phenomenon in terms of the underlying complex dielectric functions of the various elements, especially the electric field strength and spectral position of their respective interband transitions. Finally, we show how a range of interesting optical effects could be achieved in such hybrid nanostructures.

[1] G. Fletcher, M.D. Arnold, T. Pedersen, V.J. Keast and M.B. Cortie, "Multipolar and dark mode plasmon resonances on drilled silver nano-triangles" *Optics Express* **23**(14), 18002-18013 (2015)

WP29

Helium ion implantation dose dependent microstructure and laser damage of sapphire

Z.Sui

Shanghai Institute of Laser Plasma, Shanghai, 201800, China

Sapphire is used in diagnostic systems for the International Thermonuclear Experimental Reactor (ITER), where it will play important roles as electrical insulation and optical components. It is one of the optical candidate materials to be used in the high power solid-state laser driver for inertial confinement fusion (ICF). It is thus necessary to investigate the radiation effect in alumina generated by radiation such as energetic electrons, ions, neutrons or photons. In this work, the (0001) sapphire samples are irradiated with 60 keV helium ions at the fluences up to 1×1018 ions/cm^2 at room temperature. The microstructure evolution and optical properties as well as laser induced damage threshold are investigated. The density and amount of defects increase with the increasing implantation fluence. The surface becomes rough because of the aggregation of helium bubbles and migration towards the surface. There is a lattice expansion up to ~ 4.5% in the implanted area and the lattice distortion measured from dispersion of (110) diffraction is ~ 4.6deg. Such strain of crystal lattice is rather large and leads to contrast fluctuation at scale of 1 ~ 2 nm (the bubble size), shown in Fig. 1. The laser induced damage threshold (LIDT) is investigated to understand the effect of helium ion beam irradiation on the laser damage resistance of sapphire components and the results show that the LIDT decreases from decreases significantly from 5.43 J/cm^2 to 4.62, 3.71, 2.64, and 1.80 J/cm^2, respectively, with the increasing implantation fluence due to the absorptive color centers, helium bubbles and defects induced by helium ion implantation. The laser damage morphologies of samples before and after ion implantation are also presented in Fig. 2.

WP30

Theory of controlling avalanche process of carrier in short pulse laser irradiated dielectrics

X. Yuan[1], H. Deng[2] and X. Zu[2]

[1] *Research Center of Laser Fusion, China Academy of Engineering Physics, Sichuan, China*

[2] *University of Electronic Science and Technology of China, Sichuan, China, 610051*

Short pulse lasers (<10 ps) are used routinely for the investigations of high peak-power laser-matter interactions, such as laser micromachining [1-2], laser-driven accelerators, ultrafast dynamics in atoms and solids, and laser modulation spectrum in solids. However, laser-induced damage (LID) in optical components is still a limiting factor for the development of higher power laser systems and optical devices[3]. For decades, LID of dielectrics has been extensively studied by numerous theoretical and experimental methods. It is agreed that the generation of conduction band electrons (CBEs) in solids plays a critical role of LID and the damage threshold is determined by the density of CBEs for short pulse laser[4]. There are two processes to generate the CBEs in a solid. One is the valance band to conduction band photon ionization process and the other is avalanche process. Avalanche process is usually the dominant process for the generation of CBEs as the pulse width is not ultra-short (>100 fs). Thus, if the avalanche is effectively suppressed, the damage threshold of solids will be dramatically improved. In this work, a theory for controlling avalanche process of carrier during short pulse laser irradiation is proposed. The theory provides a way to suppress avalanche process and a direct judgment for the long existing debate about the dominant channel in generation of CBE for ultra-short pulse (<100 fs) in fused silica (some previous reports such as Refs.5 showed that the avalanche process is a dominant channel for the generation of CBE; whereas, some other reports such as Refs.6 showed that photon ionization process is dominant channel). The obtained temperature dependent rate equation shows that the laser induced damage threshold of dielectrics, e.g., fused silica, increase nonlinearly with the decreases of temperature. Thus present theory predicts a new approach to improve the laser induced damage threshold of dielectrics.

[1] Gattass R R and Mazur E, *Nature Photon* **2,** 219 (2008)

[2] Li Y, Stoica V A, and Endicott L, *Appl. Phys. Lett*. **99**, 121903 (2011)

[3] Deng H X, Zu X T, Xiang X, and Sun K, *Phys. Rev. Lett*. **105**, 113603 (2010)

[4] Stuart B C, Feit M D, et al. *Phys. Rev. B* **53**, 1749 (1996)

[5] Joglekar A P, Liu H H, et al. *Proc. Natl. Acad. Sci.***101**, 5856 (2004)

[6] Wu A Q, Chowdhurg I H, and Xu X F *Phys. Rev. B* **72**, 085128 (2005)

WP31

Cooperative Behaviour of Physical Systems

T. Finlayson[1] and J. Lashley[2]

[1] *University of Melbourne, Victoria 3010, Australia*

[2] *Los Alamos National Laboratory, New Mexico, United States*

Natural systems exhibiting critical phenomena are driven by fluctuations and have become the focus of attention across many branches of the physical and biological sciences. In the field of neuroscience for example, neurons in the brain appear to sit near a critical point where, on the one side there is stability with neurons ready to respond to stimuli, while on the other side, they fire in a chaotic manner, leading to seizure. Likewise, criticality can be spotted on the macroscale in the flocking of birds, the swarming of insects or the schooling of fish. In the case of bird flocking, for example, correlations have been established using direct measurements of displacements and velocities of particular birds. The statistical analysis of such data [1] has illustrated a diffusive behaviour within flocking with an increasing mean squared displacement of the form $(\delta x)^2 = Dt^{\alpha}$ with the exponent, $\alpha \sim 1.7$ and the diffusion coefficient small, resulting in slow rearrangements. As for such biological systems, in condensed matter physics, critical point behaviour which often accompanies a phase transition, results from interparticle (i.e., interatomic) correlations but unlike the biological systems, it becomes impossible to measure the behaviour of specific "particles." The collective behaviour is observed as an avalanche, or noise, in a particular physical property [2]. Somewhat surprisingly, the statistical analyses of such noise spectra, show results which resemble those for biological systems. In this paper, a brief review of these ideas will be presented and some of our recent measurements and analysis of noise spectra in shape-memory alloys will be illustrated

[1] A. Cavagna and I. Giardina, *Ann. Rev. Condens. Matter Phys.* **5**, 183-207 (2014)

[2] J.C. Lashley, K. Gofryk, B. Milhaila, J.L. Smith and E.K.H. Salje, *J. Phys.: Condens. Matter* **26**, 035701 (2014)

WP32

EPR Study of a 'Capsule' Brewed Coffee and its Decaffeinated Version

G. Troup[1] and S. Drew[2]

[1] *School of Physics, Monash University, VIC 3800, Australia*

[2] *Florey Department of Neuroscience, and Mental Health, University of Melbourne, Victoria*

Ten or fifteen years ago or less, sensory evaluation of a decaff. coffee would easily recognize it from its caffeinated form. With the development of the capsule method of coffee brewing, this is no longer true. Take-home coffee machines for this method are readily available, and give accurate volumes of hot water for the style of coffee required, e.g. short black, long macchiato. Does the EPR signal change with modern decaffeination of particular coffees? A complete coffee and its decaff. version were examined by EPR. The 'solutions' had an accurate same volume, and the filling factor in the spectrometer was the same for both. A Bruker ~3cm. wavelength EPR with a 'super Q' was used at room temperature, with signal averaging employed in detection. The spectrum of the usual Mn^{2+} signal was the same for both samples, and the ratio of the free radical signal to the Mn^{2+} was also the same. Further details will be given in the full MS.

WP33

An EPR Study of Tawny Ports, and Coffee Favoured Liqueurs

G. Troup[1] and S. Drew[2]

[1] *School of Physics, Monash University, VIC 3800, Australia*

[2] *Florey Department of Neuroscience, and Mental Health, University of Melbourne, Victoria*

This study is the delayed continuation of a project started in 1994, with red and white wines. The delay was by requested studies on whiskies and brandies. It now continues with Australian tawny ports (fortified wines) and coffee flavoured liqueurs. Four well known Australian tawny ports and two imported coffee liqueurs were purchased commercially. The EPR spectrometer was a Bruker with a 'super"Q' resonant cavity, operating at ~3cm wavelength. Temperature was room or 77K as required, and signal averaging was used when necessary. Three of the tawny ports showed expected Mn^{2+} signals of the expected intensity, but the fourth a signal almost one tenth of that of the others. All showed free radical signals, with the fourth specimen showing an unidentified, slightly broader system, as well. The 'pursuit' of further samples of number four with more Mn^{2+} failed.

The two coffee liqueurs showed coffee EPR spectra!

Further details, discussion, and conclusions will be in the full report. An antioxidant test for each kind of beverage is worthwhile

TP1

First spectrum measured on EMU, the cold-neutron backscattering spectrometer at the Bragg Institute, ANSTO

N. De Souza, A. Klapproth and G. Iles

ANSTO, Lucas Heights, NSW 2234, Australia

The cold-neutron backscattering spectrometer, EMU, one of the four spectrometers at ANSTO received its commissioning licence in 2015. This allowed opening the neutron beam onto the instrument and after measuring nominal background radiation we made our first measurements with the instrument. EMU is based on Si(111) crystal backscattering and extracts neutrons from a cold neutron guide via a double HOPG (002) crystal premonochromator setup. Backscattering occurs through implementation of spherical focusing between the Si (111) crystal monochromators and analyser arrays, aiming to deliver a spectrometer FWHM energy resolution in the order of 1.2 μeV. EMU also features a 7-metre long focusing guide located between the two premonochromators, a so-called graphite chopper alternating beam delivery to the backscattering crystal monochromator and then into the secondary spectrometer [1] and a linear Doppler drive modulating incident neutron energies over ± 31 μeV. Scattered, analysed neutrons are counted in 3He LPSD arrays. We measured two samples, one a vanadium sample can and secondly a polyethylene sheet. Using event counting obtained from two temporarily placed 3He detector tubes, we were able to obtain a backscattered spectrum. It is critical to ensure that detected neutrons have been backscattered. Backscattered neutrons travel a further distance than those that scatter immediately at the sample and therefore the timing signal must be known accurately, to distinguish between spurious and actual data. Future work will involve developing MANTID software for data treatment and analysis.

[1] B. Frick and M. Gonzalez, *Physica B* **301**, 8 (2001)

TP2

Development of high-pressure single-crystal neutron diffraction on the Laue diffractometer, KOALA, at OPAL

J. Binns[1], G. McIntyre[1], K. Kamenev[2], S. Moggach[3] and S. Parsons[3]

[1] ANSTO, Lucas Heights, NSW 2234, Australia

[2] School of Engineering and Centre for Science at Extreme Conditions, The University of Edinburgh, Scotland

[3] EaStCHEM School of Chemistry and Centre for Science at Extreme Conditions, The University of Edinburgh, Scotland

Hydrogen bonds are one of the most important classes of intermolecular interaction, and accurate H-atom positions are critical for analysis of the energy terms which determine the thermodynamic stability of molecular crystals. At ambient pressure and low temperatures, H atoms can often be located by X-ray diffraction, and X-ray data can provide an accurate picture of the intermolecular contacts. High-pressure experiments do not afford this luxury. The high systematic errors introduced by the pressure cell and low completeness mean that H-atom positions are not revealed in X-ray Fourier maps. In some compounds H-atom positions can be inferred from the positions of other atoms, but this is not possible in all cases. Neutron diffraction data are much more sensitive to H than are X-ray data, and they are essential in cases where accurate H-atom location is important. Neutron powder patterns of complex molecular systems suffer from extensive peak overlap, and single-crystal diffraction therefore has a huge advantage; there is also no need to deuterate. The main disadvantage of neutron diffraction is that a large sample is usually required, which is at odds with the decreasing volumes possible with increasing pressure with existing pressure-cell materials. Modern neutron Laue diffraction and large moissanite anvil cells offer some respite 1, but complementing high-pressure X-ray data with high-pressure neutron data is still fraught with technical challenges to obtain identical conditions. Initial developmental experiments using a miniature diamond-anvil cell with a single crystal of size typical for X-ray diffraction on the KOALA Laue diffractometer at OPAL have shown the feasibility of the Laue technique for single-crystal neutron studies at high pressure. Remarkably, data completeness is similar to ambient-pressure measurements, despite the presence of the pressure cell. It is now possible to perform joint X-ray and neutron studies on the same sample under identical conditions. The implications of the high-pressure sample environment for neutron Laue diffraction will be explored and the results from experiments on hexamine presented.

[1] G.J. McIntyre, L. Mélési, M. Guthrie, C.A. Tulk, J. Xu and J.B. Parise, *J. Phys.: Condens. Matter 17*, **S3017** (2006)

TP3

Advanced Sample Environment Support for Neutron Instruments at the Bragg Institute, ANSTO

P. Imperia, N. Booth, G. Davidson, S. Lee, T. D'Adam and A. Manning
ANSTO, Lucas Heights, NSW 2234, Australia

Over the last few years a number of advancements have been made in sample environments available to scientists visiting the Neutron Beam Facility run by the Bragg institute at ANSTO (Lucas Heights). Conventional sample environment equipment allows experiments to be carried out from 35mK to 1700K, magnetic fields up to 12T and electric fields up to 10kV. These extremes are not available on all neutron instruments nor with one piece of equipment. However combinations of temperature, magnetic and electric fields are also possible. These conventional sample environments will not be covered here. This presentation will outline advances made in the gas handling, vapour delivery, differential scanning calorimetry (DSC) and spectroscopy at extreme temperatures all carried out simultaneously with neutron data collection. Some examples of the complimentary data collected are also presented. Our automated gas handling system allows gas mixing (up to 4 gases), dosing (volumetric Sievert analysis) up to 200Bar, gas flow and molecular analysis with a dedicated mass spectrometer for kinetics investigations. The Hiden Isochema system is based on their commercial IMI system with the standard reaction chamber removed and replaced by thermalised capillary lines to allow the gas delivery to a sample reactor placed within a cryostat or furnace on the sample stage of our neutron instruments. Two options are available for vapour delivery. For samples that do not outgas a static system can be used where computer controlled valves control the vapour pressure. One valve is used to lower the pressure using a turbo pump and the second one to allow the vapour from the reservoir to increase the vapour pressure. Any non-corrosive liquid can be used in this system. The second vapour system, dynamically controls the vapour and dry gas flow allowing mixing of two vapours and a dry stream of gas or the recirculation of a saturated vapour through a sample reactor The DSC system is based on A Mettler Toledo model DSC1. The furnace has been moved to allow the passage of the neutron beam and Bragg designed crucibles are used to allow scattering experiments to be carried out while DSC data are collected. Quartz and Aluminium crucibles are available and temperature range of 550C to -100C is achievable Using Ocean Optics spectrometer equipment we have successfully carried out NIR spectroscopy down to 4K while collecting Neutron diffraction data. The use a standard NIR reflection probe and modification of the cryostat sample stick allows the probe to be introduced into the cryostat. A second spectrometer is available for UV-Vis spectroscopy and can be used in a similar method. These spectrometers are also available for use on other scattering instruments over a limited temperature range.

TP4

Vibrational studies using neutrons

A. Stampfl

ANSTO, Lucas Heights, NSW 2234, Australia

Several neutron spectrometers are available for use at the Bragg Institute. In particular a low energy band pass neutron spectrometer that operates in the range of $\sim 50 - 1200\ cm^{-1}$ has very recently been commissioned and first experiments run on TAIPAN. The so-called Beryllium-filter spectrometer is predominantly used to obtain vibrational density of states spectra from those materials that contain hydrogen, thus making this instrument especially important in the chemical, biological, geological and environmental sciences. In many aspects a neutron spectrum obtained using the Beryllium-filter spectrometer is very similar to spectra obtained in the far-infrared or terahertz regime making neutron spectroscopy a complementary technique to other spectroscopies such as photon (electromagnetic radiation)-based techniques. The neutron's properties are unique amongst other fundamental probes like light, such as outstanding materials penetrability, isotopic sensitivity, magnetic sensitivity and lack of vibrational selection rules. Furthermore because hydrogen possesses a large incoherent scattering cross-section much of the observed vibrational modes are molecular in origin.

Calculation using DFT-codes and/or molecular dynamics approaches is an integral part of a complete study investigating any material with neutron spectroscopy. A number of interesting examples are presented that highlight the capabilities of the Be-filter spectrometer along with a description of the spectrometer itself, how it works and the analysis involved.

TP5

Development of a compact X-ray source

E. Yap[1,2], R. Preston[2], J. Tickner[1] and J. Daniels[2]

[1] *CSIRO Mineral Resources*

[2] *The University of New South Wales, NSW 2052, Australia*

Since their discovery by Wilhelm Röntgen in 1895, X-rays have become a valuable tool for characterising the composition and structure of matter. The X-ray tube has long been central to techniques such as X-ray fluorescence (XRF) and X-ray diffraction (XRD) analysis. However, the external high-voltage power supply, size and costs associated with X-ray tube technology have limited the wider application of X-ray analysis. There has recently been a renewed interest in using materials exhibiting coupling mechanisms such as pyro- and piezoelectricity to generate X-rays [1, 2]. The surfaces of these materials inherit an intrinsic charge due to a spontaneous polarisation, induced by either temperature change or mechanical stress. This can be exploited to generate a high voltage in a low pressure gas, capable of both ionising the gas and accelerating the liberated electrons into a target to produce X-rays. This allows more portable X-ray sources to be built, with power supply voltages dramatically reduced from over 10 kV to a few volts [3-5]. The compact X-ray generator is being developed based around the pyroelectric effect. A vacuum chamber testbed has been constructed for the characterisation and optimisation of these novel X-ray generators. Mass flow controllers are used in conjunction with a turbo-molecular and diaphragm pump to control the gas pressure in the chamber. An Arduino microcontroller is employed to operate a thermoelectric cooler, which cycles the temperature of the pyroelectric crystal under-test. The microcontroller is also used to record temperature and pressure readings. A silicon drift detector is installed to characterise the X-ray output. Along with the details on the experimental apparatus, initial measurements using $LiNbO_3$ crystals will be presented.

[1] J. D. Brownridge and S. Raboy, "Investigations of pyroelectric generation of x-rays," *Journal of Applied Physics* **86**, 640 (1999)

[2] B. Gall, S. D. Kovaleski, J. A. Van Gordon, P. Norgard, A. Benwell, B. H. Kim, et al., "Investigation of the Piezoelectric Effect as a Means to Generate X-Rays," *IEEE Transactions on Plasma Science* **41**,106-111 (2013)

[3] G. L. Clark, Applied X-rays, Fourth ed. London: McGraw-Hill Publishing Company Ltd., 1955.

[4] E.F. Kaelble, Ed., "Handbook of X-rays: For diffraction, emission, absorption and microscopy" New York, U.S.A.: McGraw-Hill, Inc. (1967)

[5] J. A. Geuther and Y. Danon, "Electron and positive ion acceleration with pyroelectric crystals," *Journal of Applied Physics* **97**, 074109 (2005)

TP6

Investigations of the Structural and Magnetic Phase Behaviour of $MnSb_{2-x}Ta_xO_6$ Solid Solutions

H-B Kang, F. Suzuki and T Söhnel

The University of Auckland, New Zealand

Recently, the trigonal modification (sg. P321) of $MnSb_2O_6$ has drawn significant attention as it could be an unusual type of multiferroic behaviour and weakly polar material [1]. The magnetic susceptibility of $MnSb_2O_6$ shows a short range ordering below 200 K and long range ordering is observed below the Neel temperature (TN = 12.5 K) resulting in an incommensurately ordered three-dimensional Heisenberg antiferromagnet [2]. $MnTa_2O_6$ adopts the orthorhombic $MgNb_2O_6$ structure type (sg. Pbcn) and it shows a monoclinic magnetic structure: P2'1/c symmetry at 4.2 K (TN = 4.4 K) [3]. In this solid solution, Ta could occupy the MnO interlayers and it will induce the decrease of the magnetic inter layer coupling. According to the Lab X-ray diffraction studies, a new tetragonal modification can be observed between x = 0.2 and 1.8. The powder can be refined as mixtures of the trigonal $MnSb_2O_6$ structure and a tetragonal tri-rutile modification, which is known for other MSb_2O_6 compounds, for the refinement from x = 0.6 to x = 1.2. The tri-rutile modification could be refined as the sole phase between x = 1.4 to 1.6. The orthorhombic $MnTa_2O_6$ modification could only be observed from x = 1.7 - 2.0. Interestingly, the tri-rutile modification has previously been described as a meta-stable modification for $MnTa_2O_6$ [4].

[1] R. D. Johnson, K. Cao, L. C. Chapon, F. Fabrizi, N. Perks, P. Manuel, J. J. Yang, Y. S. Oh, S-W. Cheong and P. G. Radaelli, *Phys. Rev. Lett*. **111**, 017202 (2013)

[2] J. N. Reimers and J. E. Greedan, *J. Solid State Chem*. **79**, 263 (1989)

[3] H. Weitzel and S. Klein, *Solid State Comm*. **12**, 113 (1973)

[4] S. Esmaeilzadeh and J. Grins, *Solid State Sciences* **4**, 117 (2002)

TP7

Low Pressure Synchrotron X-ray Powder Diffraction of $Cu_{5-x}M_xSbO_6$ (M = Cr, Mn, W)

D. Wilson[1], T. Soehnel[1], K. Smith[1], H. Brand[2], C. Ulrich[3], P. Graham[3], F. Chang[3], M. Allison[4] and N.H Vyborna[1]

[1] *The University of Auckland, New Zealand*

[2] *Australian Synchrotron, Clayton 3168, Victoria, Australia*

[3] *The University of New South Wales, NSW 2052, Australia*

[4] *The University of Sydney, Sydney, NSW 2006 Australia*

The large crystallographic and chemical diversity of copper-based metal oxides is one of their highlighting features and cause for pursuit into copper based material research. An interesting feature seen in copper based metal oxides is the coexistence of different copper oxidation states, in different crystallographic positions, within the same compound [1-3]. This can lead to a mixture of magnetically active Cu^{2+} and magnetically inactive Cu^{1+} within the same compound, with different structural motifs. One interesting compound that demonstrates this coexistence of mixed copper oxidation states is Cu_5SbO_6, which crystallises in a modified delafossite structure type ($CuFeO_2$) [4]. Here, the magnetically active brucite-like CuO_2 layer was diluted in an ordered fashion with non-magnetic Sb^{5+}. These layers were separated by linearly coordinated, magnetically inactive Cu^{1+}. Rietveld refinements on a range of preparation temperatures revealed a low-temperature (LT) and high-temperature modification (HT) phase transition. This is related to an ordering (HT)/disordering (LT) effect of the Sb^{5+}/Cu^{2+} brucite-like layers between the Cu^{1+} ions. Substituting the Cu^{2+} or Sb^{5+} in the layers with other transition metals (Cr, Mn, W) could present interesting changes to the properties of the material, and potentially influence the ordered/disordered stacking of the layers. By using solid-state Raman spectroscopy, we could show that this structure displayed a pressure-induced phase transition at room temperature for the ordered modification, which was not observed for the disordered modification. Lowering the pressure from ambient down to 20 mbar showed phonon modes at about 700 cm^{-1} and 550 cm^{-1} disappeared almost completely. Neutron powder diffraction experiments were conducted at atmospheric and low pressure on both ordered and disordered modifications. On analysis of the neutron diffraction patterns, we could show a very small shift in the reflections, and thus changes in the unit cell parameters, for the ordered modification, while these shifts were not observed for the disordered modification. These shifts should also be observed in synchrotron powder diffraction patterns. Therefore, we investigated the nature of this phase transition with variable pressure synchrotron X-ray powder diffraction.

[1] S. Seki, Y. Yamasaki, M. Soda, M. Matasuura, K. Hirota, Y. Tokura, *Phys. Rev. Lett.*, **100**, 127201 (2008)

[2] V. Aji, A. Shekhter, C. M. Varma, *Phys. Rev. B* **78**, 094421 (2008)

[3] M. Gruninger, D. van der Marel, A, Damascelli, A. Erb, T. Nunner, T. Kopp, *Phys. Rev. B* **62**, 12422 (2000)

[4] A. Pabst, *Amer Miner* **23**, 175 (1938)

TP8

Neutron diffraction study of double tungstates Li_2M (M=Co and Ni)

C-W. Wang[1], S. Karna[2], F. C Chou[2] and R. Sankar[2]

[1] *National Synchrotron Radiation Research Centre, Hsinchu City, Taiwan 300*

[2] *Center For Condensed Matter Science, National Taiwan University*

Neutron diffraction study of double tungstates $Li_2MII(WO_4)_2$ (M=Co and Ni) The isostructural $Li_2Co(WO_4)_2$ and $Li_2Ni(WO_4)_2$ crystallize in the triclinic structure (space group P-1, Z =1). The crystal structures can be viewed as alternating layers of WO layers and Li-MO layers alone the b-axis. The WO layers built up of edge-sharing WO_6 octahedra forming infinite zigzag chains alone the a-axis as in many other tungstates. The edge-sharing LiO_6 octahedrons also form infinite chains extending along the c-axis. The divalent ions, Co^{2+} and Ni^{2+}, are locating in the octahedral oxide environment, in the mesh forming by crossing LiO and WO chains, isolated from each other. Due to the lack of direct connection of the MO_6 octahedral, the magnetic coupling between the nearest neighboring M cannot through the strong M-O-M superexchange path (SE). Nevertheless the magnetic coupling can be achieved through more complex pathways, which is bridging by the oxygen ions in LiO_6 or WO_6. In $Li_2MII(WO_4)_2$ the weak M-O-O-M pathways, known as super-superexchange (SSE) form complex network with magnetic frustrations, gives raise to complex magnetic behaviors. The temperature dependent magnetic susceptibility and heat capacity clearly mark the two magnetic transition temperatures of each of the two compounds. In $Li_2Ni(WO_4)_2$ the two magnetic transition temperatures are TN1 = 12.8 K and TN2 = 17.5 K, whereas the slightly lower TN1 = 7.2 K and TN2 = 9.5 K for $Li_2Co(WO_4)_2$. The magnetic structures have been determined from neutron powder diffraction measurement conducted on Wombat and Echidna at ANSTO. For both compounds the magnetic correlation develops below TN1, as an incommensurate modulation and the magnetic moments order into commensurate super cells below TN2. Both compounds possess collinear antiferromagnetic spin configurations in the magnetic order phases. Surprisingly the magnetic unit cells of the two isostructural compounds are different. The magnetic unit cell of $Li_2Ni(WO_4)_2$ is (2a b 2c), and the magnetic moment of Ni2+ at 3 K is 1.925 mB , roughly pointing along the a direction. Whereas a much larger magnetic unit cell of (2a 4b 4c) is realized in $Li_2Co(WO_4)_2$ below TN2. Co spins in the {+ + - -} sequence are observed when moving to the neighboring magnetic sites along b and c-axis. The magnetic moment of Co2+ is 2.836 mB at 5.5 K closely align along the a-axis as well. The different magnetic ground states in the two compounds might be resulted from to the slight differences in the crystal structure and magnetic couplings

TP9

Low-energy crystal-field excitations observed using inelastic Neutron Scattering

G. Iles[1], G. Stewart[2], R. Mole[2], W. Hutchison[2], S. Cadogan[2]

[1] *ANSTO, Lucas Heights, NSW 2234, Australia*

[2] *The University of New South Wales, UNSW Canberra, Canberra, ACT 2600, Australia*

The time-of-flight spectrometer, PELICAN, at ANSTO operates two choppers which provide a fixed initial energy of neutrons to the sample. Configuring the instrument to a wavelength of 4.75Å, sets this initial neutron energy to 3.6meV. By phasing the choppers, however, harmonic wavelengths can be obtained such as λ/2, etc. By measuring a powder sample of ErNiAl4 at λ/2 (λ = 4.75Å) we could observe a greater range of positive energy transfers (to the sample) and, after appropriate background removal, confirm the presence of an excitation at 7meV. This excitation represents the emission from the crystal field level at 7meV to 0meV confirming the result obtained in a previous experiment.

TP10

Dynamical Mechanism of Phase Transitions in A-site Ferroelectric Relaxor $(Na_{1/2}Bi_{1/2})TiO_3$

G. Deng[1], S. Danilkin[2], H. Zhang[2], P. Imperia[1], X. Li[1], X. Zhao[1] and H. Luo[1]

[1] *ANSTO, Lucas Heights, NSW 2234, Australia*

[2] *Shanghai Institute of Ceramics*

The dynamical phase transition mechanism of $(Na_{1/2}Bi_{1/2})TiO_3$ (NBT) was studied using inelastic neutron scattering. Softening of multiple phonon modes were observed to correlate with the phase transition sequence of NBT. As usual, the softening of the zone centre transverse optic (TO) modes Δ5 and Σ3 was observed in (200) and (220) zone, showing the Ti vibration instabilities in TiO_6 octahera for both cubic-tetragonal (C-T) and tetragonal-rhombohedral (T-R) phase transitions. In this two phase transitions, however, Ti^{4+} has different preferential displacement directions. Surprisingly, the longitudinal optic (LO) mode also soften significantly toward zone centre in the vicinity range of the transition temperature, indicating the Na^+/Bi^{3+} vibration instability against TiO^6 octahera during the R-T phase transition. Strong inelastic diffuse scattering shows up near M(1.5, 0.5, 0) and R(1.5, 1.5, 0.5) in the tetragonal and rhombohedral phases, respectively, indicating the condensations of the M3 and R25 optic modes for the corresponding phase transitions. This reveals the rotation instabilities of TiO_6 in the corresponding phase transition temperature range. Bottleneck or waterfall features were observed in the dispersion curves at certain temperatures, but did not show the close correlations to the formation of polar nanoregions (PNRs). Additional instabilities are the origin of the complexity of phase transitions and crystallographic structures in NBT.

TP11

Kaolinite and halloysite – does octahedral Fe^{2+} introduce the extra water into halloysite?

J. Cashion[1], W. Gates[2], J.M. Cadogan[3], G.J. Churchman[4] and L. Aldridge[1]

[1] *School of Physics and Astronomy, Monash University, Melbourne, Vic 3800*

[2] *Department of Civil Engineering, Monash University, Melbourne, Vic 3800*

[3] *School of Physical, Environmental and Mathematical Sciences, UNSW Canberra at ADFA, PO Box 7916, Canberra BC 2610*

[4] *School of Agriculture, Food and Wine, University of Adelaide, Adelaide SA 5005*

Halloysite is a member of the kaolinite (kandite) group of minerals. The kaolinite structure is made up of a tetrahedral silica sheet and an octahedral alumina sheet, bonded together into an aluminosilicate layer. Kaolinite can be written as $Al^2Si_2O_5(OH)4$, while halloysite is ideally $Al_2Si_2O_5(OH)_4.2H2O$, and usually has a high degree of disorder. The additional water molecules occur as partially confined interlayer water, which can be removed resulting in a reduction of the c-axis from approximately 1.0 nm to the kaolinite value of 0.7 nm. A long-standing unanswered question is why does halloysite contain water, while kaolinite (and the closely related dickite and nacrite) do not 1? Common theories have been that the incorporation of impurities (e.g., Al^{3+} for Si^{4+} in the tetrahedral sheet, Fe^{2+} or Fe^{3+} for Al^{3+} in the octahedral sheet, or other impurities in the octahedral sheet, which may be hydrated, etc) may create a charge imbalance which can encourage the incorporation of exchangeable cations. However, NMR measurements [2] have shown that there is no more tetrahedral Al in the Si layer than in kaolinites. Also, quasielastic neutron scattering analysis of interlayer water [3] has shown that halloysite has no exchangeable cations. This leaves octahedral Fe^{2+} as the most likely remaining charge impurity. To determine the Fe^{2+} concentrations, we have taken Mössbauer measurements of three New Zealand halloysites: Opotiki, Te Akatea and Te Puke. The first two have appreciable Fe^{2+} concentrations of approximately 10% of the total Fe (respectively, ~1.7 and ~0.4 mmol Fe^{2+}/100g) which may provide measureable layer charge, while the Te Puke has a much smaller concentration (~1%) of a total Fe concentration of 14.06 mmol/100g [4] giving ~0.1 mmol Fe^{2+}/100 g. Unambiguous fitting of the spectra of these minerals is difficult because of the very broad lines, which reduces resolution. There is also the possibility of the presence of trace goethite and of slow paramagnetic relaxation in the structural Fe^{3+}. Progress in solving this riddle of halloysite will be detailed.

[1] Bailey, S.W. *Proc. 9th Int. Clay Conf., Strasbourg, Vol II, Sciences Géologiques* **86**, 89-98 (1990)

[2] Newman, R.H. Childs, C.W. and Churchman, G.J. *Clay Min*. **29** (1994)

TP12

An ^{57}Fe Mössbauer Study of the Ordinary Chondrite meteorite Lynch-001

N. Elewa and S. Cadogan

The University of New South Wales, UNSW Canberra, Canberra, ACT 2600, Australia

The Lynch-001 meteorite is classified as an ordinary chondrite of the petrologic group L5-6 that has undergone 'minor to moderate' terrestrial weathering (A/B class). It was found in the Nullarbor desert in Western Australia in 1977 at the coordinates 31°1'S/127°13' [1]. Here, we report the characterization of the Fe-bearing phases in this chondrite using ^{57}Fe Mössbauer spectroscopy carried out over the temperature range 13 to 295 K. The paramagnetic doublets of olivine and pyroxene dominate the spectra, accounting for 62(3)% of the spectral area at room temperature. On the basis of the room temperature quadrupole splitting of 2.93(1) mm/s we estimate the olivine composition to be $Fa_{30(5)}$[2]. Besides the olivine and pyroxene, there is a paramagnetic ferric component that amounts to 15(2)% of the spectral area at room temperature. The presence of this Fe^{3+} component attests to the weathering of this meteorite. The spectrum also includes troilite (FeS) with a relative spectral area of 12(2)%, Fe-Ni metal (4(2)%) and magnetite/maghemite (7(2)%). The total relative proportion of Fe^{3+} allows us to estimate the terrestrial age of Lynch-001 to be around 6,000 yr, consistent with the value of 6,700 ± 1,300 yr determined by ^{14}C dating [3].

[1] M. M. Grady, *Catalogue of Meteorites, 5th ed* (Cambridge University Press, 2000) 689

[2] O. N. Menzies, P. A. Bland and F. J. Berry, *Lunar Planet. Sci. XXXII*, pp. 1967–1968, (2001)

[3] A.J.T. Jull et al., *Meteoritics & Planetary Sci.* **45**, 1271-1283 (2010)

TP13

Spin transitions in cementite

S. Clark

Department of Earth and Planetary Sciences, Macquarie University, NSW 2109. Australia

It was proposed over 45 years ago by W.S. Fyfe that the effect of pressure deep inside the Earth may be to collapse the atomic orbitals of iron from the high-spin to the low-spin state. This transition would represent a major change in chemical-bonding character for one of the most important elements in the Earth with predictions suggesting as much as a 45% collapse in the ionic volume of ferrous iron in silicates and oxides. Elastic moduli, thermal conductivity, electrical transport, and other physical and chemical properties of Fe-bearing minerals could be dramatically altered due to this transition. Consequently, there has been much interest in the high- to low-spin transition, and high-pressure studies of the past decade have demonstrated that it can indeed take place in oxides similar to those thought to be present in the deep mantle.

In this talk I will outline the basic physics of spin transitions in iron and consider experimental results for magnesiowustite to demonstrate the general effect on mantle properties. Details of recent experiments on cementite will then be presented.

TP14

Non-equilibrium field theory and decay widths: a new golden rule

H. Scammel and O. Sushkov
The University of New South Wales, NSW 2052, Australia

Motivated by magnetic quantum systems in the regime of finite temperatures and close vicinity to a quantum critical point, we develop a generalisation of the Fermi Golden Rule appropriate to handle the calculation of large decay widths. The 'generalised golden rule' is a self-consistent procedure, and the central results are generic. However, the present study specifically considers an O(3) non-linear field theory; $\bar{\varphi}^4$ theory, as a toy application of the generalised golden rule. Following this, we directly apply our results to the real quantum antiferromagnet $TlCuC_{l3}$, which is very well described by the O(3) field theory with an anisotropic term. We compare our results to the very recent INS data and find excellent agreement.

TP15

Incommensurate magnetic order in $PrNiAl_4$

R. White[1], W. Hutchison[1] , M. Avdeev[2] and K. Nishimura[3]

[1] *The University of New South Wales, UNSW Canberra, Canberra, ACT 2600, Australia*

[2]*ANSTO, Lucas Heights, NSW 2234, Australia*

[3]*Faculty of Engineering, University of Toyama, Japan*

The RNiAl4 intermetallic series (where R = Ln^{3+}) has been the subject of much investigation over a number of years. These compounds are known to possess some interesting magnetic behaviours including multiple magnetic phases and metamagnetism. $TbNiAl_4$, $ErNiAl_4$ and $NdNiAl_4$ are all known to have incommensurate magnetic structures determined from neutron diffraction[1-3], whereas the presence of an incommensurate magnetic phase in $PrNiAl_4$ is more tentative, based only on specific heat and magnetisation measurements[4]. Recent neutron powder diffraction experiments have confirmed the presence of this incommensurate magnetic phase at 7 K and 7.5 K, well within the range of 6.9-8.1 K predicted by the specific heat data. Analysis of the diffraction patterns puts the propagation vector of the magnetic phase at k = (0.071(1), 1, 0), with the magnetic moments pointing along the a-axis.

[1] Hutchison W D, Goossens D J, Nishimura K, Mori K, Isikawa Y and Studer A *J Journal of Magnetism and Magnetic Materials* **301** 352 (2006)

[2] Hutchison W D, Goossens D J, Saensunon B, Stewart G A, Avdeev M and Nishimura K *31st Annual Condensed Matter and Materials Meeting*, (Wagga Wagga) **1** (Australian Institute of Physics) (2007)

[3] Mizushima T, Isikawa Y, Sakurai J, Mori K, Fukuhara T, Maezawa K, Schweizer J and Ressouche E *Physica B* **194** 225 (1994)

[4] Nishimura K, Yasukawa T, Mori K, Isikawa Y, Hutchison W D and Chaplin D H *Japanese Journal of Applied Physics* **42** 5565 (2003)

TP16

Skyrmions and Hopfions in frustrated ferromagnets

Y. Kharkov[1], M. Mostovoy[2] and O. Sushkov[1]

[1] *The University of New South Wales, NSW 2052, Australia*

[2] *Zernike Institute for Advanced Materials, University of Groningen, Nijenborgh 4, 9747 AG Groningen, Netherlands*

Magnetic skyrmion is a two-dimensional 'hedgehog-like' spin texture, characterized by non-zero topological number. Stability of skyrmions is topologically protected, therefore they can be potentially used as information carriers in magnetic memory devices.

Skyrmions have been experimentally observed in several materials, such as chiral magnets and thin magnetic films with long-range dipolar interaction. Recent theoretical works [1,2] proposed frustrated ferromagnets (FFM) on triangular lattice as new skyrmion materials, that can host isolated skyrmions, skyrmion lattice and other exotic magnetic phases.

In the present work we show that stable skyrmions can exist in the FFM on the simple square lattice with spin anisotropy. This finding broadly enhances the scope of possible skyrmion materials. We also found attraction of skyrmions with opposite helicity, that leads to existence of stable skyrmions with very high topological numbers.

Hopfion is a three-dimensional topological object, which is similar to torroidal vortex. Hopfions have been predicted in various physical systems such as Bose-Einstein condensates [3], liquid He^3 [4], and vortex-like dynamical spin precession in a collinear uniaxial ferromagnet [5]. Extending our skyrmion work and considering 3D FFM on simple cubic lattice, we for the first time predict existence of a static magnetic hopfion.

[1] T. Okubo, S. Chung, and H. Kawamura, *Phys. Rev. Lett*. **108**, 017206 (2012).

[2] A. O. Leonov and M. Mostovoy, *Nature Comm*. **10** 1038 (2015).

[3] Y. V. Kartashov, B. A. Malomed, Y. Shnir, and L. Torner, *Phys. Rev. Lett.* **113** 264101 (2014).

[4] G.E. Volovik, V.P.Mineev, *JETP Letters* **46** 401 (1977).

[5] A.B. Borisov, F.N. Rybakov, *JETP Letters* **88** 264 (2008).

TP17

The magnetic properties and magnetocaloric effect in $(Mn_{1-x}Ni_x)CoGe$

Q. Ren[1], W. Hutchison[2], J. Wang [3], A. Studer[4] and S. Campbell[1]

[1] *School of PEMS, UNSW Canberra, Canberra, ACT 2600, Australia*

[2]*The University of New South Wales, UNSW Canberra, Canberra, ACT 2600, Australia*

[3] *University of Wollongong, Wollongong, New South Wales 2522, Australia*

[4]*ANSTO, Lucas Heights, NSW 2234, Australia*

Magnetic refrigeration based on magnetocaloric effect is considered as a potential alternative to the conventional gas-compression based refrigeration [1], because the former can improve energy efficiency and reduce emission of environment-harmful chemicals. Materials with firstorder magneto-structural transitions are of great interest for large magnetocaloric effect, e.g. $Gd_5(Si,Ge)_4$ and Heusler alloys [3]. Magneto-structural transition and large magnetocaloric effect were also observed in MnCoGe-based alloys. For MnCoGe-based alloys, there are two stable crystallographic structures: nominally low temperature TiNiSi-type orthorhombic structure (Pnma, martensitic phase) and the high temperature Ni_2In-type hexagonal structure (P63/mmc, austenitic phase), with a martensitic transformation around TM ~650 K [4]. Both phase present as ferromagnetic state at low temperature with Curie temperature of ~345 K and ~275 K, for the martensitic and austenitic phases, respectively. When the martensitic transition temperature TM is moved into the temperature range of the two Curie temperatures, e.g. Fe doping $(Mn_{1-x}Fe_x)CoGe$ [5], coupling of magnetic and lattice structures is obtained and hence present a magneto-structural transition from the ferromagnetic martensite to the paramagnetic austenite.

In this work, Ni was used as substitute for Mn to drive the martensitic transformation temperature. The crystallographic structures and magnetic properties of annealed $(Mn_{1-x}Ni_x)CoGe$ (x = 0.02, 0.03, 0.04, 0.05, 0.06 and 0.07) were studied via X-ray diffraction (T = 20-310 K) and magnetisation (T = 5-340 K) measurements. Then the magneto-structural transition were confirmed by neutron diffraction experiments (T = 5-320 K), and the influence of magnetic field on the magnetostructural transition were investigated using magnetic-field neutron diffraction (B = 0-9 T). The magnetic entropy changes have been derived in the conventional way from a series of isothermal magnetisation experiments, e.g. $-Sm \sim 8.8$ J kg^{-1} K^{-1} for a magnetic field change of B = 0-5 T in $(Mn_{0.95}Ni_{0.05})CoGe$.

[1] E. Brück, *J. Phys. D: Appl. Phys*. **38,** R381 (2005)

[2] V. K. Pecharsky and K. A. Gschneidner Jr, *Phys. Rev. Lett*. **78**, 4494 (1997)

[3] J. Liu, T. Gottschall, K. P. Skokov, J. D. Moore and O. Gutfleisch, *Nat. Mater*. **11**, 620 (2012)

[4] N. T. Trung, L. Zhang, L. Caron, K. H. J. Buschow and E. Brück, *Appl. Phys. Lett*. **96**, 172504 (2010)

[5] Q. Y. Ren, W. D. Hutchison, J. L. Wang, S. Muñoz Pérez, J. M. Cadogan and S. J. Campbell, Phys. Status Solidi (a) 211, 1101 (2014); *Phys. Status Solidi (a)* **211**, 2898 (2014)

TP18

Azimuthal dependence of planar orbits in the crossed fields diamagnetic Kepler problem in silicon

C. Bleasdale and R. Lewis

University of Wollongong, Wollongong, New South Wales 2522, Australia

The diamagnetic Kepler problem has been the basis of much work since the observation of oscillations in the spectrum of Barium in an external magnetic field by Garton & Tomkins [1]. These oscillations were related to the chaotic motion of the electron perpendicular to the applied magnetic field. Further work lead to a great understanding of the effects classical chaos has on quantum atomic systems. Much of the work was focused on systems with cylindrical symmetry in which the azimuthal dependence of classical trajectories was of little importance. However, if an electric field is applied perpendicular to the magnetic field, this breaks the rotational symmetry and complicates the investigation [2,3,4]. In 2009, oscillations were first observed in phosphorus doped silicon [5]. This system is not spherically symmetric due to the presence of conduction band valleys. One would expect that classical orbits launching, and returning, in the vicinity of these conduction band valleys to contribute stronger oscillations to experimental data than they may otherwise.

This work analyzes the azimuthal dependence of planar orbits in the crossed field diamagnetic Kepler problem utilizing a much simplified theoretical framework we recently proposed [6]. In the numerical calculations, the magnetic field is aligned along z-axis with the two identical conduction band valleys of silicon, and the electric field along one of four equal conduction band valleys in the x-y plane. We look to identify if varying the ratio of applied fields of the electron will shift the positions of closed orbits in the x-y plane to align themselves with the positions of the four conduction band valleys. We find that for zero classical and low electric field, the so called "Garton-Tomkins" orbit, and the majority of its associated harmonics, shows a two-fold azimuthal dependence as expected. The minimum return distance for these orbits fall outside the conduction band valleys and we therefore expect a significant drop in the recurrence strengths associated with these orbits. However, every third harmonic shows much higher stability to changes in electric field strength and instead yield a four-fold azimuthal dependence as the electric field is increased. Not only has this not been noted in previous , the minimum return distances all fall on conduction band valleys. We would therefore expect the influence of these harmonics to be greatly enhanced in experimental measurements.

[1] W. R. S. Garton and F. S. Tomkins, *The Astrophysical Journal* **158**, 839 (1969).

[2] J. von Milczewski and T. Uzer, *Phys. Rev. E*. **55**, 6540 (1997).

[3] C. Neumann, R. Ubert, S. Freund, E. Flöthmann, B. Sheehy, K. H. Welge, M. R. Haggerty, and J. B. Delos, *Phys. Rev. Lett.* **78**, 4705 (1997).

[4] D. M. Wang and J. B. Delos, *Phys. Rev. A.* **63**, 043409 (2001).

[5] Z. Chen, W. Zhou, B. Zhang, C. H. Yu, J. Zhu, W. Lu, and S. C. Shen, *Phys. Rev. Lett.* **102**, 244103 (2009).

[6] C. Bleasdale, A. Bruno-Alfonso, and R. A. Lewis *(under consideration)* (2015).

TP19

Temperature and magnetic field dependent magnetization of nanoparticulate $ZnFe_2O_4$ produced by mechanochemical synthesis

F. Nesa[1] , X. Wang[2], J. Wang[2], S. Kennedy[3], S.Campbell[4] and M. Hoffman[5]

[1]*ANSTO, Lucas Heights, NSW 2234, Australia*

[2]*University of Wollongong, Wollongong, New South Wales 2522, Australia*

[3] *European Spallation Source, Lund, Sweden*

[4] *School of PEMS, UNSW Canberra, Canberra, ACT 2600, Australia*

[5] *FRM-II, TU München, Lichtenbergstrasse 1, Garching, Germany*

$ZnFe_2O_4$ is basically a non-inverted ferrite which is enormously used as ferrofluids, magnetoelectric refrigeration and contrast agent for magnetic resonance imaging. A series of nanoparticulate $ZnFe_2O_4$ of average sizes F ~ 9 nm to 90 nm with a range of inversion 0.008 to 0.35 has been produced by mechnochemical synthesis. The blocking temperature of the investigated samples has increased with increasing crystallite size and accordingly behaved as Curie-Weiss paramagnetic materials [1, 2]. The temperature dependent magnetic behavior of these nanoparticulates has been investigated over the temperature range from 5 K to 300 K at a magnetic field of 100 oe. DC magnetization over a magnetic field range of 0 oe to 10000 oe at 5 K, 150 K and 200 K has been observed which interpreted that the samples are superparamagnetic materials [3]. All the samples showed the normal magnetic hysteresis below blocking temperature which also shows that the coercively increases with decreasing inversion 1. The frequency dependent magnetic behaviour of nanoparticulate $ZnFe_2O_4$ of 90 nm crystallite size has also been studied over a frequency range of 10 Hz to 10000 Hz which interpreted that with the increase of frequency the magnetization of this sample increased to saturation magnetization for all samples are approximately at 100 K temperature [4].

[1] Qi Chen and Z. John Zhang, *Applied Physics Letters* **73** 3156 (1998)

[2] S. J. Stewart *et al. Journal of Alloys and Compounds* **495** 506 (2010)

[3] H. M. Widatallah *et al*. *J. Magn. Magn. Mater.* **320** 324(2008)

[4] M. Hoffman *et al*. *Mater. Sci. Lett.* **39** 5057 (2004)

TP20

Pressure induced, reversible, fourfold enhancement of the magnetic ordering temperature in transition metal monomers

C. Woodall[1] and J. Martienz Lillo[2]

[1] *The University of Edinburgh, Scotland*

[2] *Departament de Química Inorgànica/Instituto de Ciencia Molecular (ICMol), Universitat de València, Spain*

Since the discovery of Single-Molecule Magnets (SMMs) in 1993 there has been extensive interest in understanding,[1] developing and tuning the nature of magnetic interactions within molecules the with emphasis on potential device miniaturisation and a bottom-up approach to building components. More recently attention has shifted from large polymetallic clusters of paramagnetic metal ions known as SMMs to include other classes of materials such as Single-Ion Magnets (SIMs),[2] where monometallic complexes are able to order via through space dipole intermolecular interactions arising from the combination of large magnetic anisotropy and spin-delocalisation from metal to ligand.[3,4]

We report a high-pressure study of two ReIV SIMs, $[ReCl_4(MeCN)_2]\cdot MeCN$ (1) and $[ReBr_4(bpym)]$ (2) (bpym = 2,2'-bipyrimidine) with the intention of investigating the role that pressure may play on their magnetic and structural properties. Both compounds display magnetic ordering at low temperatures (Tc = 6.7 K, 19.0 K respectively) via a spin canting mechanism controlled by the strength of the intermolecular interactions with the crystal structure, making it likely to be highly susceptible to pressure. Both compounds have been investigated using high-pressure SQUID magnetometer and the results correlated with high-pressure crystallography and computational analysis to reveal up to a four-fold increase in Tc despite only moderate increases in pressure (ambient to 4 GPa) that correlates directly with significant reductions in intermolecular Re-X…X interactions as pressure increases

[1] Sessoli, R.; Tsai, H. L.; Schake, A. R.; Wang, S. Y.; Vincent, J. B.; Folting, K.; Gatteschi, D.; Christou, G.; Hendrickson, D. N. *Journal of the American Chemical Society* **115**, 1804 (1993)

[2] Craig, G. A.; Murrie, M. *Chemical Society Reviews* **44**, 2135 (2015)

[3] Martínez-Lillo, J.; Faus, J.; Lloret, F.; Julve, M. *Coordination Chemistry Reviews* **289**, 215 (2015)

[4] Wang, X.-Y.; Avendaño, C.; Dunbar, K. R. *Chemical Society Reviews* **40**, 3213 (2011)

TP21

Physical, thermal and ^{57}Fe Mössbauer studies of $Y_2Fe_2Si_2C$

R. Susilo[1] , S. Cadogan[1], C-H. Hsu[2], H.Lin[2], W. Hutchison[3] and S. Campbell[1]

[1] *School of PEMS, UNSW Canberra, Canberra, ACT 2600, Australia*

[2] *Centre for Advanced 2D Materials and Graphene Research Centre, National University of Singapore, Singapore 117546*

[3] *The University of New South Wales, UNSW Canberra, Canberra, ACT 2600, Australia*

$R_2Fe_2Si_2C$ (R = rare-earths) compounds crystallise in the monoclinic $Dy_2Fe_2Si_2C$-type structure with the C2/m space group. Previous magnetic studies revealed no magnetic phase transition in $Y_2Fe_2Si_2C$ down to 2 K 1, thus indicating that $Y_2Fe_2Si_2C$ acts as an ideal non-magnetic reference material for investigating the magnetism of the $R_2Fe_2Si_2C$ system. Accordingly, we have used $Y_2Fe_2Si_2C$ as a reference material to estimate the magnetic contribution to the total specific heat of magnetic $R_2Fe_2Si_2C$ compounds [2-4]. Despite the significance of $R_2Fe_2Si_2C$ for enhanced understanding of the magnetism of $R_2Fe_2Si_2C$ compounds, no detailed studies have so far been reported for $Y_2Fe_2Si_2C$.

In this work, we report our detailed investigations of the structural and thermal properties, specific heat (CP) together with ^{57}Fe Mössbauer studies and first-principles calculations on $Y_2Fe_2Si_2C$. The thermal expansion of $Y_2Fe_2Si_2C$ follows the Debye-Grüneisen relation with no pronounced anomalies observed between 20 K and 300 K. By comparison, the CP data over the temperature range of 2 K - 300 K cannot be described adequately by the Debye model; rather, the CP data have been described fully by the Debye-Einstein model including anharmonic corrections, suggesting the importance of optical contributions (Einstein terms) to the phonon spectrum in $Y_2Fe_2Si_2C$. The low-temperature CP measurements (2 - 17 K) yield a rather large Sommerfeld coefficient g = 16.3(5) mJ/mol. K2, reflecting a large density of states (DOS) at the Fermi energy (EF) which suggests that $Y_2Fe_2Si_2C$ might be an itinerant ferromagnet. On the other hand, ^{57}Fe Mössbauer spectra measured from 10 K to 300 K show no magnetic splitting, confirming that the Fe atom is in a non-magnetic state. While electronic structure calculations reveal a large DOS at the Fermi energy, the DOS of the Fe-3d states at EF is only 1.1 states/eV per Fe atom. This value corresponds to N(EF)I = 0.51 which is far below the Stoner criterion for ferromagnetism, thereby establishing that $Y_2Fe_2Si_2C$ is far from being magnetic.

[1] D. Schmitt, D. Paccard, and L. Paccard. *Solid State Commun.,* **84**, 357 (1992)

[2] R.A. Susilo, J.M. Cadogan, W.D. Hutchison and S.J. Campbell, *Physica Status Solidi (A),* **211**, 1087 (2014)

[3] R.A. Susilo, J.M. Cadogan, R. Cobas, W.D. Hutchison, M. Avdeev and S.J. Campbell, *J. Appl. Phys.*, **117**, 17C113 (2015)

[4] R.A. Susilo, J.M. Cadogan, W.D. Hutchison, M. Avdeev, R. Cobas, S. Muñoz Pérez and S.J. Campbell, *J. Alloys Compd.*, **654**, 392 (2016)

TP22

Mechanism of enhancement of the electron g-factor in quantum point contacts

G. Vionnet[1] and O. Sushkov[2]

[1] *Institute of Theoretical Physics, Ecole Polytechnique Federale de Lausanne (EPFL), 1015 Lausanne, Switzerland*

[2] *The University of New South Wales, NSW 2052, Australia*

The electron g-factor measured in a quantum point contact by source-drain bias spectroscopy is significantly larger than its value in a two-dimensional electron gas. This enhancement, established experimentally in numerous studies, is an outstanding puzzle. In the present work we explain the mechanism of this enhancement in a theory accounting for the electron-electron interactions. We show that the effect relies crucially on the non-equilibrium nature of the spectroscopy at finite bias.

TP23

Towards understanding the magnetic structure of DyN, a ferromagnetic semiconductor

J. Evans[1], G. Stewart[2], S. Cadogan[2], W. Hutchison[2], E. Mitchell[3] and J. Downes[1]

[1] MQ Photonics Research Centre, Department of Physics and Astronomy – Macquarie University, NSW 2109, Australia

[2] School of PEMS, UNSW Canberra, Canberra, ACT 2600, Australia

[3]CSIRO Materials Science and Engineering, Lindfield, NSW, Australia

The rare-earth nitride (REN) series has attracted considerable research interest because of the co-existence of semiconducting and ferromagnetic properties, a feature ideal for spintronic devices. Dysprosium nitride (DyN) is a promising candidate whose electronic structure is relatively well understood. However, its magnetic structure has received little attention until recently. In particular, its low temperature bulk magnetic moment of about 4μB/ion is significantly lower than the predicted magnetic moment, which is much closer to the free-ion value of 10μB/ion 1. Because of this, we are attempting to understand the detailed magnetic structure of DyN using conventional magnetometry combined with ^{161}Dy Mössbauer spectroscopy. Using ion-assisted deposition, we have grown thick 3-4 μm DyN films on both sapphire and Kapton substrates. Because the characteristic measurement time for ^{161}Dy Mössbauer spectroscopy is of the order of nanoseconds, the spectrum recorded at 5 K was sensitive to rapid thermal fluctuation between the low-lying levels of the Dy^{3+} crystal field scheme. The spectrum was successfully analysed in terms of flipping between a pair of levels with moments of the same magnitude, 10 μB, but opposite sign. Based on the fitted energy separation, the longer-time, thermal-averaged moment can be estimated at about 85% of the full free ion value. However, such a simple 2-level crystal field ground state model would require a breaking of the cubic symmetry appropriate for the Dy^{3+} site in bulk DyN.

[1] D. L. Cortie *et. al.*, *Phys. Rev. B* **89**, 064424 (2014)

TP24

G-factors of hole bound states in spherically symmetric potentials in cubic semiconductors

D. Miserev and O. Sushkov

The University of New South Wales, NSW 2052, Australia

Holes in cubic semiconductors have effective spin 3/2 and as a result they have very strong spin orbit interaction as compared with that of electrons. High spin 3/2 provides the complex kinematic structure in coupling between spin and momentum. The strength/complexity creates a variety of new opportunities for spintronics, semiconductors' based artificial topological materials, quantum point contacts and other spin related effects/applications.

In the present study we develop a new technique and then calculate analytically Lande factors of hole bound states in arbitrary spherically symmetric confining potentials. Previously, this problem for a special case of acceptor states was addressed numerically and a very strong suppression of g-factors was noted [1]. The origin of this suppression was not understood. Our analysis explains the suppression and, more importantly, allows making predictions for arbitrary bound states which can be used in spintronics applications.

[1] Schmitt, W. O. G., Schmitt, E., Bangert, G., Landwehr, *J. Phys. Condens. Matter* **3** (1991).

TP25

A ^{161}Dy-Mössbauer spectroscopy investigation of $DyCrO_4$

G. Stewart[1], W. Hutchison[2] and D. Ryan[2]

[1] *The University of New South Wales, UNSW Canberra, Canberra, ACT 2600, Australia*

[2] *The Centre for the Physics of Materials, McGill University, Montreal, H3A 2T8, Canada*

The rare earth (R) chromates $RCrO_4$ form with the tetragonal zircon type structure (space group I41/amd). They are of interest because of competing ferromagnetic and antiferromagnetic super-exchange interactions between the 3d ($Cr^{5+)}$ and 4f (R^{3+}) sites, believed to be responsible for the giant magnetocaloric effect observed recently for R = Gd, Dy and Ho [1,2]. The ^{161}Dy-Mössbauer spectroscopy measurements on $DyCrO_4$ reported here were prompted by earlier ^{169}Tm- and ^{155}Gd-Mössbauer spectroscopy results for $TmCrO_4$ [3] and $GdCrO_4$ [4], respectively. In both instances, it was necessary to interpret the Mössbauer spectra in terms of a superposition of two sub-spectra (approx. 80:20 intensity ratio) despite there being only a single crystallographic R(4a) site. In addition, the magnetic transitions exhibited first order character, which is contrary to bulk magnetic measurements.

$DyCrO_4$ is reported to undergo a small crystal distortion to an orthorhombic (Imma) structure somewhere between 27 and 40 K and to order ferromagnetically at TC = 22.4 K [5]. Our ^{161}Dy-Mössbauer results show a simple magnetically-split spectrum at 5 K. Compared to the reference Dy metal spectrum there is a small increase in the line width. However, contrary to the earlier Mössbauer work [3,4], a second sub-spectral component is not immediately evident. The spectra are paramagnetic above TC with the quadrupole splitting and Wegener relaxation broadening diminishing as the temperature increases to room temperature.

This work was supported by AINSE, grant number 14547.

[1] Midya A. et al. *Appl. Phys. Lett.* **103** 092402. (2013)
[2] Midya A. et al. *J. Appl. Phys*. **115** 17E114. (2014)
[3] Jiménez E. et al._*J. Magn. Magn. Mater*. **272** 568 (2004)
[4] Jiménez-Melero E. et al. *J Phys. Chem. Mater*. **18** 7893 (2006)
[5] Long Y. et al. *J. Magn. Magn. Mater*. **322** 1912. (2010)

TP26

Spin drift in Rashba systems with tilted magnetic fields

S. Bladwell and O. Sushkov

The University of New South Wales, NSW 2052, Australia

It is well known in Plasma physics that combinations of electric and magnetic fields lead to the drift of charge particles. In this work, we show that with the addition of a tilted magnetic field, drift analogous to that observed in plasmas occurs in systems with Rashba SO interactions. The resulting drift of the charge carriers has a direction dependent on the spin, rather than the charge of the electron or hole, reflecting the origin of this effect in the spin-orbit interaction. From this theoretical analysis we present proposals for experimental observation.

TP27

Epitaxial (001) $BiFeO_3$ thin-films with excellent ferroelectric properties by chemical solution deposition - The role of gelation

Q. Zhang and N. Valanoor

The University of New South Wales, NSW 2052, Australia

High quality phase pure (001) epitaxial bismuth ferrite ($BiFeO_3$; BFO) thin films have been realized by chemical solution deposition. A thorough chemical investigation of the precursor molecular changes during gelation reveals that control of the delicate balance between gelation and metal nitrate precipitation through solvent evaporation is the key to a homogenous gel, necessary to ultimately obtain high-quality films. Spin-coating the precursor on a preheated $SrTiO_3$ (001) (STO(001)) substrate (~70 °C) and subsequent heating at 90°C leads to a suitable gel film, which is then heated to 650°C for crystallization. Pure phase BFO thin films of 150 nm thickness prepared by this route on lanthanum strontium manganite ($La_{0.67}Sr_{0.33}MnO_3$; LSMO) buffered STO(001) substrates are shown to have not only epitaxial nature, but also robust ferroelectric properties with low coercive field. Critically we show that these films can be achieved using stoichiometric 0.25 M precursors (with no Bi excess), thus obviating complexities typically arising from secondary phases associated with precursors having excess Bi. Square hysteresis loops with a high remnant polarization of $2Pr$ =97.8 $\mu C/cm^2$ and a low coercive field of $2E_c$ = 203.5 kV/cm are obtained at room temperature. Frequency-dependent hysteresis loops reveal a switching mechanism that is nucleation dominated. In addition, polarization direction dependent resistive switching behaviour is also observed. The findings here thus show it is possible to realize high-quality bismuth ferrite thin films via chemical process techniques.

TP28

Complex Magnetic Structure in strained nanoscale bismuth ferrite thin films

C. Ulrich[1], J. Bertinshaw[1], R. Maran[2], S. J. CAllori[1], V. Ramesh[1], J. Cheung[1], S. Danilkin[1], S. Hu[1]
J. Siedel[1] and N. Valanoor[1]

[1] *The University of New South Wales, NSW 2052, Australia*

[2]*ANSTO, Lucas Heights, NSW 2234, Australia*

Multiferroic materials demonstrate excellent potential for next-generation multifunctional devices, as they exhibit coexisting ferroelectric and magnetic orders. Bismuth ferrite ($BiFeO_3$) is a rare exemption where both order parameters coexist far beyond room temperature, making it the ideal candidate for technological applications. In particular, multiferroic thin films are the most promising pathway for spintronics applications. Therefore we have investigated $BiFeO_3$ thin films by neutron diffraction. At present, the underlying physics of the magnetoelectric coupling is not fully understood and competing theories exist with partly conflicting predictions. For example, the existence of spin cycloid is a mandatory requirement to establish a direct magnetoelectric coupling. Thus far internal strain in epitaxially grown films has limited the stability of the spin cycloid for $BiFeO_3$ films with less than 300 nm thickness, causing the spin cycloid to collapses to a collinear G-type antiferromagnetic structure. Our neutron diffraction experiments have demonstrated that we were able to realize a spin cycloid in films of just 100 nm thickness through improved electrostatic and epitaxial constraints. This underlines the importance of the correct mechanical and electrical boundary conditions required to achieve emergent spin properties in mutiferroic thin film systems. The discovery of a large scale uniform cycloid in thin film $BiFeO_3$ opens new avenues for fundamental research and technical applications that exploit the spin cycloid in spintronic or magnonic devices.

TP29

Nanoscale Ferroelectric domain structure of bismuth ferrite $BiFeO_3$ under different strains

A. Alsubaie, P. Sharma, and J. Siedel

The University of New South Wales, NSW 2052, Australia

The effect of induced epitaxial strain on ferroelectric properties of thin films has received increased research interest in recent years. Researching studies have shown that the polarization1, piezoelectricity[2], domain structure[3], and phase stability[2] of these materials in thin films can be modified by strain because of the inherent coupling between the elastic and ferroelectric phenomena [4]. Ferroelectric domain structure under mechanical tensile stress in bismuth ferrite (BFO) was observed using piezo response force microscopy (PFM) under different strain conditions. For this purpose a newly designed bending stage has been developed for tensile and compressive bending stress application. We have found that the ferroelectric domain structure changes under tensile stress and domain walls are displaced along the uniaxial strain direction. The change of domain structure is clearly seen in PFM with and without applied stress. Furthermore, in-plane polarization-electric field (P-E) hysteresis loops are recorded under different strains. We found that the positive coercive voltages are slightly changed in contrast with the negative coercive voltages under moderate tensile strain of the BFO film.

[1]. Choi, K.J., *et al*., Enhancement of ferroelectricity in strained BaTiO3 thin films. *Science*. **306** 1005. (2004)

[2]. Zeches, R., *et al*., A strain-driven morphotropic phase boundary in BiFeO3. *Science*. **326** 977 (2009)

[3]. Chen, Z., *et al*., Low symmetry monoclinic MC phase in epitaxial BiFeO3 thin films on LaSrAlO4 substrates. 2010.

[4]. Chen, Z., *et al*., Study of strain effect on in-plane polarization in epitaxial BiFeO3 thin films using planar electrodes. *Physical Review B*. **86**(23) 235125. (2012)

TP30

Generalised requirements for ferroelectric domain sharing over grain boundaries

S. Mantri , and J. Daniels

The University of New South Wales, NSW 2052, Australia

Ferroelectric materials are utilised in a range of technologically important devices. For cost reasons, they are mostly used in the polycrystalline form. Observations of the microstructure and domain structure in polycrystalline ferroelectrics and its effect on ferroelectric performance has been extensively studied. Some of these observations show the frequent occurrence of continuous ferroelectric domain boundaries across grain boundaries. This continuity of domains is suspected to lead to collective dynamics behaviour, particularly during ferroelectric domain wall motion during material excitation. The presented research relates to this domain sharing between neighbouring grains. The requirements for plane matching across grain boundaries is studied, which in turn is used to analyse the proportion of grain boundaries that can allow for plane matching for various grain misorientations using simulations. These simulations are then compared to the microstructures recorded using near field 3D-XRD methods to understand the grain-scale heterogeneous response of these materials under applied electric field.

TP31

Rational design of multiferroic superlattices

C. Cazorla

The University of New South Wales, NSW 2052, Australia

Multiferroics, materials that typically display ferroelectricity and magnetism, have generated a tremendous flurry of interest in recent years due to their fundamental complexity and potential for applications in nanoelectronics and energy conversion. Finding in nature single-phase compounds with those properties, however, has proved extremely difficult. Such a scarcity of bulk multiferroic materials has motivated researchers to investigate oxide-based materials in thin film and superlattices geometries where i) the properties of the ferroelectric can be tuned almost at will by choosing an appropriate substrate lattice parameter, (ii) the electrostatic coupling between different oxide layers can be exploited, and iii) interfaces, rather than the oxide itself, can show novel multi-functional properties which are absent in either of the bulk constituents. In the development of this field first-principles simulations have played a major role, leading to the present situation in which theory often leads the way to new devices.

In this talk, I will present a general first-principles approach to predict the behaviour of perovskite oxide superlattices based exclusively on the properties of their individual bulk constituents. Such a formalism combines constrained electric displacement strategies with a rigorous description of interface polarity. As a result, a clear separation between genuine interface and bulk effects is possible. Crucially, the present method allows one to quantify straightforwardly the impact that interface polarity has on the equilibrium (and metastable) phases of a superlattice. As a proof of concept I apply this formalism to $[PbTiO_3]_m/[BiFeO_3]_n$ heterostructures and show that (i) earlier first-principles predictions obtained in ultrashort-period superlattices with explicit supercell simulations are accurately reproduced, and (ii) by assuming interface terminations with different nominal charge, radical changes in the overall ferroelectric properties of the superlattice are disclosed that lead to the stabilization of otherwise inaccessible bulk phases.

TP32

Positive effect of an internal depolarization field in ultrathin epitaxial ferroelectric films

G. Liu and N. Valanoor

The University of New South Wales, NSW 2052, Australia

The effect of intentionally introducing a large depolarization field in (001)-oriented, epitaxial $Pb(Zr_{0.2}Ti_{0.8})O_3$ (PZT) ultra-thin films grown on $La_{0.67}Sr_{0.33}$ MnO_3 (LSMO) buffered $SrTiO_3$ (STO) substrates is investigated. Inserting between 3 to 10 unit cells of STO between two 3nm thick PZT films significantly influences the out-of-plane (c) lattice constant as well as the virgin domain state. Piezoresponse force microscopy images reveal a nanoscale (180) polydomain structure in these films. In comparison, a "reference" single layer PZT sample (6 nm thick without STO spacer) exhibits an elongated PZT c-axis (0.416nm) and is preferentially "down"-polarized with large regions of monodomain contrast. It shows asymmetric switching loops (i.e. imprint) coupled with sluggish domain switching under external bias. We show that the insertion of STO drives a monodomain to 180 polydomain transition in the as-grown state, which reduces the imprint by 80%. The insertion of the STO also profoundly improves dielectric leakage and hence the distribution of the applied electric field. Consequently, the critical pulse duration of the electric field required to initiate domain switching is reduced by two orders of magnitude relatively to the reference sample. These results demonstrate the possibility of manipulating the depolarization field in such a way that it has positive effects on the ferroelectric behaviour of ultrathin PZT films. This work is published in *Advanced Electronic Materials* DOI: 10.1002/aelm.201500288

TP33

Determining fundamental properties from diffraction: electric field induced strain and piezoelectric coefficient

M. Hinterstein[1] , A. Studer[2] and M. Hoffman[1]

[1] *The University of New South Wales, NSW 2052, Australia*

[2] *The Bragg Institute, ANSTO, Lucas Heights, NSW 2234, Australia*

Piezoelectric ceramics exhibit the remarkable property to couple elastic strain and polarization under the influence of an applied electric field. Among the various types of piezoelectric devices, especially actuators rely on high electric fields to generate high strains and forces. Prominent examples for actuators are multilayer stack actuators used for nanopositioning or in modern combustion engines for automobiles to control injection cycles. The two most important characteristics of this class of materials are macroscopic strain and piezoelectric coefficient. Despite extensive studies and elaborated measurement techniques, the correlation between macroscopic strain and structural response is still not fully understood. Most of the relevant systems found up to now are compositions close to phase boundaries linking highly correlated phases. This results in major challenges for structural analyses due to overlapping reflections. Apart from the well-known field induced structural responses such as domain switching and the converse piezoelectric effect we recently identified field induced phase transitions in different systems as an additional poling mechanism [1,2]. In order to resolve all three involved poling mechanisms within only one experiment we developed a structural analysis technique with in situ X-ray and neutron powder diffraction data [3]. The results not only separately reveal the contributions of each poling mechanism to the macroscopic strain, but also different behaviours of the individual phases. The calculation of the elastic strain perfectly matches the macroscopic observations, confirming the accuracy of the applied models. Since this method yields fundamental information such as the crystal structure as a function of applied electric field, we were able to calculate the piezoelectric coefficient for the individual phases based on information on the atomic scale. In this contribution we present the latest research on the elucidation of strain mechanisms and fundamental properties in piezoceramics.

[1] M. Hinterstein, M. Knapp, M. Hoelzel, W. Jo, A. Cervellino, H. Ehrenberg and H. Fuess, *J. Appl. Phys*. **43**, 1314 (2010).

[2] M. Hinterstein, J. Rouquette, J. Haines, Ph. Papet, M. Knapp, J. Glaum and H. Fuess, *Phys. Rev. Lett*. **107**, 077602 (2011).

[3] M. Hinterstein, M. Hoelzel, J. Rouquette, J. Haines, J. Glaum, H. Kungl, M. Hoffman, *Acta Mater*. **94**, 319 (2015).

TP34

Diffuse X-ray Scattering: Probing the Nano-scale Disorder in the Lead-Free Piezoelectric $Na_{0.5}Bi_{0.5}TiO_3$

P.Tung[1], M. Major[2], J. Huspeth[3] and J. Daniels[1]

[1] *The University of New South Wales, NSW 2052, Australia*

[2]*Technische Universitat Darmstadt, 64287 Darmstadt, Germany*

[3]*European Synchrotron Radiation Facility*

Understanding the relationship between the properties of piezoelectrics and its atomic structure is important in enhancing their properties. With the addition of enforced legislations motivating the removal of lead in all electronic products, research into the fundamental properties of lead-free piezoelectric materials is vital.

A promising lead-free piezoelectric is $Na_{0.5}Bi_{0.5}TiO_3$ (NBT), however it is a highly complex perovskite material and the room temperature structure is still debated. The use of conventional scattering methods to analyse Bragg peaks gives information on the long-range average structure that permeates throughout the whole material, and hence it can be difficult to extract information on deviations away this average structure, i.e. the disorder. Scattering that originates from this disorder is known as diffuse scattering. Here, diffuse X-ray synchrotron scattering was employed to deduce the short- to medium-range structures that diverge away from the long-range structure.

Analysis of the diffuse scattering has revealed a diverse range of disorder occurring in NBT, which includes octahedral stacking faults, A-site size effects and structural modulations on the order of 10 unit cells. Preliminary modelling of the A-site occupancy has been carried out and modelling of the remaining disordered structures is currently being performed.

By understanding the nano-scale atomic mechanisms that contribute to the electromechanical properties in NBT, we will be closer to exploiting and controlling such properties in future functional materials to allow them to replace current lead technologies.

TP35

Combinatorial synthesis of piezoelectric materials using an inkjet printer

F. Marlton, J. Daniels and O. Standard

The University of New South Wales, NSW 2052, Australia

Piezoelectrics are used in a wide variety of technology applications and currently their best performing compositions are lead-based. Legislative requirements will impose serious restrictions on the use of these lead-based materials in consumer devices over the coming years and currently no viable lead-free alternative exists. A potential pathway for the discovery of such a unique material is through combinatorial techniques. Combinatorial chemistry is the rapid synthesis and analysis of large numbers of compositions, through many combinations of a relatively small number of starting compounds.

Inkjet printing is currently at the threshold of becoming a standard fabrication tool, with a wide range of materials science applications. It is regarded as one of the most promising techniques for the creation of functional metal oxides on various substrates because it has an automatically controlled printing scheme with precise and flexible droplet volumes and offers rapid mass production. This project aims to produce a ternary phase diagram with a compositional resolution of 1% using ceramic suspensions and inkjet printing technologies.

This study outlines the challenges and methods for producing high quality ceramic inks. Using rapid, high energy milling techniques, ceramic inks with a maximum particle size of 200 nm have been developed. This has been used to print single phase Barium Titanate on Alumina substrates using a commercial printer.

This technique has the potential to lead to the development of novel environmentally-friendly lead-free compositions of piezoelectrics and a state-of-the-art combinatorial synthesis technique for functional materials discovery.

TP36

Stress and electric-field dependence of the induced phase symmetry in BNT-xBT

M.J. Hossain[1], Z. Wang[1], N. Khansur[1], P.Tung[1]and J. Daniels[1]

[1] *The University of New South Wales, NSW 2052, Australia*

The solid solution system $Bi_{0.5}Na_{0.5}TiO_3 - xBaTiO_3$ (BNT-BT) has attracted wide research interest in the scientific community as a potential high-strain lead-free piezoelectric material. The electro-mechanical coupling mechanisms in a series of BNT-BT solid solutions with the BT content ranging from 5 mol% to 8 mol% in 0.25 mol% steps have been studied using in situ high-energy synchrotron X-ray diffraction (XRD). Unipolar stress cycling with a maximum stress ~600 MPa, and bipolar electric-field cycling with maximum field of 5 kV/mm were applied in two separate experiments. In the initial state, the BNT-xBT series exhibited a region of pseudo-cubic symmetry between x~5-8. During application of both stress and electric field, lower BT content samples ($x < 5.25$) tended to transform to rhombohedral symmetry, while higher BT content ($x > 7.75$) tended to go tetragonal. Compositions between these tended to transform to mixed phase symmetry. The results show that the stress and electric-field-induced phase transformation mechanisms are highly analogous in this material system within the range studied here.

TP37

Contrasting strain mechanisms in lead-free piezoelectric ceramics

N. Khansur and J. Daniels

The University of New South Wales, NSW 2052, Australia

Piezoelectric ceramics find a wide range of applications in advanced technological fields. Most of the currently used electro-active ceramics contain lead (Pb). Environmental concerns and limitations in high temperature performances of lead based compositions have spurred the field of lead-free electroceramics research. Compositions based on bismuth sodium titanate (BNT), sodium potassium niobate (NKN), bismuth ferrite (BF) and barium titanate (BT) have long been considered as candidates to replace lead based electroceramics. Although lead-free compositions based on these systems exhibit piezoelectric properties for potential device application, further enhancement is required. To improve their properties, extensive knowledge of structure-property relationships, especially during the field-on condition is essential. Diffraction is a useful technique to highlight structure-property relationships. To understand the microscopic origin of strain in lead-free electroceramics several compositions based on BNT, NKN, BF and BT has been studied using in situ high energy X-ray diffraction. Their microscopic strain response has been elucidated under electric field. Both the intrinsic (lattice) and extrinsic (domain switching and/or phase transformation) strain contributions have been analysed for each system and have been correlated with their macroscopic properties. This comparative study of their strain responses will enable us to focus on some important aspects that are essential to improve electro-mechanical properties in future lead-free systems.